

Cell Capacity Analysis of Relay Enhanced LTE-A Systems

Von der Fakultät für Elektrotechnik und Informationstechnik
der Rheinisch-Westfälischen Technischen Hochschule Aachen
zur Erlangung des akademischen Grades eines Doktors der
Ingenieurwissenschaften genehmigte Dissertation

vorgelegt von

Diplom-Informatiker
Yuan Chen

aus Shanghai, China

Berichter: Universitätsprofessor Dr.-Ing. Bernhard Walke
Universitätsprofessor Dr.-Ing. Anke Schmeink

Tag der mündlichen Prüfung: 21. Dezember 2020

Zellulare digitale Breitband-Mobilfunksysteme der 4. Generation laut Standard 3rd Generation Partnership Project (3GPP) Long Term Evolution- Advanced (LTE-A) wurden in Release 10 durch ein neues Netzelement ergänzt: ortsfixe in Schicht 2 des ISO/OSI¹ Modells übertragende Relaisknoten (RNs). RNs werden seit ihrer Erfindung bei ComNets (1999) weltweit beforscht. Sie verbessern die Funkversorgung von Mobilstationen (MSs) in Mobilfunkzellen und erhöhen unter geeigneten Umständen die Zellkapazität und die Spektrum Effizienz. Bisherige Ergebnisse zur Charakterisierung der Mittelwerte von Leistungsparametern von RN-verstärkten Zellen stammen von Untersuchungen mit ereignisgesteuerter stochastischer Systemsimulation. Obwohl diese Werkzeuge von Mobilfunkausrüstern und Netzbetreibern die Systeme sehr detailliert repräsentieren, zeigen bekannte Ergebnisse von 12 Firmen zur Leistungsfähigkeit von RN sehr unterschiedliche Resultate. Die Simulationsmodelle sind offenbar bzgl. Qualität und gemachter Annahmen nicht vergleichbar. Es fehlt ein transparentes mathematisches Verfahren, um wichtige Leistungsparameter von RN-verstärkten LTE-A Systemen zu ermitteln.

Diese Arbeit stellt sich dieser Aufgabe und löst sie sehr überzeugend. In einem ersten wichtigen Beitrag erstellt die Arbeit - unter Nutzung aller von ITU-R² für die Bewertung des LTE-A Systems für ein Stadtszenario (UMa) bereitgestellten Parameter und Funkausbreitungsmodelle - ein mathematisches Modell. Es berechnet für kleine 5×5 m Flächenele-

¹Open Systems Interconnection Modell der Internationalen Standardisation Organisation

²International Telecommunication Union - Radio Sektor

mente eines vielzelligen Mobilfunknetz-Modells für die Abwärtsstrecke (DL), abhängig vom Ort der MS, die Verteilungen von Nutz-zu-Störsignalabstand (SINR), Fehlerrate, Durchsatz und Spektrum Effizienz. Das Modell berücksichtigt die physikalischen Übertragungseigenschaften des Funkkanals, adaptive Modulation und Codierung (AMC) und zugehörige Fehlerraten bei der Durchsatzberechnung. Es modelliert auch die in Schicht 2 des ISO/OSI Modells in der MAC³ Teilschicht ablaufenden Funktionen des hybriden ARQ⁴ Protokolls bzw. des in der darüber liegenden RLC⁵ Teilschicht ausgeführten Selective Repeat-ARQ Protokolls, wobei auch Fehler bei der Übertragung von Protokoll-Steuerinformation und die Zahl zulässiger wiederholter Übertragungen eines Nutzdatenblocks berücksichtigt werden. In relaisverstärkten Systemen werden zwei sequentielle Funkstrecken betrieben, jede auf Basis der genannten Protokolle.

Die Verteilung erfolgreich übertragener Pakete bzw. deren belegte Funkbetriebsmittel ergibt die Durchsatzverteilung des ortsabhängigen Flächenelements. Summierung über alle Flächenelemente ergibt die Durchsatzverteilung bzw. die Spektrum Effizienz am DL der Zelle. Damit wird der Protokollstapel zur Funkübertragung von IP-Paketen vollständig berücksichtigt. Mit Wahrscheinlichkeit auftretende Mehrfachübertragungen derselben Nutzdaten, eventuell auch durch im Protokollstapel tiefer liegende Protokollschichten führen zu unübersichtlichen mathematischen Ausdrücken für den Betriebsmittelverbrauch. Diese Arbeit nutzt aus der Literatur bekannte Signalflussgraphen (SFG), um die mathematischen Ausdrücke zu vereinfachen und überschaubar zu machen.

Ein kleinerer Beitrag der Arbeit betrifft systematische Untersuchungen zur Spektrum Effizienz bei verschiedener Aufteilung der Funkbetriebsmittel einer Zelle auf direct, backhaul und

³Medium Access Control

⁴Automated Repeat on ReQuest

⁵Radio Link Control

access Link⁶. Die optimale Aufteilung wird vorgestellt; sie vermeidet verkehrstheoretische Engpässe. Bemerkenswert ist, dass dabei der meiste Verkehr der Zelle über RNs läuft und die Varianz des Nutzdurchsatzes minimal wird. Diese Arbeit parametrisiert das vorgestellte Modell so wie in einer früher bei ComNets bearbeiteten Dissertation (K. Sambale), die durch Simulation die Zahl und Orte von RNs pro Zelle optimiert, um Zellkapazität und Spektrum Effizienz zu maximieren. Es gelingt, die Mittelwerte eigener Resultate durch Ergebnisse der genannten Arbeit und einer von Nokia Mitarbeitern publizierten Simulationsarbeit zu validieren. Diese Arbeit untersucht auch den Fall, dass Pico-Zellen (als out-of-band RNs bzw. mit Kabelanschluss) anstelle von RNs an deren Standorten eingesetzt werden. Da dann keine Betriebsmittel für den backhaul Link benötigt werden, verdoppelt sich die Systemkapazität der Zelle. Der Rechenaufwand für einen bestimmten Parametersatz zur Charakterisierung der untersuchten 800×800 m großen Versorgungsfläche beträgt etwa 10 Tage auf einem 64 Blade PC-Cluster. Am DL erzeugen andere BSs Interferenz, am UL sind es alle Mobilstationen. Weil die Zahl MS erheblich größer ist als die der BSs, erfordern statistisch vertrauenswürdige Simulationsergebnisse einen riesigen Rechenaufwand, den noch niemand investiert hat.

Das vorgestellte Verfahren eignet sich auch zur Berechnung von Durchsatz, Kapazität und Spektrum Effizienz (SE) am UL für Zellen ohne und mit Relais. Das ist ein dritter besonders wichtiger Beitrag der Arbeit. Um die Interferenz durch MSs zu modellieren, wird eine Zelle in Partitionen mit exklusiv zugewiesenen Funkbetriebsmitteln aufgeteilt. Die Aufteilung wird im vielzelligen Funknetz so gewählt, dass Gleichkanal Interferenz an geometrisch möglichst weit entfernten Orten entsteht. Partitionen mit gleichen Funkbetriebsmitteln sind in einem regelmäßigen Muster über alle Zellen hinweg angeordnet. Einzelne Partitionen derselben Zelle können zu einer Division

⁶Direct link: BS \leftrightarrow MS; backhaul link: BS \leftrightarrow RN; access link: RN \leftrightarrow MS.

gruppiert werden, wobei der verkehrstheoretische Bündelgewinn gegenüber dem einer Partition steigt. Aus diesem Modell resultiert bei der BS aus den kleinen Flächenelementen systemweit eine ziemlich gleichmäßige SINR- bzw. SE-Verteilung. Gegenüber einer nicht partitionierten Zelle steigt die SE mit Partitionierung nur wenig an, aber die Standardabweichung sinkt erheblich. MSs können also unabhängig vom Ort in der Zelle etwa gleich fair bedient werden. Für den UL relaisverstärkter Zellen wird exemplarisch anhand eines Parametersatzes gezeigt, dass Relais die Spektrum Effizienz am UL deutlich erhöhen können.

ABSTRACT

Cellular digital broadband mobile radio systems of the 3rd Generation Partnership Project (3GPP) Long Term Evolution-Advanced (LTE-A) standard (4th generation) were supplemented with a new network element in Release 10: fixed Relay Nodes (RN) operating on Layer 2 of the International Organization for Standardization/Open Systems Interconnection (ISO/OSI) model. Since their invention by ComNets in 1999, RNs have been researched worldwide. They improve the radio signal received by Mobile Stations (MS) in mobile radio cells and, if deployed properly, increase cell capacity and spectrum efficiency. Present results, which characterize mean values of performance parameters for relay enhanced cells, are based on evaluations with event-driven stochastic system simulation. Although these simulators of equipment vendors and network operators represent the systems in great detail, results known from 12 companies on the performance of RNs show very different findings. The simulation models are obviously not comparable to each other in terms of quality and assumptions. There is no transparent analysis method to calculate important performance parameters of relay enhanced LTE-A systems.

This work faces up to this task and solves it very convincingly. In a first important contribution the work develops a mathematical model, taking into account all parameters and radio propagation models given by International Telecommunication Union Radiocommunication Sector (ITU-R) for the evaluation of LTE-A systems for a Urban Macro-cell (UMa) scenario. It calculates the distributions of Signal to Interference plus Noise Ratio (SINR), error rate, throughput and spectrum efficiency depending on the location of a MS for each small 5×5 m area element of a multi-cell mobile radio network for the downlink (DL). The model takes into account the physical

transmission properties of the radio channel, Adaptive Modulation and Coding (AMC) and corresponding error rates by calculating throughput. It also models the functions in Layer 2 of the ISO/OSI model, namely the Hybrid Automatic Repeat Request (HARQ) protocol running in the Medium Access Control (MAC) sublayer and the Selective Repeat Automatic Repeat Request (SR-ARQ) protocol performed in the Radio Link Control (RLC) sublayer above MAC, where transmission errors of protocol control information and the number of allowable re-transmissions of a user data block are also taken into account. In relay enhanced systems two sequential radio links are operated, each based on the protocols mentioned above.

The distribution of successfully transmitted packets or their consumed radio resources results in the throughput distribution of the location-dependent area element. Summing up over all area elements results in the throughput distribution or the spectrum efficiency on DL of the cell. Thereby the protocol stack for radio transmission of IP packets is fully taken into account. Multiple transmissions of the same user data, which occur with probability, possibly also through lower-lying protocol layers in the protocol stack, lead to unclear mathematical expressions for resource consumption. This work uses Signal Flow Graphs (SFG) known from literature to simplify the mathematical expressions and make them comprehensible.

A smaller contribution of the dissertation concerns systematic investigations of spectrum efficiency with different partition of radio resources of a cell on direct ($BS \leftrightarrow MS$), backhaul ($BS \leftrightarrow RN$) and access link ($RN \leftrightarrow MS$). The optimal partition is presented; it avoids bottlenecks in traffic theory. It is worthy of note that most of the cell's traffic runs via RNs and the variance of the user throughput becomes minimal. This work parameterizes the presented model just as in a dissertation (K. Sambale) completed previously at ComNets, which uses simulation to optimize the number and locations of RNs per cell in order to maximize cell capacity and spectrum efficiency. This work succeeds in validating the mean values of its own results against

the results of the work mentioned above and a simulation work published by Nokia employees. This work also investigates the case, that pico cells (as out-of-band RNs or with cable connection) are deployed instead of RNs at their locations. Since in this case no resources are required for the backhaul link, the system capacity of a cell doubles. The computational effort for a certain parameter set to characterize the studied 800×800 m service area is about 10 days on a 64-PC-cluster. On DL other BSs make interference, while on uplink (UL) interferers are all MSs. Because the number of MSs is substantially larger than that of BSs, statistically trustworthy simulation results require an enormous amount of computational effort, which no one has yet invested.

The presented method is also suitable for calculating throughput, capacity and spectrum efficiency on UL for cells with and without relays. This is a third particularly important contribution of the work. In order to model the interference from MSs, a cell is partitioned into divisions with exclusively allocated radio resources. The partitioning is chosen in the multi-cell radio network in such a way that co-channel interference appears at locations that are geometrically as far away as possible. Divisions with the same radio resources are arranged in a regular pattern across all cells. Multiple divisions of the same cell can be grouped into a partition, where the traffic-theoretical trunking gain increases compared to that of individual divisions. In the case with BS only, this model results in a fairly even distribution of SINR or spectrum efficiency over small area elements across the system. Compared to a non-partitioned cell, the spectrum efficiency with partitioning increases only slightly, but the standard deviation decreases significantly. Therefore, MSs can be served fairly equally regardless of their locations in the cell. For UL of relay enhanced cells it is shown in an exemplary way with a parameter set, that relays can distinctly increase the spectrum efficiency on UL.

Contents

Kurzfassung	iii
Abstract	vii
1 Introduction	1
1.1 Motivation	1
1.2 Objectives	1
1.3 Contribution of Thesis	2
1.4 Outline	3
2 3GPP LTE-A Standard	5
2.1 LTE Radio Frame	5
2.1.1 Downlink	6
2.1.2 Uplink	8
2.2 LTE Protocol Stack	10
2.2.1 AMC Scheme on PHY Layer	13
2.2.2 HARQ Protocol on MAC Layer	15
2.2.3 ARQ Protocol on RLC Layer	17
2.2.4 Protocol Overhead	19
2.3 LTE Relaying	21
2.3.1 Threshold Based Association	23
2.3.2 Backhaul Physical Channels	24
2.3.3 Backhaul HARQ	28
2.3.4 Relay versus Pico Cell	30
2.4 5G NR versus 4G LTE	31
3 ITU-R IMT-A Scenario	35

Contents

3.1	Scenario	35
3.2	Channel Model	36
3.2.1	LoS Probability	37
3.2.2	Path Loss	38
3.2.3	Shadow Fading	39
3.2.4	Antenna Pattern	39
3.3	Two-hop Channel Model	40
3.4	Performance Measures	40
3.4.1	Cell Spectral Efficiency	42
4	Related Work	43
4.1	Background	43
4.2	3GPP Self-Evaluation	44
4.2.1	Nokia Siemens Networks [NN10]	45
4.2.2	Alcatel-Lucent [AA09]	47
4.2.3	Intel (UK) [Int10]	48
4.2.4	Motorola [Mot09]	49
4.2.5	Qualcomm [Qua10]	50
4.2.6	Panasonic [Pan10]	51
4.2.7	NEC [NEC10]	51
4.2.8	NTT Docomo [NTT11]	52
4.2.9	LG Electronics [LG 10]	52
4.2.10	Huawei [Hua09]	53
4.2.11	ZTE [ZTE09]	53
4.2.12	China Mobile [CMC09b]	54
4.3	Summary	54
4.4	Validation Reference	55
4.4.1	Sambale	55
4.4.2	Saleh	56
4.5	Further Work	57
4.5.1	Minelli	58
5	Analytical Framework	61
5.1	Non-Relay System	61
5.2	Relay Enhanced System	63

6	SINR Calculation	65
6.1	Downlink	65
6.1.1	Relay Enhanced Cell	67
6.2	Uplink	69
6.3	Maximum Ratio Combining	75
7	Signal Flow Graph Models	77
7.1	Mathematic Fundamentals	77
7.2	SFG Models for LTE Performance Evaluation . .	82
7.3	SFG Model for AMC Scheme of PHY Layer . . .	83
7.3.1	Block Error Rate	87
7.3.2	Number of Physical Resource Block Pairs . .	88
7.4	SFG Model for HARQ Protocol of MAC Layer . .	90
7.5	SFG Model for ARQ Protocol of RLC Layer . . .	100
8	Throughput Capacity Calculation	103
8.1	Resource, Error and Efficiency	103
8.2	User Throughput	104
8.3	Cell Capacity	105
8.3.1	Relay Enhanced Cell	106
8.4	Cell Spectral Efficiency	107
9	Results for Downlink	109
9.1	Scenario and System Parameters	109
9.1.1	UMa Scenario Parameters	110
9.1.2	Relay Deployment Parameters	113
9.1.3	LTE System Parameters	121
9.2	Resource, Error and Efficiency	122
9.2.1	Protocol Layers	124
9.2.2	Maximum of Retransmissions	126
9.3	Throughput and Capacity	127
9.3.1	Map of User Throughput	128
9.3.2	CDF of Aggregate Throughput	132
9.3.3	Mean of Aggregate Throughput	134
9.4	Validation	136
9.4.1	Impact of Scheduling on Capacity	137

Contents

10 Resource Partitioning in Relay Enhanced Cells	139
10.1 Introduction	139
10.2 Results for Downlink of Relay Enhanced Systems	140
11 Uplink under Reuse Partitioning	145
11.1 Introduction	145
11.2 Reuse Partitioning	147
11.3 New Concept Reuse Partitioning	148
11.4 Results for Uplink under Reuse Partitioning . . .	152
11.5 Results for Uplink of Relay Enhanced Systems .	160
12 Conclusions	163
12.1 Conclusions	163
Bibliography	171
Acronyms	183
Curriculum Vitae	189

Introduction

Content

1.1 Motivation	1
1.2 Objectives	1
1.3 Contribution of Thesis	2
1.4 Outline	3

1.1 Motivation

In order to satisfy the International Telecommunication Union Radiocommunication Sector (ITU-R) International Mobile Telecommunications-Advanced (IMT-A) performance requirements, 3rd Generation Partnership Project (3GPP) Long Term Evolution-Advanced (LTE-A) needs a variety of features beyond Long Term Evolution (LTE) including the relaying technique, the enhanced Multiple Input Multiple Output (MIMO) support and the Coordinated Multiple Point (CoMP) operation. It has been shown, that the relaying technique can improve capacity in LTE-A systems and various parameters for the relay deployment have impact on the degree of capacity enhancement. However, it is still unknown to what degree the deployment of relays in LTE-A systems can meet or even exceed the IMT-A performance requirements.

1.2 Objectives

In this work, it will be explored under the basic conditions of the ITU-R IMT-A evaluation guidelines, to what degree

the relaying technique can enhance cell capacity of the 3GPP LTE-A system. The performance evaluation will be conducted through mathematical analysis. Analytical models, which represent various details of LTE standardized protocols to a high degree, will be developed to calculate cell capacity. Results of the mathematical analysis will be validated by results of a stochastic, event driven simulation, where scenario and system assumptions made in the analysis comply with those in the external simulation.

1.3 Contribution of Thesis

This work consists of following components, which are contribution of the thesis.

- As far as I know the methodology presented here is the first mathematical model able to calculate cell capacity of LTE systems with detailed modeling of Physical (PHY), Medium Access Control (MAC) and Radio Link Control (RLC) protocol layers in a multi-cell scenario with realistic inter-cell interference, where a macro cell is enhanced with multiple small cells, either relays with wireless backhaul or pico cells with wired backhaul;
- Local user throughput and cell capacity are analytically calculated with signal flow graph models for a given scenario with predefined parameters, taking LTE protocol specific characteristics, e.g. Adaptive Modulation and Coding (AMC) on PHY layer, Hybrid Automatic Repeat Request (HARQ) on MAC layer and Automatic Repeat Request (ARQ) on RLC layer, etc. into consideration in detail;
- Different infrastructures of mobile radio networks, e.g. deployments with versus without relay or pico cells etc., are compared among one another in terms of local user

throughput and cell capacity achieved, where LTE protocol specific features considered could even be neglected;

- Optimum radio resource partitioning among base station, relay nodes and backhaul links is found for the down-link deployment of relays, which maximizes cell capacity and minimizes variance of local user throughput, thereby achieving maximum possible user fairness;
- A novel reuse partitioning concept is proposed to mitigate uplink cochannel interference in cellular networks. Various ways for reuse partitioning are introduced, which aim at the improvement of throughput for users at cell edge and the achievement of homogeneous distribution over a whole cell area.

1.4 Outline

The thesis is structured as follows.

Chapter 2 gives an introduction to the 3GPP LTE-A mobile radio system to be evaluated. Chapter 3 introduces evaluation criteria, namely the ITU-R IMT-A scenario and its related channel model. Chapter 4 gathers a dozen of reports published by different companies such as Nokia Siemens Networks, Alcatel-Lucent, etc. during the 3GPP self-evaluation process, and lists their results on the gain in cell capacity for the deployment of relays.

Chapters 5 - 8 describe a methodology to mathematically analyze LTE systems with respect to cell capacity. Chapter 5 gives an overall description of the analytical framework. Chapter 6 specifies how to calculate a probabilistic distribution of Signal to Interference plus Noise Ratio (SINR)s based on probabilistic radio channel states. Chapter 7 explains how to apply signal flow graph methods to modeling LTE aspects such as AMC, HARQ and ARQ in detail, which is the core of the ana-

lytical methodology. Chapter 8 specifies how to calculate local user throughput and cell capacity for a relay enhanced LTE system.

Chapter 9 shows, among others, results of cell capacity for LTE systems enhanced with relays and pico cells, respectively, where parameters of scenario and system are configured in the first section and results of this work are validated by external results in the last section. Chapter 10 optimizes resource partitioning for downlink and shows results under different resource partitioning conditions. Chapter 11 proposes a novel reuse partitioning concept for uplink and shows results in various ways for reuse partitioning.

3GPP LTE-A Standard

Content

2.1	LTE Radio Frame	5
2.1.1	Downlink	6
2.1.2	Uplink	8
2.2	LTE Protocol Stack	10
2.2.1	AMC Scheme on PHY Layer	13
2.2.2	HARQ Protocol on MAC Layer	15
2.2.3	ARQ Protocol on RLC Layer	17
2.2.4	Protocol Overhead	19
2.3	LTE Relaying	21
2.3.1	Threshold Based Association	23
2.3.2	Backhaul Physical Channels	24
2.3.3	Backhaul HARQ	28
2.3.4	Relay versus Pico Cell	30
2.4	5G NR versus 4G LTE	31

2.1 LTE Radio Frame

The 3GPP LTE Release 10 has been accepted as an IMT-A system by ITU-R. Only from this release on LTE-A has come into standard; Previous releases are all called LTE. In this thesis, 3GPP LTE-A standard comes into consideration and then LTE is interchangeably written instead of LTE-A for the sake of simplicity.

A specification of LTE radio frame configuration is given in [3GP10d]. In the two-dimensional time-frequency domain radio resources are divided as follows. In the time domain, a

10 *ms* radio frame is divided into ten 1 *ms* subframes, each of which is further subdivided into two 0.5 *ms* slots. Each slot comprises seven Orthogonal Frequency Division Multiplexing (OFDM) symbols by applying normal cyclic prefix. In the frequency domain, the system bandwidth consists of a number of 180 *kHz* subchannels. Each subchannel is composed of twelve 15 *kHz* subcarriers.

A basic granularity of radio resource assigned for data transmission is a Physical Resource Block Pair (PRBP), which consists of a bandwidth of one subchannel for a duration of one subframe. A bandwidth of one subchannel for a duration of one slot is termed a Resource Block (RB). A smallest unit of radio resource is a Resource Element (RE), which consists of a bandwidth of one subcarrier for a duration of one OFDM symbol. An RB and a PRBP are then made up of 84 and 168 REs, respectively.

Only the frame structure applicable to Frequency Division Duplex (FDD) is considered in this work, where uplink and downlink transmissions are separated in frequency domain and operated in paired radio spectra.

2.1.1 Downlink

For downlink transmission an LTE radio frame [BM11] is configured as shown in Fig. 2.1.

In the middle, one radio frame consists of 10 subframes in the time dimension and the maximal bandwidth consists of 110 subchannels in the frequency dimension. The Physical Broadcast Channel (PBCH) shown in green is located in the 1st subframe and within a minimal bandwidth of 6 subchannels in the middle of the frequency band. The synchronization sequences shown in blue are located in the 1st and the 6th subframes and within the minimal bandwidth. Typically, up to 3 of the first OFDM symbols in each subframe are used for signaling by downlink control channels shown in yellow, which include the Physical Control Format Indicator Channel (PCFICH), the

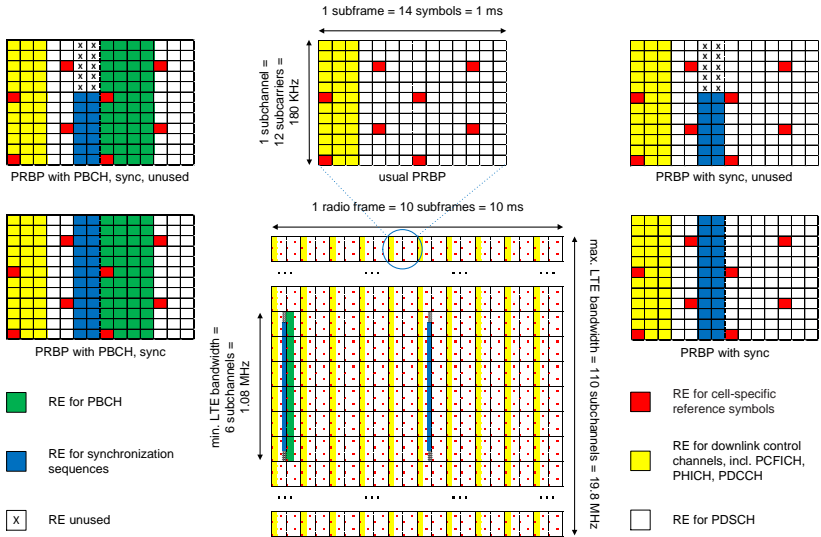


Figure 2.1: LTE radio frame for downlink transmission

Physical Hybrid-ARQ Indicator Channel (PHICH) and the Physical Downlink Control Channel (PDCCH). In case of one antenna port, 8 REs per PRBP are reserved by cell specific Reference Signal (RS)s (pilot) shown in red; In case of two and four antenna ports, 16 and 24 REs per PRBP are reserved by cell specific RSs, respectively. All the aforementioned REs shown in green, blue, yellow and red are regarded as overhead and only the remaining REs shown in white are available for Physical Downlink Shared Channel (PDSCH) to carry user data on downlink.

Besides, on top in the middle of Fig. 2.1, an example of PRBP comprises REs occupied by the downlink control channel in yellow and cell specific RSs in red; Such PRBPs carry least control signaling but most user data. On the right, both PRBPs comprise REs for synchronization sequences in blue in addition to yellow and red REs. On the left, both PRBPs comprise

REs for PBCH in green in addition to yellow, red and blue REs; Such PRBPs carry least user data but most control signaling, very different from the PRBP on top in the middle. On both left and right sides, some PRBPs comprise unused REs marked with "x".

2.1.2 Uplink

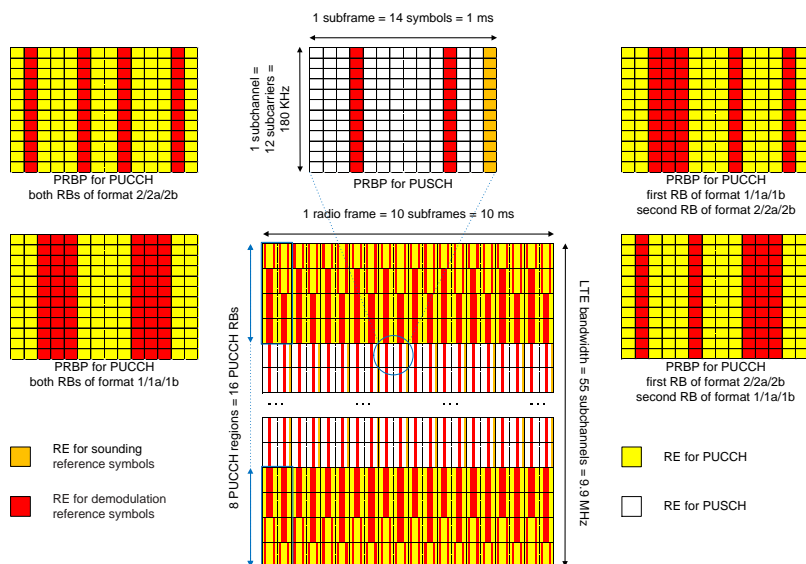


Figure 2.2: LTE radio frame for uplink transmission

For uplink transmission an LTE radio frame [LN09] is configured as shown in Fig. 2.2.

A Physical Uplink Control Channel (PUCCH) region is comprised of a single RB in the first slot of a subframe at or near one edge of system bandwidth, and another RB in the second slot of the subframe at or near the opposite edge of system bandwidth. Typical numbers of PUCCH regions are given in Table 2.1 for different LTE bandwidths. PUCCH RBs of format

2/2a/2b are mapped to band-edge RBs and followed by those of format 1/1a/1b. As illustrated in the middle of Fig. 2.2, 8 PUCCH (yellow) regions are available to a 10 MHz bandwidth in every subframe, namely 8 PUCCH RBs on upper band edge and another 8 on lower band edge. Among 8 PUCCH RBs at or near each edge, 3 at edge are of format 2/2a/2b and the other 5 near edge are of format 1/1a/1b.

Table 2.1: Typical numbers of PUCCH regions [LN09]

Bandwidth [MHz]	Number of PUCCH RBs	Number of PUCCH regions
1.4	2	1
3	4	2
5	8	4
10	16	8
20	32	16

The amount and positions of Demodulation Reference Signal (DM RS) associated with PUCCH depend on the type of uplink control information transmitted. 3GPP specifies the number of reference symbols per slot and indices of reference symbols in a slot for different PUCCH formats as shown in Table 2.2 and Table 2.3, respectively. As illustrated on the left in Fig. 2.2, the upper PRBP consists of two PUCCH RBs of format 2/2a/2b, each of which comprises two DM RS (red) symbols per slot, namely 2nd and 6th symbols. The lower PRBP is composed of two PUCCH RBs of format 1/1a/1b, each of which comprises three, namely 3rd, 4th and 5th DM RS symbols in a slot. On the right, the upper/lower PRBP is made up of one PUCCH RB of format 1/format 2 in the first slot and the other PUCCH RB of format 2/format 1 in the second slot.

Except PUCCH regions all the other PRBPs in a radio frame are used by Physical Uplink Shared Channel (PUSCH). A PRBP of PUSCH is illustrated on top in the middle of Fig. 2.2. A single DM RS (red) associated with PUSCH (white) occupies

Table 2.2: Number of DM RS symbols per slot for different PUCCH formats [3GP10d]

PUCCH format	Normal cyclic prefix	Extended cyclic prefix
1,1a,1b	3	2
2, 3	2	1
2a, 2b	2	N/A

Table 2.3: Indices of DM RS symbols in a slot for different PUCCH formats [3GP10d]

PUCCH format	Normal cyclic prefix	Extended cyclic prefix
1, 1a, 1b	2, 3, 4	2, 3
2, 3	1, 5	3
2a, 2b	1, 5	N/A

the center Single Channel Frequency Division Multiple Access (SC-FDMA) symbol in each slot, i.e. 4th and 11th symbols in every subframe. An Sounding Reference Signal (SRS) (orange) is always present on the last i.e. 14th SC-FDMA symbol in every subframe.

Control signaling is transmitted on PUCCH regions. User data is not permitted on SC-FDMA symbols designated for DM RS and SRS, but transmitted on PUSCH, only. In summary, all the colored REs in the figure are regarded as overhead.

2.2 LTE Protocol Stack

The basic protocol stack of the user plane of the 3GPP LTE system is shown in Fig. 2.3. The protocol stack of the control plane is not discussed here, since it is not related to the analysis of user throughput and cell capacity in this work.

From bottom to top, the LTE protocol stack comprises a PHY

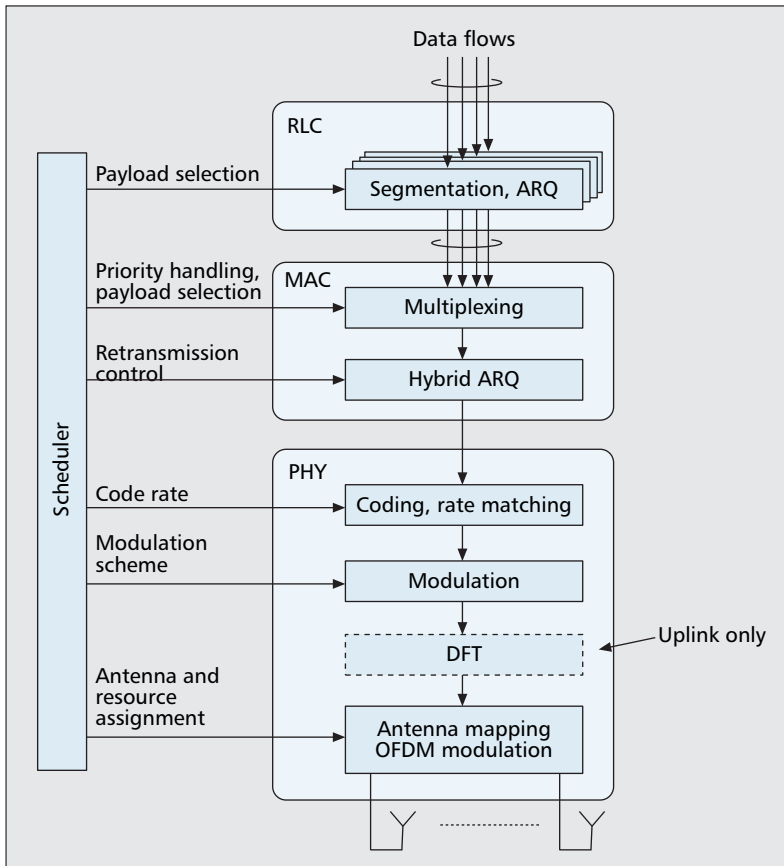


Figure 2.3: LTE user plane protocol stack (simplified) [ADF+09]

layer [3GP10c], a MAC layer and a RLC layer [3GP10g].

In PHY layer, data to be transmitted are first turbo coded for Forward Error Correction (FEC), and then modulated with a Quadrature Phase Shift Keying (QPSK), or 16-Quadrature Amplitude Modulation (QAM), or 64-QAM scheme, and finally modulated based on inverse Fast Fourier Transform (FFT) algorithms to result in OFDM signals. AMC is applied here to take SINR conditions of radio links into account: If link con-

dition is not good enough, a more robust low-rate Modulation and Coding Scheme (MCS) is used to reduce Block Error Rate (BLER) at a cost of more radio resource consumption; Otherwise, a less robust high-rate MCS is adopted.

Orthogonal Frequency Division Multiple Access (OFDMA) is used for LTE downlink radio transmission, where data are transmitted on a large number of parallel, narrow-band subcarriers. Since transmit power available at User Equipment (UE)¹ on uplink is expensive, SC-FDMA is adopted for LTE uplink, where data are transmitted on a single 15 kHz subcarrier. In addition, a Discrete Fourier Transform (DFT) precoder is employed prior to the OFDM modulator to preserve single carrier properties.

Data is transmitted on the PDSCH/PUSCH in units known as Transport Block (TB)s. During data transmission, errors may occasionally occur due to noise, interference and/or fading. To further protect the bit pipe against transmission errors, LTE applies a Cyclic Redundancy Check (CRC) that is attached to TBs by the PHY layer on the transmitting side. The PHY layer on the receiving side forwards only error-free TBs to its upper layer. If the PHY layer on the receiving side detects bit errors in a TB, the TB is repeated by the transmitter on request of the receiver making use of an ARQ protocol.

To handle uncorrectable transmission errors at the receiver, LTE employs a two-layered retransmission mechanism: A HARQ protocol located in the MAC sublayer is complemented by a Selective Repeat Automatic Repeat Request (SR-ARQ) protocol residing in the RLC sublayer. Both ARQ protocols retransmit erroneous data units up to a maximum of retransmission attempts to reduce residual error rate at the cost of extra radio resource consumption. In particular, the HARQ protocol employs multiple stop-and-wait ARQ processes instead of a single stop-and-wait scheme to allow continuous transmission.

¹UE in LTE-A is also referred to as User Terminal (UT) in IMT-A.

Most errors are captured and corrected by the fast and light-weight HARQ protocol with low latency and low feedback overhead, while only rarely residual errors are detected and resolved by the highly reliable but in terms of latency and overhead more expensive SR-ARQ protocol. With this two-layered retransmission design for LTE, upper layers are affected only rarely by erroneous packets.

Besides retransmission handling, the RLC and MAC layers are responsible for segmentation of a data flow and multiplexing of data flows, respectively.

2.2.1 AMC Scheme on PHY Layer

Transmission algorithms try to achieve high spectral efficiency under varying signal quality of radio links. This is commonly referred to as link adaptation and is based on AMC. For AMC the degrees of freedom are modulation order and code rate, which result in individual MCSs [3GP10e].

3GPP defines LTE MCS tables for PDSCH and PUSCH, respectively, see Table 2.4 and Table 2.5. Modulation order determines the number of data bits transmitted per modulated symbol. Code rate represents the ratio of user bits normalized by user bits plus redundant FEC bits of a data stream. An MCS selects a modulation order and a code rate, which product determines its reference efficiency. Code rate is not specified in Table 2.5 for PUSCH but can be calculated as the quotient of reference efficiency and modulation order.

Two individual MCS tables are proposed for PDSCH and PUSCH instead of a common one, thereby link performance is optimized for OFDMA on downlink and SC-FDMA on uplink, respectively. In both tables MCS index ranges from 0 to 28, modulation order takes an ascending value 2, 4 or 6, code rate increases with MCS index in each block of a same modulation order, and reference efficiency keeps an increment throughout the whole MCS indices. Worth mentioning is that the first MCS in the block of a higher modulation order equals the last MCS in

Table 2.4: LTE MCSs for PDSCH [Mot08]

MCS index	modulation order	code rate $[\frac{1}{1024}]$	reference efficiency
0	2	120	0.2344
1	2	157	0.3057
2	2	193	0.377
3	2	251	0.4893
4	2	308	0.6016
5	2	379	0.7393
6	2	449	0.877
7	2	526	1.0264
8	2	602	1.1758
9	2	679	1.3262
10	4	340	1.3262
11	4	378	1.4766
12	4	434	1.69535
13	4	490	1.9141
14	4	553	2.1602
15	4	616	2.4063
16	4	658	2.5684
17	6	438	2.5684
18	6	466	2.7305
19	6	517	3.0264
20	6	567	3.3223
21	6	616	3.6123
22	6	666	3.9023
23	6	719	4.21285
24	6	772	4.5234
25	6	822	4.8193
26	6	873	5.1152
27	6	910	5.33495
28	6	948	5.5547

Table 2.5: LTE MCSs for PUSCH [EPM08]

MCS index	modulation order	code rate $[\frac{1}{1024}]$	reference efficiency
0	2		0.20
1	2		0.25
2	2		0.31
3	2		0.41
4	2		0.50
5	2		0.62
6	2		0.73
7	2		0.86
8	2		0.98
9	2		1.11
10	2		1.23
11	4		1.23
12	4		1.41
13	4		1.60
14	4		1.80
15	4		2.01
16	4		2.14
17	4		2.28
18	4		2.52
19	4		2.77
20	4		3.01
21	6		3.01
22	6		3.25
23	6		3.51
24	6		3.77
25	6		4.02
26	6		4.26
27	6		4.45
28	6		4.63

the block of a previous lower modulation order with respect to reference efficiency. E.g., in Table 2.4 for PDSCH the first MCS of modulation order 4 (MCS index 10) equals the last MCS of modulation order 2 (MCS index 9) with respect to reference efficiency 1.33.

Comparing MCS table of PDSCH to that of PUSCH, a same modulation order does not cover an aligned range of MCS index. E.g., the modulation order 4 ranges from MCS index 10 to 16 for PDSCH, while from MCS index 11 to 20 for PUSCH. Further, code rates adopted by PDSCH are basically different from those adopted by PUSCH. Consequently, reference efficiencies available for PDSCH are other than those for PUSCH.

AMC chooses proper MCSs taking current radio link conditions at the respective receiver into account. A lower order MCS is more robust against transmission errors, since it has more tolerance to interference and noise. Therefore, it can be used in a poor link condition, but provides a lower bit rate. A higher order MCS is more prone to transmission errors, since it has more sensitivity to interference and noise. Hence, it offers a higher bit rate, but can be useful only when SINR is sufficiently high.

2.2.2 HARQ Protocol on MAC Layer

For the HARQ protocol on MAC sublayer [3GP10h] various signaling errors and their effects on LTE system performance are described in [TLW09]. Since the protocol is modeled, completely, in this work, it is described in the following.

In downlink, a TB is transmitted on the PDSCH, and each transmission is announced to a respective UE by a downlink assignment on the PDCCH. When the UE correctly receives the downlink assignment, it will try to decode the TB on PDSCH. When the UE decodes the TB correctly, it sends an Acknowledgement (ACK) on the PUCCH to report success. When the UE fails to decode the TB, it sends a Negative Acknowledgement (NAK) to report failure. If the UE misses the

Table 2.6: HARQ protocol

forward channel	reverse channel	retransmission	result
TB reception correct	ACK → ACK	✗	✓
	ACK → NAK	✓	✓
	ACK → DTX	✓	✓
TB reception erroneous	NAK → NAK	✓	dependent
	NAK → ACK	✗	✗
	NAK → DTX	✓	dependent
resource assignment failed	DTX → DTX	✓	dependent
	DTX → ACK	✗	✗
	DTX → NAK	✓	dependent

downlink assignment, it does not send any feedback.

The signal of an HARQ feedback sent on PUCCH is detected by a responsible Enhanced Node-B (eNB)² through two thresholds, so that ACK, NAK and Discontinuous Transmission (DTX) (silence) can be distinguished. If the eNB detects an ACK, it will not start an HARQ retransmission. If the eNB detects a NAK, it will retransmit the corrupted TB. In case soft combining supports Incremental Redundancy (IR), eNB will retransmit another Redundancy Version (RV) of the TB than transmitted in a previous transmission. If the eNB detects a DTX, it will retransmit the missed TB. In case of IR, eNB will retransmit a same RV as before.

Owing to transmission errors, however, an HARQ feedback may be misinterpreted by the eNB as summarized in Table 2.6.

If the eNB erroneously detects a DTX or NAK as an ACK, no HARQ retransmission will be performed. This misdetection results in a packet loss on MAC layer, which is recovered by SR-ARQ retransmission on RLC layer, in case RLC Acknowledged Mode (AM) is used.

²eNB in LTE-A is also referred to as Base Station (BS) in IMT-A.

If the eNB detects a NAK instead of a DTX, it will retransmit the data using another RV instead of a same RV used before. Vice versa, if the eNB detects a DTX instead of a NAK, it will retransmit the data using a same RV used before instead of another RV. Both misdetections result in reduced efficiency to decode the retransmission, since the IR gain is lost by applying a wrong RV.

If the eNB misdetects an ACK as a NAK or DTX, it will retransmit the data. The UE will recognize the data as a repetition, and retransmit an ACK. This also causes an extra retransmission and additional overhead.

The aforementioned signaling errors are taken into account to investigate the HARQ process. Whether a TB needs to be retransmitted does not depend on what HARQ feedback is sent out by the UE, but is dependent on what HARQ feedback is interpreted by the eNB, see Table 2.6.

When the resource is successfully assigned and the TB is correctly received on PHY layer, the transmission on MAC layer succeeds regardless of retransmission on PHY layer, see Table 2.6 first three rows. Both in case of successful resource assignment and erroneous reception of TB on PHY layer, and in case of resource assignment failure, the transmission on MAC layer fails, if no retransmission of TB is carried out on PHY layer, see fifth and eighth rows. In both cases, whether the transmission on MAC layer succeeds or fails, depends on whether the retransmission of TB is correct or erroneous on PHY layer, see the other rows.

2.2.3 ARQ Protocol on RLC Layer

The ARQ protocol on RLC sublayer in AM [3GP10i] realizes a generalized SR-ARQ process [ZRM97]. Since the protocol is modeled in detail in this work, it is described here, accordingly.

Referring to the generalized SR-ARQ process, a transmitter sends data blocks and a receiver acknowledges receptions by means of feedback messages. Each feedback message contains

Table 2.7: Generalized SR-ARQ protocol

data block	feedback message	upcoming feedback	retransmission	result
received	received	n/a	✗	✓
	lost	in time	✗	✓
		timeout	✓	✓
lost	received	n/a	✓	dependent
	lost	in time	✓	dependent
		timeout	✓	dependent

ACKs and NAKs about all past data blocks. A NAK indicates loss of a corresponding data block and triggers a retransmission of the data block. Upon reception of such a feedback message, all erroneous data blocks are scheduled for retransmission.

In the presence of feedback losses, the generalized SR-ARQ process waits for further feedback information, rather than retransmitting, immediately. For this purpose a timeout counter is assigned to each data block, and activated when the data block is transmitted. When the timeout expires, the absence of feedback is equivalent to a NAK and the data block is scheduled for retransmission.

Regarding the LTE ARQ protocol, the receiving side of RLC AM entity sends a STATUS report to the transmitting side of its peer RLC AM entity. A STATUS report comprises *NAK_SN* sequence numbers (SNs), one for every data block, which has not been correctly received and is stated as outstanding, and *ACK_SN* an SN of the data block, which is next to be received and is not stated as missing. Thereby the STATUS report indicates NAKs for the data blocks with $SN = NAK_SN$ and ACKs for the others with $SN < ACK_SN$ and $SN \neq NAK_SN$. Upon reception of a NAK corresponding to a data block, the transmitting side triggers a retransmission of the data block. Obviously, a STATUS report complies with a

feedback message specified in the generalized SR-ARQ process.

When the receiving side of an RLC AM entity detects reception failure of an data block, namely a gap in the sequence of received data blocks based on the RLC SNs, it starts a timer $t_{Reordering}$, assuming that the missing data block is still being retransmitted by the HARQ protocol on MAC sublayer below. If the receiving side can receive the missing data block in time, it stops and resets the reordering timer; Otherwise, it lets the timer be running until expiry. When the reordering timer expires, the receiving side triggers a STATUS report and indicates a NAK for the missing data block, to inform the transmitting side to retransmit this data block. Clearly, a timer $t_{Reordering}$ corresponds to a timeout counter described in the generalized SR-ARQ process.

The generalized SR-ARQ process is taken into account to investigate the LTE ARQ protocol. Whether a data block needs to be retransmitted depends on three following factors and all possible cases are summarized in Table 2.7.

1. Whether the data block is received or lost on forward channel,
2. Whether its feedback message is received or lost on reversal channel, and
3. Whether any upcoming feedback message is received in time or out of time.

2.2.4 Protocol Overhead

Fig. 2.4 depicts the data flow of an Internet Protocol (IP) packet from the IP layer, through the data link layer down to the PHY layer. The data link layer comprises three sublayers and they are from above to below respectively the Packet Data Convergence Protocol (PDCP) sublayer, the RLC sublayer and the MAC sublayer.

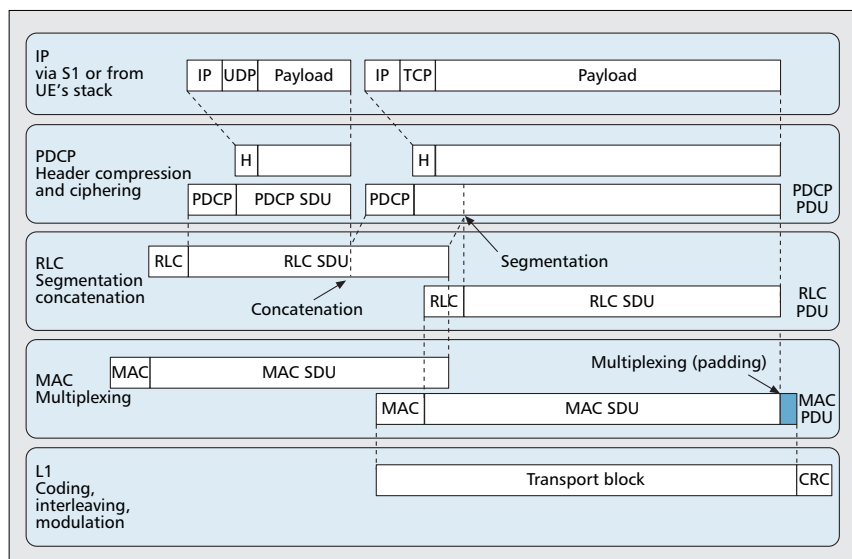


Figure 2.4: Data flow through LTE protocol stack [LLM⁺09]

The figure shows, how each protocol layer processes the Protocol Data Unit (PDU) of its upper layer to form its own Service Data Unit (SDU) and then adds its protocol header to the SDU to constitute its layer specific PDU. E.g., a PHY SDU (TB) corresponds to a MAC PDU and a PHY PDU is composed of a TB and a CRC.

An IP header has a size of 20 bytes for IPv4 and 40 bytes for IPv6, respectively. A Transmission Control Protocol (TCP) header has 20 bytes. In general payload can have variable sizes; for TCP services packet sizes are typically 1500 bytes. A PDCP header, an RLC header, a MAC header and a PHY CRC are 1 byte, 4 bytes, 3 bytes and 3 bytes, respectively.

The PDCP sublayer is mainly responsible for IP header compression and ciphering. An IP header together with a TCP header are compressed to 8 bytes for both IPv4 and IPv6 cases. Payload remains unaffected.

The RLC sublayer mainly comprises ARQ functionality and

supports data segmentation and concatenation. The latter two are illustrated in the figure with an example: A second PDCP PDU is segmented into two parts. Its first part is concatenated to a first PDCP PDU to constitute a first RLC SDU. Its second part alone constitutes a second RLC SDU.

The MAC sublayer mainly has HARQ functionality and provides data multiplexing. The data multiplexing is performed in case multiple data flows are taken into account; this is not illustrated in the figure, which only shows a single data flow.

2.3 LTE Relaying

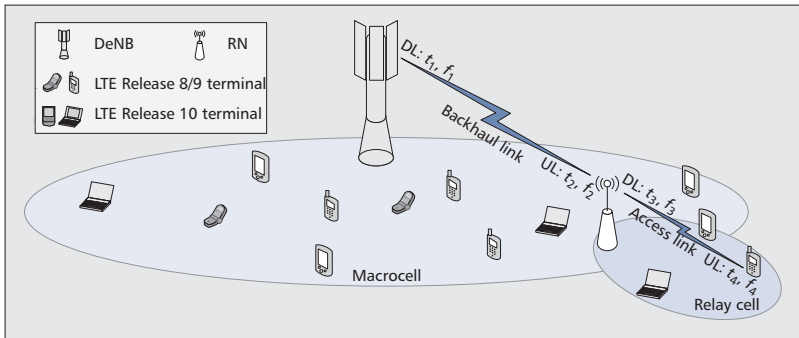


Figure 2.5: Relay deployment example [HCM⁺12]

Relaying is one of the salient features for 3GPP LTE-A. 3GPP LTE Release 10 is the first revision in LTE standard series to support relaying [3GP10g].

In Fig. 2.5, both LTE Release 8/9 terminals and LTE Release 10 terminals denote UEs. As illustrated in the figure, by deploying an Relay Node (RN), a radio link between the eNB and a UE is divided into two hops. The radio link between the eNB and the RN is referred to as a backhaul link, while the radio link between the RN and the UE is referred to as an access link. If instead of the two hops there exists a radio link between the eNB

and the UE, it is referred to as a direct link. The source eNB, from which the RN receives its signal, is also called a Donor Enhanced Node-B (DeNB). The coverage areas of the RN and the eNB are referred to as a relay cell and a donor cell, respectively.

The RN has a dual personality: On one hand, it appears as a UE from the eNB point of view; On the other hand, it behaves like an eNB from the perspective of the UE under its control. The RN relies on the backhaul link to receive/transmit data from/to the eNB and leans on the access link to transmit/receive data to/from the UE in downlink/uplink case.

With the help of the RN, both the backhaul link and the access link may have better radio propagation conditions than the direct link. In particular, if the backhaul link is operated at a significantly high SINR, which, e.g., results from Line-of-Sight (LoS) between the serving eNB and the RN and Non-Line-of-Sight (NLoS) between interfering eNBs and the RN, relaying technique offers good potential to capacity improvement besides coverage extension and shadowing reduction at relatively low cost.

The spectral efficiency of a two-hop link is greater than that of a one-hop link [CW14], if

- the total amount of radio resources needed on both the backhaul link and the access link for the two-hop transmission is less than the radio resources required on the direct link for the one-hop transmission, and
- the remaining packet error rate left over from the two-hop transmission is less than the residual error rate left from the one-hop transmission.

If a wired instead of a wireless backhaul is used, an RN degenerates to a pico eNB. As illustrated in Fig. 2.6, by deploying a pico eNB, the coverage areas of the pico eNB and the macro eNB are referred to as a pico cell and a donor cell, respectively. The access link between the pico eNB and a pico UE may have

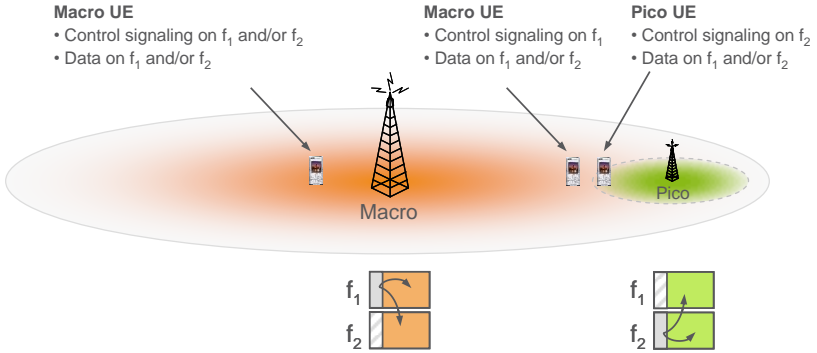


Figure 2.6: One example of heterogeneous deployments [3GP10b]

better radio propagation condition than the direct link between the macro eNB and the pico UE.

2.3.1 Threshold Based Association

Threshold based association [CW14] is adopted for a more flexible control of association of UEs to Radio Access Point (RAP)s. Under the SINR threshold based association strategy, a UE associates with the eNB, if the difference between the SINR it perceives from the eNB and the SINR it perceives from the RN is greater than a given SINR threshold, otherwise it is served by the RN.

Setting the threshold to 0 dB, a UE associates with its RAP exactly the same way as under the best SINR association strategy, namely a UE is served by the eNB, if it receives higher SINR from the eNB than from the RN, and otherwise it is served by the RN.

Increasing the threshold to some positive value, the UE requires higher SINR from the eNB than from the RN to associate with the eNB. Further increasing the threshold to $+\infty$ dB, the UE never associates with the eNB. Decreasing the threshold to some negative value, the UE needs higher SINR from the RN

than from the BS to be served by the RN. Further decreasing the threshold to $-\infty$ dB, the UE is never served by the RN.

2.3.2 Backhaul Physical Channels

In case of inband relaying, backhaul link and access links operate in the same frequency band. Thus, a mechanism is necessary for a half duplex operating relay to separate activity on access links and backhaul link in time domain, namely the relay is neither transmitting/receiving on access links nor receiving/transmitting on backhaul link at the same time.

In general, in order to support inband relaying in LTE-A system, the relay requires some transmission/reception gaps on access links to be able to communicate with its DeNB to receive/transmit on backhaul link.

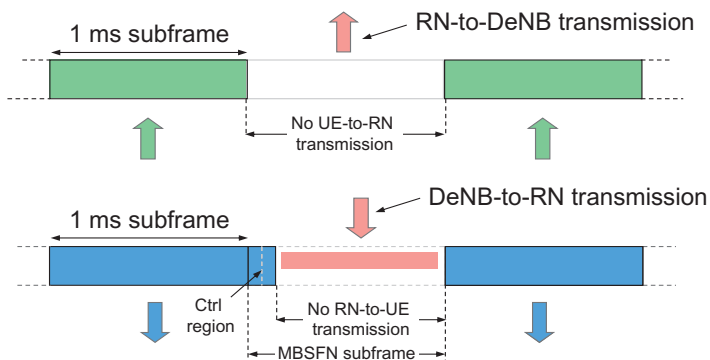


Figure 2.7: Multiplexing between access and backhaul links [DPS11]

In uplink, as illustrated at the top of Fig. 2.7, a relay may schedule that it need not receive data on access links in a certain subframe and may then use this subframe to transmit on backhaul uplink. The uplink radio frame shown in Fig. 2.2 is also valid for relay deployment without modification.

In downlink, as illustrated at the bottom of Fig. 2.7, Multicast

Broadcast Single Frequency Network (MBSFN) subframes are used for time division multiplexing between backhaul and access links for relaying. The downlink radio frame in Fig. 2.1 is adapted for relaying solution.

MBSFN subframes were already introduced in 3GPP LTE Release 8. In an MBSFN subframe as specified in Release 8 UEs expect control signals and reference signals in the first one or two OFDM symbols and ignore the rest of the subframe. In Release 10 (LTE-A) MBSFN subframes in addition are used to transmit relay data.

RNs declare MBSFN subframes in a downlink radio frame. MBSFN subframes can be declared only for 6 out of 10 subframes in each 10 ms radio frame, namely the 2nd, 3rd, 4th, 7th, 8th and 9th subframes. However, the 1st, 5th, 6th and 10th subframes cannot be designated as MBSFN subframes due to the presence of synchronization and broadcast signaling channels.

The configuration of a relay downlink backhaul subframe is illustrated in Fig. 2.8. An RN uses the first few OFDM symbols of an MBSFN subframe for transmitting cell specific reference signals and control signaling on access links to its UEs. The RN can then use the remainder of such an MBSFN subframe for receiving backhaul downlink transmission from its DeNB.

Some subchannels of an MBSFN subframe are used by Relay Physical Downlink Control Channel (R-PDCCH) for control signaling on backhaul links from DeNB to its RNs; The other subchannels of the same MBSFN subframe are used by PDSCH for data transmission, not only intended for backhaul links but also available for direct links from eNB to its own UEs.

R-PDCCH uses the first slot for backhaul downlink assignments and the second slot for backhaul uplink grants. If the first slot but not the second slot is occupied by R-PDCCH, the second slot can be utilized by PDSCH for data transmission of backhaul downlink. However, if not the first slot but the second slot is occupied by R-PDCCH, the first slot can not be utilized by PDSCH and must be left unused.

A subset of OFDM symbols in an MBSFN subframe is avail-

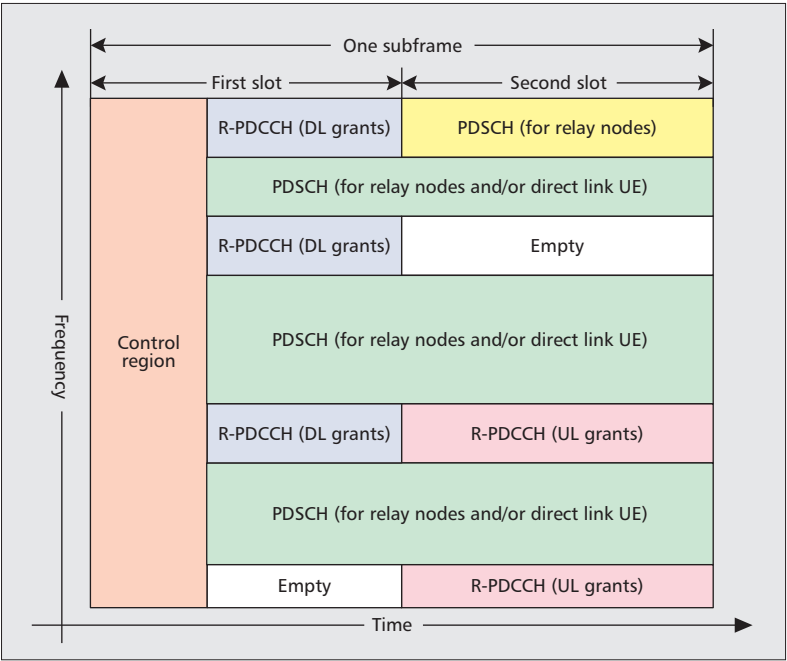


Figure 2.8: Relay DL backhaul design [HCM⁺12]

Table 2.8: OFDM symbols usable for DeNB-to-RN transmission in the first slot [3GP10f]

Configuration	Start symbol index	End symbol index	Useful symbols
0	1	6	6
1	2	6	5
2	3	6	4

able for backhaul downlink transmission. 3GPP specifies the OFDM symbols to be used of the first and second slot in Table 2.8 and Table 2.9, respectively. R-PDCCH and PDSCH are mapped to REs in such OFDM symbols.

Fig. 2.9 shows exemplarily an LTE radio frame for down-

Table 2.9: OFDM symbols usable for DeNB-to-RN transmission in the second slot [3GP10f]

Configuration	Start symbol index	End symbol index	Useful symbols
0	0	6	7
1	0	5	6

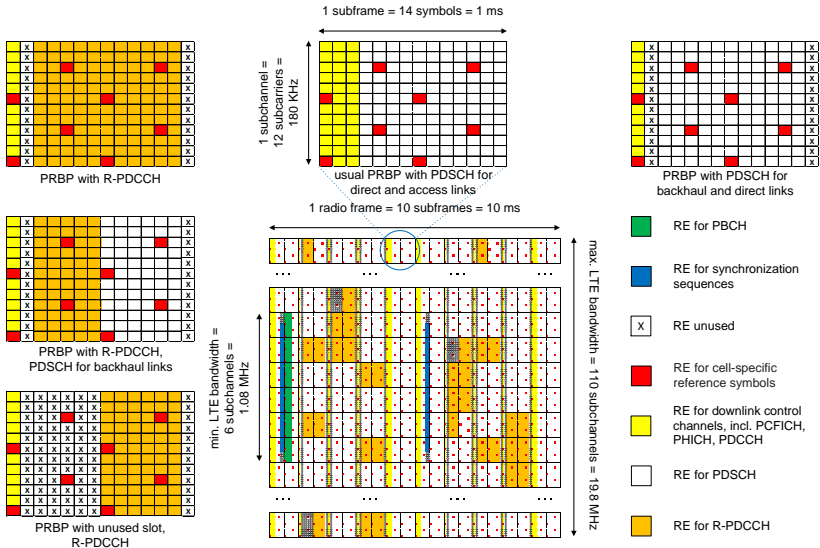


Figure 2.9: LTE radio frame for downlink transmission in relay enhanced system

link transmission in a relay enhanced system. The 2^{nd} , 3^{rd} , 4^{th} , 7^{th} , 8^{th} and 9^{th} subframes are configured to be MBSFN subframes. Only the 1^{st} OFDM symbol of an MBSFN subframe is configured for RN-to-UE transmission. The 2^{nd} and the 14^{th} OFDM symbols of an MBSFN subframe are not usable and OFDM symbols therebetween are then configured for DeNB-to-RN transmission.

Some PRBPs in an MBSFN subframe are available for R-PDCCH. E.g., in the 2nd subframe, the 2nd and the 5th of the 6 PRBPs in the middle frequency band afford both the first and the second slot to R-PDCCH; The PRBP at the very top gives the first slot to R-PDCCH but leaves the second slot to PDSCH; The PRBP at the very bottom gives the second slot to R-PDCCH but leaves the first slot unused. Such PRBPs for R-PDCCH can be configured and distributed arbitrarily in an MBSFN subframe in terms of type, quantity, order and pattern.

The other PRBPs in an MBSFN subframe are available for PDSCH, e.g. all the PRBPs in the 7th subframe except the 2nd, 3rd, 4th, 5th of the 6 PRBPs in the middle frequency band. Some of them are utilized for data transmission over backhaul links from DeNB to its RNs. The others are merely used for direct links from eNB to its own UEs, but not for access links between RNs and their own UEs.

All PRBPs in non-MBSFN subframes are available for PDSCHs, e.g. all the PRBPs in the 1st subframe. They are shared by eNB and RNs to serve their UEs over direct links and access links, respectively.

On downlink the inband backhaul link is supported with the MBSFN method: During MBSFN subframes (backhaul subframes) an eNB may transmit backhaul traffic to its RNs and access traffic to its macro UEs; During non-MBSFN subframes (access subframes) the eNB and the RNs may transmit access traffic to its macro UEs and their relay UEs, respectively. MBSFN subframes are (semi-)statical and have the same format for all the cells.

2.3.3 Backhaul HARQ

For LTE-A with relaying, HARQ protocol is not only operated on access links but also on backhaul links. In order to ensure backward compatibility with LTE Release 8, no changes are made to the access link HARQ operation, but only slight modifications to the backhaul HARQ operation.

In downlink, the access link HARQ is operated in an asynchronous manner, namely each downlink resource assignment on PDCCH explicitly indicates the HARQ process number of data transmission. The same design is applied to the backhaul downlink HARQ, where downlink resource assignment is signaled on R-PDCCH.

In uplink, the access link HARQ is operated as a synchronous protocol with a periodicity of 8 ms , namely an uplink subframe follows 4 ms after a downlink subframe to implicitly identify the HARQ process. The backhaul uplink HARQ retains the synchronous aspect.

For access links, the PDCCH can still be available in every subframe, even in MBSFN subframes. For backhaul links, however, the R-PDCCH can be located in MBSFN subframes, only. Thus, the backhaul HARQ is slightly different from the access link HARQ, which is briefly summarized according to [HLG⁺11] and [DPS11]:

1. In order to match the HARQ Round Trip Time (RTT) on access link, a subframe configured for uplink backhaul always follows 4 ms after a subframe for downlink backhaul;
2. As the possible configuration of MBSFN subframes has a 10 ms structure while the HARQ timing follows an 8 ms periodicity, backhaul downlink subframes are configured with a basic pattern of 8 subframes, however, exclude those that cannot be declared as MBSFN subframes, even if it were necessary to do so to follow the 8 ms periodicity;
3. Since an uplink data transmission on PUSCH needs to be assigned by an uplink resource grant 4 ms earlier on R-PDCCH, if a subframe cannot be used for backhaul downlink transmission, then the subframe 4 ms later cannot be used for backhaul uplink transmission, either;
4. Some subsequent backhaul uplink subframes may be

spaced 16 *ms* apart due to the MBSFN subframe restriction, and others are 8 *ms* apart, as usual.

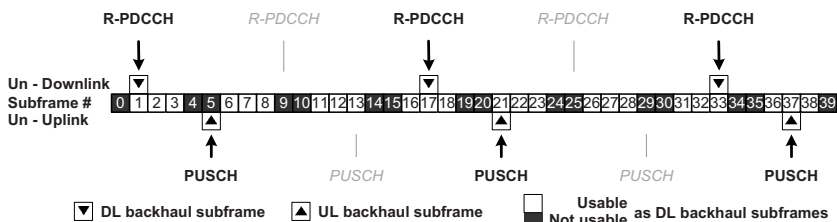


Figure 2.10: Uplink backhaul HARQ timing with 8 ms periodicity (FDD) [HLG+11]

As illustrated exemplarily in Fig. 2.10, data cannot be transmitted on backhaul uplink in the subframes marked 13 and 29, since their resource grant cannot be correspondingly assigned on backhaul downlink 4 *ms* earlier in the subframes marked 9 and 25.

In summary, the HARQ operation spends an RTT of 8 *ms* on access links, while on backhaul links the RTT is 8 *ms* at least. In this work, not the latency but the throughput is analyzed and, hence, the same analytical model can be applied to both the access link HARQ and the backhaul HARQ operation.

Obviously, the ARQ operation on RLC layer, which is operated on top of the HARQ operation on MAC layer, is all the same for both access links and backhaul links.

2.3.4 Relay versus Pico Cell

It is stated in [3GP10b], that "at least Type 1 and Type 1a relay nodes are part of LTE-Advanced." Both types of RNs have common characteristics as follows:

- An RN is in control of one or several cells of its own, each of which appears to UEs as a separate cell distinct from a donor cell and has a unique physical layer cell identity;

- An RN transmits all its own physical channels, e.g. synchronization channels, reference symbols, etc.;
- UEs in cells controlled by an RN receive PDCCH directly from the RN and send PUCCH directly to the RN;
- An RN is non-transparent to UEs, i.e., every UE is aware of whether or not it is communicating with the mobile radio network via the RN;
- An RN appears as a regular eNB to all its UEs, i.e., from a UE perspective there is no difference in accessing cells controlled by an RN and cells controlled by a eNB;
- Cells controlled by an RN also support LTE Release 8 UEs, while to LTE-A UEs, the RN appears more than an LTE Release 8 eNB to allow further performance enhancement.

Both Type 1 and Type 1a RNs have all the same set of features as mentioned above, except that Type 1 RNs operate inband while Type 1a RNs outband. An RN is said to be inband if its backhaul link shares the same frequency band with its access links; while outband, if its backhaul link does not operate in the same frequency band as its access links. Another view on an outband RN is a pico eNB.

In this work, system capacity is compared between small cells enhanced LTE networks either based on inband RNs or pico eNBs, which also enables a comparison between Type 1 and Type 1a RNs.

2.4 5G NR versus 4G LTE

3GPP 5th Generation (5G) New Radio (NR) Release 15 has been accepted by ITU-R for International Mobile Telecommunications-2020 (IMT-2020).

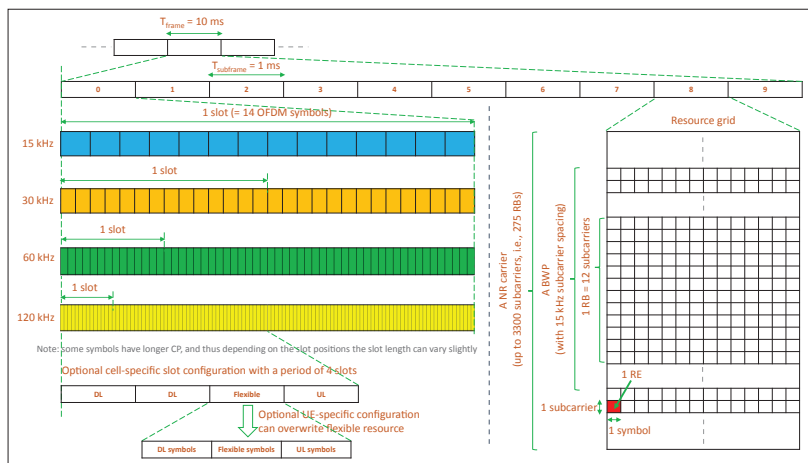


Figure 2.11: Illustration of 5G NR transmission structure and basic terminologies [LLB⁺19]

Fig. 2.11 depicts how radio resources of a NR radio frame [3GP19] are partitioned in time and frequency domains. NR adopts OFDM with a cyclic prefix for both downlink and uplink transmissions. An RB consists of 12 consecutive subcarriers in the frequency domain. A frame has a duration of 10 ms and consists of 10 subframes of 1 ms. Each subframe consists of 2^μ slots with 14 OFDM symbols each. An RE occupies one subcarrier in frequency and one OFDM symbol in time. This is the same as in LTE when $\mu = 0$.

Scalable numerologies are key to support NR deployment in a wide range of spectrum. NR adopts flexible subcarrier spacing of $2^\mu \cdot 15$ kHz for $\mu = 0, 1, \dots, 4$ scaled up from the basic 15 kHz subcarrier spacing in LTE. Accordingly, cyclic prefix and also OFDM symbol are scaled down by a factor of $2^{-\mu}$ from LTE cyclic prefix length of 4.7 microseconds and OFDM symbol length of 1/14 ms, respectively. This allows configuration of a NR radio frame identical to LTE frame structure by setting μ to zero.

A single NR carrier in Release 15 is limited to 3300 active subcarriers. At lower sub-6 GHz frequencies, subcarrier spacings of 15 kHz and 30 kHz are suitable and the maximum carrier bandwidth is 100 MHz. At higher millimeter-wave frequencies, NR supports 60 kHz and 120 kHz for data channels and the maximum bandwidth is 400 MHz. Both are much greater than the maximum LTE carrier bandwidth of 20 MHz.

In summary, NR radio frame structure is similar to LTE-A. Therefore, our analysis method developed in this work is also applicable to evaluation of 5G cellular systems.

ITU-R IMT-A Scenario

Content

3.1 Scenario	35
3.2 Channel Model	36
3.2.1 LoS Probability	37
3.2.2 Path Loss	38
3.2.3 Shadow Fading	39
3.2.4 Antenna Pattern	39
3.3 Two-hop Channel Model	40
3.4 Performance Measures	40
3.4.1 Cell Spectral Efficiency	42

3.1 Scenario

Both, IMT-A and LTE-A systems specified by ITU-R and 3GPP, respectively introduced a number of scenarios and related channel models for purpose of analyzing system performance. Urban Macro-cell (UMa) scenario introduced by ITU-R standard M.2135 [IR08b] that is also known as Case 1 scenario introduced by 3GPP standard TR36.814 [3GP10b] is the basis scenario for the investigation in this thesis.

In Fig. 3.1 (right), numbers identify 57 sector cells of this scenario and "ISD" labels an inter-site distance exemplarily. As shown in the figure, BSs are placed in a regular grid following a basic hexagon layout, performance of the central BS site is evaluated, where interference to the central BS site is modeled by a first tier of six and a second tier of twelve BS sites around it.

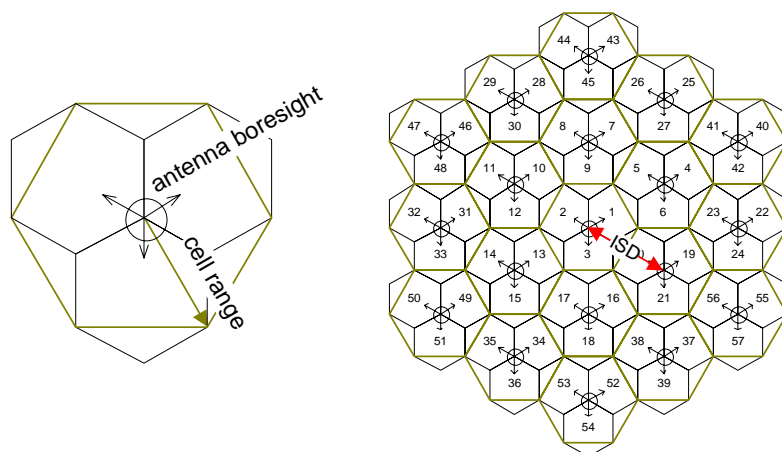


Figure 3.1: Cellular coverage layout of UMa scenario [IR08b]

In general, Inter-site distance (ISD) is the distance between an BS and its closest neighbor BS; It is the same for all BS sites. The UMa scenario has an ISD of 0.5 km to represent a small cell deployment and an interference limited environment.

Fig. 3.1 (left) shows details of a BS site employing three sector antennas. The antenna beam orientations in the macro-cell layout are 30° , 150° and 270° , respectively, with a sector angle of 120° . Each sector itself establishes a cell so that a BS sets up a three-sector site. The scenario has 19 sites, each made-up of 3 cells. UTs are assumed distributed uniformly over the whole scenario.

Both channel models related to ITU-R UMa and 3GPP Case 1 scenarios, respectively, are introduced in the following section.

3.2 Channel Model

From a mathematic point of view, the channel model of ITU-R UMa scenario [IR08b] has a more general form than that of 3GPP Case 1 scenario [3GP10b], where the ITU-R model not

only covers all parameters considered by the 3GPP model, but also introduces some extra parameters in addition. Besides, the two channel models may set different values to a parameter that both have in common, or assign different values to a common constant term, or to the coefficient of a common variable item.

These differences are presented by a comparison of the two channel models in following subsections.

The ITU-R channel model is chosen in this thesis as the basis to calculate the cell capacity of LTE-A systems, taking following perspectives into consideration.

- A model to calculate LTE-A capacity shall be built, among others, on basis of a more general channel model such as the ITU-R channel model, which may provide more insights compared to the 3GPP channel model.
- According to 3GPP's spec [3GP10b], "Table A.2.1.1.2-3 (3GPP channel model) presents the baseline parameters for initial evaluations in heterogeneous networks. More detailed modeling of new nodes propagation and channel model based on IMT.EVAL (ITU-R channel model) should be considered for performance evaluation at a later stage." I.e., 3GPP has chosen not only its own channel model but also the ITU-R channel model as the basis for LTE-A performance evaluation.
- Other researchers have chosen the ITU-R channel model instead of the 3GPP channel model to evaluate LTE-A performance, e.g. Sambale's work [Sam13] and Saleh's work [SmBR⁺11], which results are used to validate our own results in this thesis.

3.2.1 LoS Probability

Both channel models take LoS and NLoS radio propagation conditions into account, where probability of LoS p_{LoS} is

defined as a function of distance d in m .

$$p_{LoS}(d) = \min(18/d, 1) \cdot (1 - \exp(-d/63)) + \exp(-d/63) \quad (3.1)$$

$$p_{NLoS}(d) = 1 - p_{LoS}(d) \quad (3.2)$$

3.2.2 Path Loss

Both channel models specify path loss \bar{L}_{LoS} and \bar{L}_{NLoS} for LoS and NLoS radio propagation conditions, respectively.

In the 3GPP model path loss is a function alone of distance D in km , Eq. (3.3) for LoS and Eq. (3.4) for NLoS, assuming a carrier frequency of $2GHz$ and antenna heights of $32m$ at BS and $1.5m$ at UT.

$$\bar{L}_{LoS}(D) = 103.4 + 24.2 \log_{10}(D) \quad (3.3)$$

$$\bar{L}_{NLoS}(D) = 131.1 + 42.8 \log_{10}(D) \quad (3.4)$$

In the ITU-R model path loss is a function, among others, of distance d in m , center frequency f_c in GHz , antenna heights h_{BS} of BS and h_{UT} of UT in m , Eq. (3.5) for LoS and Eq. (3.6) for NLoS. In addition to the variable distance, the ITU-R model can be applied to a frequency range of $2GHz < f_c < 6GHz$, and various antenna heights of $10m < h_{BS} < 150m$ and $1m < h_{UT} < 10m$.

$$\bar{L}_{LoS}(d) = \begin{cases} 22.0 \log_{10}(d) + 28.0 + 20 \log_{10}(f_c), & 10m < d < d'_{BP} \\ 40.0 \log_{10}(d) + 7.8 - 18.0 \log_{10}(h'_{BS}) - 18.0 \log_{10}(h'_{UT}) + 2.0 \log_{10}(f_c), & d'_{BP} < d < 5000m \end{cases} \quad (3.5)$$

$$\begin{aligned} \bar{L}_{NLoS}(d) = & 161.04 - 7.1 \log_{10}(W) + 7.5 \log_{10}(h) \\ & - \left(24.37 - 3.7 \left(\frac{h}{h_{BS}} \right)^2 \right) \log_{10}(h_{BS}) \\ & + (43.42 - 3.1 \log_{10}(h_{BS})) (\log_{10}(d) - 3) \\ & + 20 \log_{10}(f_c) - 3.2 (\log_{10}(11.75 h_{UT}))^2 - 4.97 \\ & 10m < d < 5000m \end{aligned} \quad (3.6)$$

Break point distance of the piecewise function Eq. (3.5) is computed as $d'_{BP} = 4 \cdot h'_{BS} \cdot h'_{UT} \cdot f_c / c$, where f_c is the center frequency and $c = 3.0 \cdot 10^8 \text{ m/s}$ is the propagation velocity in free space. Effective antenna heights at BS and UT are given as $h'_{BS} = h_{BS} - 1.0\text{m}$ and $h'_{UT} = h_{UT} - 1.0\text{m}$, respectively, where h_{BS} and h_{UT} represent their actual antenna heights, correspondingly. The average street width and building height can be set to $W = 20\text{m}$ and $h = 20\text{m}$, respectively.

3.2.3 Shadow Fading

Both models define shadow fading as a log-normal distribution Eq. (3.7) and Eq. (3.8) for LoS and NLoS radio propagation conditions, respectively. In 3GPP model its standard deviation is $\sigma_{LOS} = 8\text{dB}$ for LoS and $\sigma_{NLOS} = 8\text{dB}$ for NLoS, while in the ITU-R model $\sigma_{LOS} = 4\text{dB}$ and $\sigma_{NLOS} = 6\text{dB}$.

$$L_{LoS}(d) \sim \mathcal{N}(\bar{L}_{LoS}(d), \sigma_{LOS}^2) \quad (3.7)$$

$$L_{NLoS}(d) \sim \mathcal{N}(\bar{L}_{NLoS}(d), \sigma_{NLOS}^2) \quad (3.8)$$

3.2.4 Antenna Pattern

Both models specify the horizontal antenna pattern used for 3-sector cell sites with fixed antenna patterns as Eq. (3.9), where the relative horizontal antenna gain $A_h(\theta)$ in dB is a function of the direction θ , $-180^\circ \leq \theta \leq 180^\circ$. $\min[\cdot]$ denotes the minimum function and A_m is the maximum attenuation. $\theta_{3\text{dB}}$ is the 3dB beamwidth. The 3GPP assumes $\theta_{3\text{dB}} = 70^\circ$ and $A_m = 25\text{dB}$, while the ITU-R assumes $\theta_{3\text{dB}} = 70^\circ$ and $A_m = 20\text{dB}$.

$$A_h(\theta) = -\min \left[12 \left(\frac{\theta}{\theta_{3\text{dB}}} \right)^2, A_m \right] \quad (3.9)$$

Similarly, both models give the vertical antenna pattern by Eq. (3.10), where the relative vertical antenna gain $A_v(\phi)$ in dB is a function of the elevation direction ϕ , $-90^\circ \leq \phi \leq 90^\circ$. ϕ_{tilt} is

the electrical antenna downtilt angle, which shall be configured for deployment scenario. ϕ_{3dB} is the elevation 3dB value and SLA_v is the elevation maximum attenuation. The 3GPP assumes $\phi_{3dB} = 10^\circ$ and $SLA_v = 20dB$, while the ITU-R assumes $\phi_{3dB} = 15^\circ$ and $SLA_v = 20dB$.

$$A_v(\phi) = -\min \left[12 \left(\frac{\phi - \phi_{tilt}}{\phi_{3dB}} \right)^2, SLA_v \right] \quad (3.10)$$

In both models, the three-dimensional antenna pattern combines the horizontal and the vertical antenna patterns.

$$A(\theta, \phi) = -\min [-(A_h(\theta) + A_v(\phi)), A_m] \quad (3.11)$$

It should be clear now, what the differences between the two channel models are and that both models have their pros and cons.

3.3 Two-hop Channel Model

The ITU-R channel model presented in preceding sections is not only valid for direct links (BS \leftrightarrow UT) in a one-hop case but also for access links (RN \leftrightarrow UT) and backhaul links (BS \leftrightarrow RN) in a two-hop case.

The basis is the statement in ITU-R evaluation guidelines [IR08b]: "The link from a relay to a mobile station can be modeled with the same models as the conventional link from a base station to a mobile station. The links from base stations to relay stations can be modeled with conventional links."

Therefore, exactly the same channel model is applied to both access links and backhaul links as to direct links.

3.4 Performance Measures

Report ITU-R M.2134 [IR08a] specifies requirements of technical performance for IMT-A radio interfaces. Eight performance measures are taken into account: Cell Spectral Efficiency

(CSE), peak spectral efficiency, bandwidth, cell edge user spectral efficiency, latency, mobility, handover and Voice over IP (VoIP) capacity. Each proposed candidate technology needs to fulfil the minimum performance requirements in order to be considered by ITU-R for IMT-A. Therefore, these eight parameters are useful for evaluation of IMT-A candidate technology.

Further, guidelines for evaluation of radio interface technologies for IMT-A are addressed in Report ITU-R M.2135 [IR08b]. Evaluation methods are recommended for performance measures. Technology proposals shall be evaluated by system level simulation for three performance metrics: CSE, cell edge user spectral efficiency and VoIP capacity. The other performance metrics shall be evaluated just by inspection, analysis and link level simulation. Hence, these three out of eight are most interesting system characteristics.

Moreover, evaluation configurations are given for each performance measure in Report ITU-R M.2135 [IR08b]. Baseline parameters in Table 8-2 and system simulation parameters in Table 8-4 are applicable to all of the three performance measures. Additional parameters in Table 8-6 are specific to VoIP capacity only, while additional parameters in Table 8-5 are available for both CSE and cell edge user spectral efficiency in common. Thus, these two out of three are closely related to each other in terms of parameters.

This is why this work focuses on CSE (cell capacity) and takes in addition cell edge user throughput into consideration¹ for evaluation of LTE-A as an IMT-A candidate technology². It

¹E.g. Fig. 9.7 and Fig. 11.12 illustrate for downlink and uplink, respectively, the map of user throughput for each location in a relay enhanced cell, which includes among others throughput achieved by users located at cell edge.

²Average spectral efficiency and 5th percentile user spectral efficiency are still important performance metrics for IMT-2020 (5G) [IR17a], which correspond to original CSE and cell edge user spectral efficiency of IMT-A (4th Generation (4G)), respectively. For both of them candidate technolo-

is worthy of note, that up to now evaluation results have only been provided by simulation; It is still an open issue to evaluate CSE of LTE-A cellular systems by analytical model.

3.4.1 Cell Spectral Efficiency

The CSE, η , is defined mathematically in Eq. (3.12), as given in ITU-R performance requirements [IR08a]. A system comprises a population of N users and a network of M cells. χ_i denotes the number of correctly received bits by a i^{th} user on downlink or from the i^{th} user on uplink. T denotes a certain period of time over which the data bits are received, and ω the channel bandwidth.

$$\eta = \frac{\sum_{i=1}^N \chi_i}{T \cdot \omega \cdot M} \quad (3.12)$$

Analyzing Eq. (3.12) in depth, three following terms user throughput, cell capacity and CSE used in this thesis, are well-defined mathematically.

The user throughput, $throughput_{user_i}$, more precisely the throughput achieved between a i^{th} UT and its serving BS, is the number of correctly received bits at or from the i^{th} UT averaged over the period of time for reception, Eq. (3.13).

$$throughput_{user_i} = \frac{\chi_i}{T} \quad (3.13)$$

The cell capacity, $capacity_{cell}$, more precisely the total throughput achieved by all UTs located in a cell, is the sum of N UTs' user throughput divided by the number of cells M , Eq. (3.14).

$$capacity_{cell} = \frac{\sum_{i=1}^N \chi_i}{T \cdot M} = \frac{\sum_{i=1}^N throughput_i}{M} \quad (3.14)$$

The CSE, CSE , is the cell capacity normalized to the channel bandwidth ω , Eq. (3.15).

$$CSE = \frac{\sum_{i=1}^N \chi_i}{T \cdot \omega \cdot M} = \frac{capacity_{cell}}{\omega} \quad (3.15)$$

gies shall be evaluated by system level simulation [IR17b]. VoIP capacity of IMT-A is no longer a performance metric adopted for IMT-2020.

Related Work

Content

4.1	Background	43
4.2	3GPP Self-Evaluation	44
4.2.1	Nokia Siemens Networks [NN10]	45
4.2.2	Alcatel-Lucent [AA09]	47
4.2.3	Intel (UK) [Int10]	48
4.2.4	Motorola [Mot09]	49
4.2.5	Qualcomm [Qua10]	50
4.2.6	Panasonic [Pan10]	51
4.2.7	NEC [NEC10]	51
4.2.8	NTT Docomo [NTT11]	52
4.2.9	LG Electronics [LG 10]	52
4.2.10	Huawei [Hua09]	53
4.2.11	ZTE [ZTE09]	53
4.2.12	China Mobile [CMC09b]	54
4.3	Summary	54
4.4	Validation Reference	55
4.4.1	Sambale	55
4.4.2	Saleh	56
4.5	Further Work	57
4.5.1	Minelli	58

4.1 Background

In 1985 B. Walke was the first to publish the structure and operation mode of a packet-switching cellular multi-hop radio

network in [WB85]. As stated in [LHX⁺10], "The first relay-based cellular radio network was proposed in [WB85], which was a consequence of merging ad hoc networks and cellular networks." In 2000 Walke adapted the relay technology introduced in 1985 to modern cellular mobile broadband systems in [EVW01], [WPS03].

ITU-R has conferred IMT-A (4G) status to two technologies: 3GPP LTE and Institute of Electrical and Electronics Engineers (IEEE) 802.16m (Worldwide Interoperability for Microwave Access (WiMAX)). Both technologies include fixed two-hop relays as one of their enablers. As of today, relays were deployed in Universal Mobile Telecommunications System (UMTS) but are rarely used in LTE networks owing to the progress made in smart antenna technology that is proved useful to save cost related to relays. Relays, however, are expected to be especially useful in 5G networks owing to the high path loss present at 3-4 *GHz* carrier frequencies used in 5G.

Relays, especially when operating in half-duplex mode, have been considered for traditional cellular networks as candidates to enhance system capacity, extend cell coverage, and improve cell edge user throughput in a cost-effective manner without incurring high site and backhaul acquisition costs [PWS⁺04].

4.2 3GPP Self-Evaluation

To be able to evaluate performance of relay enhanced LTE-A cellular systems and to promote comparison of evaluation results among candidate systems proposed, 3GPP has issued an evaluation methodology document for system level simulation, Annex A of [3GP10b]. Models to be used to account for LoS probability, path loss, shadow fading and antenna pattern on direct, backhaul and access links are defined therein along with simulation assumptions and implementation parameters.

In 3GPP RAN1 #58 meeting of 2009, the channel model for relay deployment was revised [CMC09a]. Path loss models

include two separate components for LoS and NLoS propagations instead of a combination of both for direct, backhaul and access links, respectively. Moreover, backhaul links get a bonus of 5 dB to the NLoS path loss and a higher LoS probability from each sector of donor macro site to relay site, if benefiting from optimized relay site planning.

A number of companies in cooperation with research institutes have achieved preliminary performance results in past 3GPP RAN1 meetings, as summarized in Table 4.1. In these contributions, LTE-A systems with Type 1 relays (cf. Chapter 2) are simulated on downlink for 3GPP Case 1 scenarios (cf. Chapter 3) according to the updated evaluation methodology adopting the latest agreed channel model [3GP10b]. Using a eNB only case as baseline system¹, a relay enhanced system in comparison achieves a maximum performance gain with respect to a chosen performance metric by deploying an optimum amount of RNs per cell. For each contribution, the performance gain is given in Table 4.1 along with the performance metric and the number of RNs, respectively. A cell is defined as one sector of a three-sector site.

4.2.1 Nokia Siemens Networks [NN10]

In order to improve user experience and provide good coverage at cell edge, RNs are evenly distributed over the cell-edge area, namely close to four edges, which are adjacent to neighbor sites, out of six edges of a hexagonal sector cell. The more RNs are deployed, the more UEs switch from eNB to RN; The relay coverage is increased steadily with the increase of RNs.

Relay site planning can improve SINR of backhaul links. However, backhaul links may be interfered by backhaul links of the other two sectors of the same site, which makes site planning difficult. Even when using directional antennas for backhaul links and planning relay sites carefully, some RNs

¹Both baseline scenario and baseline system refer to the scenario without relays and the non-relay system as shown in Fig. 3.1.

Table 4.1: 3GPP self-evaluation

source [doc]	RNs per cell	performance metric [unit]	performance gain
Nokia Siemens Networks [NN10]	4	aggregate throughput per sector [Mbps]	40 %
Alcatel-Lucent [AA09]	2	cell-average user throughput [bps/Hz/cell]	4 %
Intel (UK) [Int10]	3	cell spectral efficiency [bps/Hz/sector]	112 %
Motorola [Mot09]	4	aggregate throughput per sector [Mbps]	5 %
Qualcomm [Qua10]	4	median throughput per UE [kbps]	53 %
Panasonic [Pan10]	4	aggregate cell throughput [Mbps]	17 %
NEC [NEC10]	2	sector throughput [bps/Hz]	12 %
NTT Docomo [NTT11]	4	cell throughput [Mbps]	15 %
LG Electronics [LG 10]	4	mean UE throughput [kbps]	43 %
Huawei [Hua09]	3	average cell throughput [Mbps]	10 %
ZTE [ZTE09]	10	average cell throughput [Mbps]	-2 % (loss)
China Mobile [CMC09b]	4	aggregate sector throughput [Mbps]	40 %

may still suffer from inter-backhaul interference, which impacts backhaul capacity and related RNs' user throughput.

With a small number of RNs, e.g. 1 or 4 RNs per cell, SINR of direct/access links is almost not improved but remains comparable to that of cells without RNs. With a large number of RNs, e.g. 10 RNs per cell, SINR of direct/access links is deteriorated and gets even worse than that of cells without RNs, because more relays bring despite stronger signal more interference at the same time. However, more relays always allow more concurrent transmissions, which may enhance throughput performance independent of SINR.

Cell-edge user throughput is a much more important performance parameter, since most users are not close to macro eNBs but roam in cell-edge areas. To maximize cell-edge user throughput, a tradeoff in resource allocation is required between backhaul links and direct/access links. E.g., considering Time Division Multiplexing (TDM) based resource partition in an inband relay system, the best and optimum subframe configuration for 4 RNs per sector is to allocate 2 out of 10 subframes to backhaul links and the remaining 8 subframes to direct/access links, respectively.

Then it turns out that 4 RNs per sector provide 40 % gain in terms of aggregate sector throughput compared to the baseline scenario, see Table 4.1. It is found that by increasing the number of RNs deployed per sector from 1 to 4, aggregate sector throughput is improved considerably.

4.2.2 Alcatel-Lucent [AA09]

Different scheduling algorithms result in different system performance in terms of throughput and fairness. A Proportional Fair (PF) scheduler [TK09] is usually applied in LTE cellular systems, because it achieves a good tradeoff between system throughput and fairness among users.

In this study, semi-static resource allocation is assumed for relay enhanced cellular systems, i.e., disjunct resource parti-

tions of the bandwidth are allocated to the DeNB and its subordinate RNs, respectively. PF scheduling is applied per hop, i.e., resources available at DeNB are scheduled to serve its UEs and RNs via direct links and backhaul links, and resources available at each RN are scheduled to serve its UEs via access links.

For comparison purpose, downlink system performance is evaluated in terms of normalized cell-average user throughput in $\text{bps}/\text{Hz}/\text{cell}$ for both conventional cellular systems and relay-enhanced cellular systems. The study's finding is that about a 4.15 % gain is achieved in cell-average user throughput with two RNs per cell compared to cells without relays.

4.2.3 Intel (UK) [Int10]

Throughput of backhaul links is important for CSE of a relay enhanced LTE system, since backhaul links tend to be bottlenecks in two-hop eNB-RN-UE transmission.

Since backhaul links can be designed to have near LoS transmission characteristics, spatial multiplexing on backhaul links is an efficient way to improve system performance in case of multiple relays. In this study, Multi-User Multiple Input Multiple Output (MU-MIMO) is adopted for backhaul links while Single-User Multiple Input Multiple Output (SU-MIMO) is used for both direct links and access links. eNB and RNs are equipped with 4 antennas, respectively, and UEs have 2 antennas.

By using spatial multiplexing on backhaul links, an increase of CSE over cells without relays is achieved, namely up to 38 % in case of two RNs per cell. However, with three RNs per cell performance severely degrades, resulting from too much interference to backhaul links.

By employing both, directional antennas at relays and spatial multiplexing on backhaul links, CSE of relay enhanced systems is significantly improved, namely 74 % and 112 % for deployment scenarios with two and three RNs per cell, respectively, compared to a deployment without relays.

4.2.4 Motorola [Mot09]

Significant performance gains are realized with outband backhaul to serve relays over the baseline scenario in terms of both sector throughput and 5th percentile user throughput. Both of them improve with increased number of relays per sector from one to four.

For inband backhaul four models are studied: A assumes a non-optimized relay site planning with an omnidirectional antenna at relay; B incorporates an optimized relay site planning; C uses a directional antenna at relay; D combines B with C. It is found that both sector throughput and 5th percentile user throughput, generally, improve progressively for models A through D. In model D, backhaul link performance is quite poor and could be improved.

Concerning MBSFN subframe configuration it is found that sector throughput performance is degraded by configuring two backhaul subframes per frame (SFpF) compared to one backhaul SFpF. This is because the quality of backhaul links is poor on average for models A through D and the reduced throughput due to resource consumption by backhaul links is poorly compensated for by the increased throughput in relay subcells. Sector throughput performance degrades continuously with increased number of backhaul SFpF, say four and six.

On the other hand, 5th percentile user throughput is improved by configuring two backhaul SFpF compared to one backhaul SFpF, since relay-cell-edge users benefit from increased backhaul capacity. However, 5th percentile user throughput degrades for four and six backhaul SFpF, because macro-cell-edge users are impacted by loss of donor subcell capacity.

It is found that aggregate throughput per sector is better with four RNs per sector than one RN per sector. Configuring one backhaul SFpF in the best performing model D, four RNs per sector improve aggregate sector throughput by about 5 % compared to the baseline scenario.

However, 5th percentile user throughput is substantially reduced with four RNs per sector compared to one RN per sector owing to high interference experienced by relay-cell-edge users with increased number of RNs per sector. Moreover, 5th percentile throughput is generally worse with relays than in the baseline scenario, because access links to relay users increase interference to direct links to macro-cell-edge users in a relay enhanced system that applies aggressive frequency reuse.

4.2.5 Qualcomm [Qua10]

Two relaying models are compared, namely basic relays and advanced relays. With basic relays, relays may transmit data in any subframe that is not scheduled for backhaul transmission.

Advanced relays deploy a range extension cell-selection algorithm and a cooperative silencing scheme. Macro cells do not transmit but remain silent for a number of subframes during each radio frame and these subframes are used by relays to serve relay UEs that need range extension. As usual, advanced relays adopt subframe partitioning between resources allocated to access links and backhaul links. In particular, some of the subframes are used by relays to serve relay UEs, while the remaining subframes are used by the macro cell to serve both relays as well as macro UEs. This partitioning ensures that relay UEs do not see interference from high-powered macro cell signals and dominant interference from macro cells to relay UEs is effectively mitigated. In addition, only relay UEs located nearby relays are scheduled concurrently to macro cell transmission.

It is found that advanced relays provide a gain of 53 % in terms of median UE throughput by using two range extension SFpF, whilst basic relays only achieve a gain of 32 %.

4.2.6 Panasonic [Pan10]

The study says that aggregated cell throughput slightly improves by increasing the number of subframes scheduled for backhaul links. However, with 1 RN, 2 RNs and 4 RNs per cell 1-2, 2-3 and 3-4 backhaul SFpF are found sufficient, respectively. Increase of the number of backhaul subframes decreases donor-cell throughput; On the other hand, it increases relay-cell throughput.

Aggregated cell throughput is improved by increasing the number of RNs from one to four. Cell throughput gain of relay systems is about 8 %, 16 % and 17 % with 1 RN, 2 RNs and 4 RNs, respectively, compared to the baseline system.

4.2.7 NEC [NEC10]

Impact of RN placement including distance between eNB and RN, and impact of handoff bias for cell selection are investigated to give an insight into RN deployment.

Placement of RNs close to eNB antenna main lobe is found to achieve better performance in terms of sector throughput and cell-edge user throughput compared to equidistant placement of RNs. Further, eNB to RN distance shall be around 45 % of ISD, which puts relays close to cell edges.

Handoff bias in favor of RN is found to expand the relay-cell range and increase the number of UEs associated to a RN, and thus improve sector throughput. However, biased cell selection, especially with a large bias value, reduces cell-edge user throughput since UEs may choose a high interfered RN instead of a eNB to be served.

Two RNs per sector cell, among others, increase sector throughput by about 12 % compared to a non-relay system, if RNs are placed close to eNB antenna main lobe, eNB to RN distance equals 45 % ISD, unbiased cell selection is used, and two SFpF are assigned for downlink backhaul transmission.

4.2.8 NTT Docomo [NTT11]

Throughput gain of a fixed relay deployment scenario is found to be greater than that of a random relay deployment scenario. Moreover, the more relays are deployed, e.g. 4 RNs in a cell, the higher cell-edge user throughput is achieved.

With 4 RNs per cell, 40 % of all UEs approximately are served by RNs. The number of SFpF assigned to backhaul links substantially affects throughput of relay cell and 4 backhaul SFpF appear to be a good choice.

Relays can improve overall cell throughput by about 15 % compared to the baseline scenario with 4 fixed RNs per cell and 4 backhaul SFpF.

4.2.9 LG Electronics [LG 10]

The study finds that relays provide a substantial throughput gain. Further, throughput is increased in a symmetrical relay deployment compared to a random relay deployment.

With half-duplex relays, macro-UEs are interfered only by macro cells during backhaul subframes, i.e., macro-UEs naturally enjoy the "cooperative silencing" effect of relays; On the other hand, UEs are interfered by both macro cells and relays during access subframes.

Channel State Information (CSI) shall be measured and reported separately in backhaul subframes and access subframes to reflect this interference variation. Transmission to macro-UEs, which experience severe interference from nearby relays in access subframes, is multiplexed with transmission to RNs in backhaul subframes. The multiplexing transmission is found to provide noticeable throughput gains, especially, in the interference-limited Case 1 scenario.

The study reports a 37 % gain on mean user throughput for a symmetrical relay deployment with 4 relays compared to the baseline scenario. The multiplexing transmission contributes an additional gain of 6 % resulting in a sum total throughput

gain of 43 %.

4.2.10 Huawei [Hua09]

The study assumes that an eNB can schedule RNs at 6 subframes and schedule UEs at 10 subframes, while a RN can schedule UEs at 4 subframes. In order to improve cell-edge UE throughput, the PF scheduler is adjusted, so that RNs schedule more resources to cell-edge UEs in access subframes, and eNBs schedule more resources to RNs in backhaul subframes.

With 3 RNs dropped uniformly per cell, mean cell throughput is found to be about 10 % higher than in the baseline scenario.

4.2.11 ZTE [ZTE09]

Relays are shown to slightly improve data rate for users experiencing medium channel conditions, at the cost of slight degradation for users experiencing poor and good channel conditions. In summary, relays with inband wireless backhaul do not contribute to improve system capacity.

Assuming frequency reuse across eNB and RNs, given that transmit power and antenna gain of eNB is much higher compared to RNs, strong intra-cell interference from eNB to UEs served by RNs significantly limits data rate on access links, and shrinks downlink coverage area of RNs. Especially, interference limited Case 1 scenarios, where eNB and RNs are geographically crowded with aggressive frequency reuse, cannot benefit from relays.

Mean cell throughput is about 2 % lower compared to the baseline scenario with 10 RNs uniformly distributed per cell without optimization of relay placement.

4.2.12 China Mobile [CMC09b]

The resource partition ratio between access subframes and backhaul subframes is configured as 2:1 and non-allocated resources in backhaul subframes are assigned to macro UEs to improve resource utilization.

The study finds that with increasing the number of RNs per sector, the scheduling opportunity for a macro UE in a backhaul subframe decreases until it approaches zero at 2 RNs per sector. This is because resource reuse in RNs of the same sector provides an enormous access link capacity that tends to overload the available backhaul link capacity. It is argued that this causes throttling of total throughput of UEs served by RNs.

By introducing relays, aggregate sector throughput increases compared to a non-relay system. With increasing the number of RNs, sector throughput increases until 4 RNs are deployed. Sector throughput is seriously limited by capacity of backhaul links if more than 4 RNs are deployed. The maximum sector throughput gain, compared to the baseline system, is achieved with 4 RNs per sector in an amount of about 40 %.

It is said that total throughput of UEs served by RNs can further be improved by using Spatial Division Multiple Access (SDMA) on backhaul links, where multiple beams are aligned from eNB to different RNs. Then, multiple RNs in a same sector cell are served simultaneously over the same resource blocks, which provides a multiplexing gain even under increased interference level to backhaul links.

4.3 Summary

Some basic yet important factors have been studied in the aforementioned works to understand their impacts on performance of relay enhanced LTE systems. This gives some hints on design and implementation of relay deployment.

However, all these works are based on system level simulation. The throughput performance gain figures listed in Table

4.1 are quite disperse, ranging from -2% to $+112\%$. Apparently, quite differently sophisticated relay enhanced systems have been studied ranging from non-optimized placement of RNs up to spatial multiplexing applied to backhaul links using MIMO technology. This makes it impossible to compare the studies' results easily. Further, different simulation platforms and parameter settings have been used, some of which may affect the results presented substantially.

It is obvious from the studies that relay enhanced systems

- may substantially increase throughput capacity of cellular systems like LTE and 5G,
- to be effective, will benefit from technologies as usual in non-relay systems, and
- are especially sensitive to interference.

Nevertheless, relays are expected to be without competition to serve heavily shadowed areas and to serve non-hotspot locations, where fibre cabling is missing.

4.4 Validation Reference

Sambale's [Sam13] and Saleh's [SmBR⁺11] studies are used as references to validate our results. They have both simulated LTE-A systems with Type 1 relays (cf. Chapter 2) on downlink for ITU-R UMa or 3GPP Case 1 scenarios (cf. Chapter 3), and evaluated throughput capacity of both non-relay systems and relay enhanced systems.

4.4.1 Sambale

Optimum relay placement is investigated in Sambale's study [Sam13] to maximize CSE of relay enhanced cellular systems.

Three RNs per cell are found sufficient to achieve maximal possible CSE increase almost completely. One RN shall be

placed in BS antenna boresight direction at a distance of $0.95 \times \frac{2}{3} \times ISD$ from BS to RN. The other two RNs are placed symmetrically 18° apart from BS antenna boresight at a distance of $0.7 \times \frac{2}{3} \times ISD$ from BS to RN, respectively. All the three RNs shall be mounted below rooftop at a height of 6.5 m .

RN transmit power has negligible impact on CSE and 20 dBm is enough to achieve close to maximum CSE. Association of UT either to a BS or a RN according to maximum SINR, achieves almost maximum CSE increase. CSE does not benefit from association with SINR offset in favor of RNs, and thus unbiased subcell selection between donor cell and relay cell is used.

It is said that RNs shall be placed carefully to have LoS backhaul link between serving BS and RN but NLoS radio propagation condition between interfering BSs and RN. CSE increase mainly results from replacing a NLoS direct link by a LoS backhaul link and a mostly LoS access link.

BS antenna down tilt has minor impact on CSE. Directional antennas at RNs pointing towards serving BS or their UTs have negligible impact on CSE, and omnidirectional antennas at RNs are sufficient to achieve maximal CSE.

Three RNs per cell placed and configured optimally as stated above achieve an increase of 80% in CSE compared to cells without RNs.

4.4.2 Saleh

In Saleh's study [SmBR⁺11] two resource sharing models applicable to backhaul links in relay enhanced systems are compared to each other with respect to throughput.

First, the reference model decides backhaul resource shares among RNs according to proportion of the sum of throughput achieved on access links of an RN to the total throughput achieved on access links of all RNs in the cell, and prioritizes relay UEs benefiting from good channel conditions on access links by providing them with high backhaul throughput.

Second, the hop-optimization model decides backhaul resource shares among RNs according to ratio of the number of UEs served by an RN to the total number of UEs served by all RNs in the cell, and prioritizes relay UEs suffering from bad channel conditions on access links by maximizing their backhaul throughput.

It is said that these models neither improve nor reduce throughput of UEs served by direct links. It is found that the hop-optimization model achieves a gain in 5 %-ile user throughput without loss in average cell throughput, and thus provides a more homogeneous user experience in relay cells, compared to the reference model.

Compared to cells with eNB only, four RNs per cell achieve a same gain of 30 % in average cell throughput with both resource sharing models studied. The gain in 5 %-ile user throughput is 23 % with the reference model and 38 % with the hop-optimization model.

4.5 Further Work

In the Bibliography of this dissertation, the most recent related work cited dates from 2015, which is introduced in the next subsection; The bulk of papers appeared during 3GPP self-evaluation from 2009 to 2011, which are introduced in previous sections.

An extensive literature search reveals that simulation based studies on the throughput capacity of relay enhanced LTE systems deployed in the UMa scenario have been published mostly in parallel to the standardization of 3GPP LTE Release 10 finalized in 2010. No related work based on analytical models is found to complement and validate the simulation studies.

In 2015 3GPP described use cases for study on LTE support for Vehicle to Everything (V2X) services in Release 14 [3GP15]. E.g., the V2X system broadcasts a message warning vehicles approaching the congested area of a traffic jam. The message is

relayed by other vehicles on the road to extend the range of the message and gives vehicles toward the congestion ample time to change course.

In 2016 further use cases were given for study on enhancement of support for V2X services in LTE Release 15 [3GP16]. E.g., vehicles traveling on the road can dynamically form a platoon. A platoon manager real-time collects surrounding traffic data from platoon members, and relays it to road side unit; At the same time, the platoon manager real-time receives road conditions and traffic information far away from the platoon from road side unit, and relays them to platoon members.

Since then, another wave of publications is related to mobile relays as specified for machine type communications and for autonomous driving in LTE Releases 14 and 15, respectively. However, these works, which are again based on system level simulation, are not relevant to our work, since strict delay bounds are to keep, there, and delay is not a performance measure in our mathematical model.

4.5.1 Minelli

Minelli's paper [MMCG15] compares the impact of two traditional schedulers, namely PF and Round Robin (RR)² [TK09], on the sector throughput of relay-enhanced LTE-A cellular networks by means of simulation.

In case of outband relaying, sector throughput steadily increases with the number of RNs (#RNs) from 0 to 6 RNs per sector by applying either RR or PF scheduling; The increase is less significant under a lower cell load. Scheduling gain of PF over RR grows with #RNs under a high cell load, but remains approximately constant with #RNs under a low cell load.

In case of inband relaying, sector throughput constantly increases with #RNs by applying RR scheduling, whereas by ap-

²An RR scheduler, also known as a resource fair scheduling approach, assigns an equal share of PRBPs in every radio frame to each UE in turn, irrespective of their prevailing channel conditions.

plying PF scheduling sector throughput stops increasing when #RNs exceeds 3 RNs per sector. Scheduling gain of PF over RR decreases with #RNs; A PF scheduler largely outperforms an RR scheduler by deploying few RNs (less than 3 RNs per sector), whereas performance of RR scheduler approaches that of PF scheduler when #RNs grows.

Scheduling gain of PF over RR increases with the data rate on backhaul link. A PF scheduler does not gain much or even performs worse than an RR scheduler in a poor inband backhaul condition, where RNs may be in either LoS or NLoS to their serving eNB and their interfering eNBs.

It is concluded that PF scheduling does not bring a consistent performance improvement compared to RR scheduling in three cases: 1) Many RNs (more than 3 RNs per sector) are deployed in case of inband relaying, 2) data rate of backhaul link is low, 3) network load is low in case of outband relaying. A PF scheduler is not necessarily the right option for multi-hop cellular networks; An RR scheduler seems to be a good choice in the three abovementioned cases.

Analytical Framework

Content

5.1 Non-Relay System	61
5.2 Relay Enhanced System	63

5.1 Non-Relay System

Our analytical framework is able to evaluate a non-relay LTE system with BS only, see Fig. 3.1. The framework comprises modules as illustrated in Fig. 5.1: SINR distribution calculation, Signal Flow Graph (SFG) models for PHY, MAC and RLC protocol layers in LTE, numeric conversion, location averaging and user summation.

According to the IMT-A channel model (cf. Chapter 3) path loss from transmitter to receiver considers both LoS and NLoS radio propagation conditions, where LoS probability is a function of distance therebetween. Based on the channel model, probability distribution of SINR is calculated for a link between a UT position and the position of its responsible BS.

As illustrated in Fig. 5.1 (left), from Cumulative Distribution Function (CDF) of SINR for a certain link, protocol layer specific SFG models constitute Moment Generating Function (MGF) of resource consumption for this link. A protocol layer specific MGF is a transform of probability distribution of the amount of resources consumed to transmit a protocol layer specific SDU. An MGF comprises a success part corresponding to an error-free transmission and a failure part representing an erroneous transmission. SFG models specific to PHY, MAC and

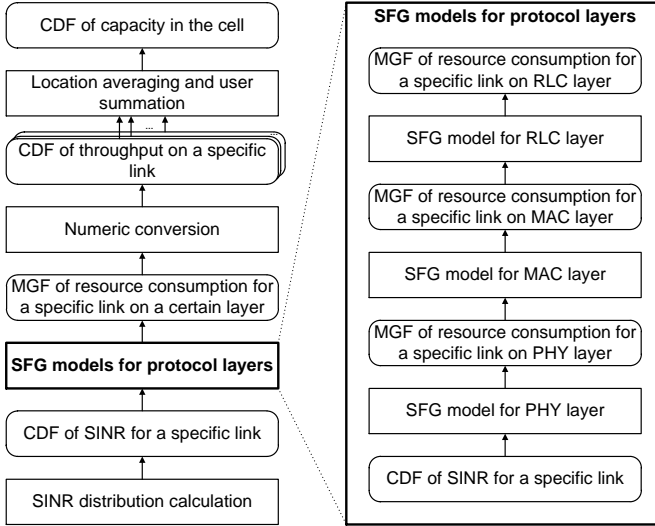


Figure 5.1: Capacity model

RLC layers deliver MGFs of resource consumption specific to these three layers, respectively, as illustrated in Fig. 5.1 (right).

MGF of resource consumption for a certain link is numerically converted to CDF of throughput for this link. By overlaying a grid onto a multi-cell scenario, say a $5\text{ m} \times 5\text{ m}$ grid over an $800\text{ m} \times 800\text{ m}$ center area of the scenario, a CDF of SINR, a MGF of resource consumption and a CDF of throughput can be derived in sequential steps for any grid element. User throughput map of multi-cell scenario shows mean throughput for each grid element representing a potential UT location in the scenario.

By location averaging, CDF of throughput for a user of a cell is derived from all CDFs of throughput for grid elements in the cell, each representing a small location area and altogether covering the whole area of the cell. By user summation, CDF of cell capacity is derived from all CDFs of throughput for multiple users located in the cell.

5.2 Relay Enhanced System

Our analytical framework is also capable to evaluate a relay enhanced LTE system with wireless backhaul operated inband as specified as mandatory in 3GPP LTE Release 10 [3GP10a]. The modeling framework is extended as illustrated in Fig. 5.2, which comprises modules two-hop operation, location averaging and user summation in a subcell, and subcell summation among the other modules introduced in Fig. 5.1. A subcell may be a relay cell or a donor cell as illustrated in Fig. 2.5, which are the area covered by an RN and a BS, respectively.

The modules SINR probability distribution calculation, SFG models for PHY, MAC and RLC layers, and numeric conversion are also applied to a scenario extended with relays to calculate CDF of SINR, MGFs of resource consumption on PHY, MAC and RLC layers, and CDF of throughput consequently, not only for direct link between BS and any arbitrary one-hop UT location, but also for backhaul link between BS and any given RN location, and access link between RN and any arbitrary two-hop UT location.

Applying location averaging, CDF of throughput for a user located in a subcell is derived from all CDFs of throughput for the user standing at various grid elements in the subcell. For a relay subcell this takes only throughput on access link into account and does not represent user throughput of two-hop link. For a donor subcell this accounts for throughput on direct link and corresponds to user throughput of one-hop link. Applying user summation, CDF of capacity for a subcell is derived from all CDFs of throughput for multiple users located in the subcell. Similarly, this considers capacity on all access links in a relay subcell and capacity on all direct links in a donor subcell.

Two-hop operation calculates one output CDF with two input CDFs: The first input is capacity on all access links of users in a relay subcell, the second is throughput on backhaul link of the relay subcell, and the output is capacity on all two-hop links of users in the relay subcell.

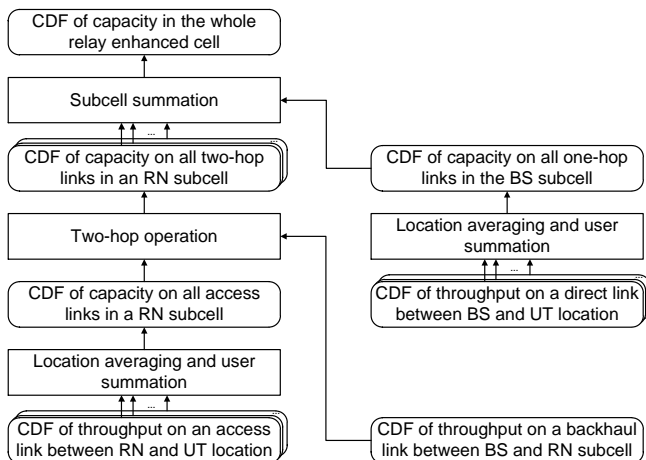


Figure 5.2: Capacity model extended for two-hop systems

Subcell summation calculates CDF of capacity for a cell, given CDFs of capacity for each of its non-overlapping sub-cells.

SINR Calculation

Content

6.1 Downlink	65
6.1.1 Relay Enhanced Cell	67
6.2 Uplink	69
6.3 Maximum Ratio Combining	75

6.1 Downlink

In cells with BS only, a UT on downlink is served by a BS and interfered by neighbor BSs. Radio propagation conditions for both signal and interferences may be either LoS or NLoS¹.

Notations are introduced as follows. Index $i = 1, 2, \dots, \#sites$ numbers sites in the scenario shown in Fig. 3.1 and $j = 1, 2, 3$ identifies sector cells in each site, where $\#sites$ is the total number of sites. Subscript i denotes a radio link from the BS site i to an observed UT location and (i, j) for a radio link from the BS sector antenna j at site i to the UT location. Among them, subscripts i_S and (i_S, j_S) denote a radio link where the one and only signal propagates; All the others are radio links where interference propagates.

A radio channel state at an observed UT location is defined as a combination of LoS and/or NLoS radio propagation conditions for signal and interferences. Each channel state has its own probability and its individual SINR at the location of observation. $b_i \in \{0, 1\}$ denotes that radio wave propagates un-

¹We assume throughout in our model that UTs are immobile thereby representing a snapshot of the system.

der either LoS or NLoS condition, where 1 and 0 represent LoS and NLoS, respectively.

The probability of a channel state is product of either LoS probability $p_{LoS,i}$ or NLoS probability $p_{NLoS,i}$ of each radio link, Eq. (6.1) for a UT served by BS. $p_{LoS,i}$ and $p_{NLoS,i}$ are calculated by Eqs. (3.1) and (3.2), respectively.

$$p_{BS} = \prod_{i=1}^{\#sites} b_i \cdot p_{LoS,i} + (1 - b_i) \cdot p_{NLoS,i}, \quad (6.1)$$

Eq. (6.2) calculates receive power of both signal and interferences². Receive power under either LoS or NLoS condition, $P_{rx,LoS}$ and $P_{rx,NLoS}$, are obtained by transmit power P_{tx} plus both antenna gains at transmitter G_{tx} and receiver G_{rx} , and minus path loss under either LoS or NLoS condition, PL_{LoS} and PL_{NLoS} , respectively. PL_{LoS} and PL_{NLoS} are calculated by Eq. (3.5) and Eq. (3.6), respectively. Both G_{tx} and G_{rx} are calculated by Eq. (3.11).

$$P_{rx,(N)LoS} = P_{tx} + G_{tx} + G_{rx} - PL_{(N)LoS} \quad (6.2)$$

In a channel state, receive signal power depends on whether signal propagates under LoS or NLoS condition, Eq. (6.3) for a UT served by BS. Receive interference power is obtained by summing up all individual receive power dependent on LoS or NLoS condition and subtracting receive signal power, Eq. (6.4) for a UT served by BS. Individual receive power under LoS and NLoS conditions, $P_{LoS,(i,j)}$ and $P_{NLoS,(i,j)}$, are calculated by Eq. (6.2). It is worth noting that for a UT served by BS, receive powers from the three sectors of a site are different from one another, however, the three radio links have a same radio propagation condition, since the three BS sector antennas are co-located at a common BS site.

$$S_{BS} = b_{i_S} \cdot P_{LoS,(i_S,j_S)} + (1 - b_{i_S}) \cdot P_{NLoS,(i_S,j_S)} \quad (6.3)$$

²Eq. (6.2) is applicable to both a UT/RN served by BS and a UT served by RN.

$$I_{BS} = \sum_{i=1}^{\#sites} \sum_{j=1}^3 b_i \cdot P_{LoS,(i,j)} + (1 - b_i) \cdot P_{NLoS,(i,j)} - S_{BS} \quad (6.4)$$

Eq. (6.5) calculates SINR in a channel state³. Receive signal power S and receive interference power I are calculated by Eqs. (6.3) and (6.4), respectively, for a UT served by BS. Noise power N in linear $[mW]$ domain is obtained by thermal noise level -174 dBm plus noise figure of receiver n_f in logarithmic $[dBm]$ domain, then times the bandwidth proportional to the number of LTE subchannels $\#sch$ in linear $[mW]$ domain, each of which spans a bandwidth of 180 kHz , Eq. (6.6).

$$SINR = \frac{S}{I + N} \quad (6.5)$$

$$N = 10^{\frac{-174 + n_f}{10}} \cdot \#sch \cdot 180 \cdot 10^3 \quad (6.6)$$

6.1.1 Relay Enhanced Cell

In cells enhanced with RNs, an RN on backhaul downlink besides the signal from its donor BS simultaneously receives cochannel interferences from neighbor BSs. A UT on direct downlink is served by a BS and interfered by neighbor BSs, while a UT on access downlink is served by an RN and interfered by neighbor RNs of its own and other sites.

The calculation in the preceding section applied to a UT served by BS in cells with BS only is also applicable to both a UT and an RN served by BS in cells enhanced with RNs. Further, the calculation is slightly modified as follows to be applicable to a UT served by RN.

In addition to notations introduced so far, index $k = 1, 2, \dots, \#RN_s$ numbers relays in each cell, where $\#RN_s$ is the number of RNs

³Eq. (6.5) is also applicable to both a UT/RN served by BS and a UT served by RN. For a UT/RN served by BS, S and I are calculated by Eqs. (6.3) and (6.4), respectively. For a UT served by RN, S and I are calculated by Eqs. (6.8) and (6.9), respectively.

per cell. Subscript (i, j, k) denotes a radio link from the RN k in cell j of site i to an observed UT location. Among them, subscript (i_S, j_S, k_S) denotes the one and only radio link of signal propagation.

The probability of a channel state is given by Eq. (6.7) for a UT served by RN, similar to Eq. (6.1) for a UT/RN served by BS. $b_{(i,j,k)} \in \{0, 1\}$ represents either LoS or NLoS radio propagation condition of a radio link. $p_{LoS,(i,j,k)}$ and $p_{NLoS,(i,j,k)}$ are LoS and NLoS probabilities of the radio link, respectively.

$$p_{RN} = \prod_{i=1}^{\#sites} \prod_{j=1}^3 \prod_{k=1}^{\#RNs} b_{(i,j,k)} \cdot p_{LoS,(i,j,k)} + (1 - b_{(i,j,k)}) \cdot p_{NLoS,(i,j,k)} \quad (6.7)$$

In a channel state, receive signal power is given by Eq. (6.8) for a UT served by RN, similar to Eq. (6.3) for a UT/RN served by BS. Receive interference power is given by Eq. (6.9) for a UT served by RN, similar to Eq. (6.4) for a UT/RN served by BS. $P_{LoS,(i,j,k)}$ and $P_{NLoS,(i,j,k)}$ are individual receive power under LoS and NLoS conditions, respectively.

$$S_{RN} = b_{(i_S,j_S,k_S)} \cdot P_{LoS,(i_S,j_S,k_S)} + (1 - b_{(i_S,j_S,k_S)}) \cdot P_{NLoS,(i_S,j_S,k_S)} \quad (6.8)$$

$$I_{RN} = \sum_{i=1}^{\#sites} \sum_{j=1}^3 \sum_{k=1}^{\#RNs} b_{(i,j,k)} \cdot P_{LoS,(i,j,k)} + (1 - b_{(i,j,k)}) \cdot P_{NLoS,(i,j,k)} - S_{RN} \quad (6.9)$$

It is known from [Sam13] that throughput capacity is close to optimum when deploying three RNs per sector cell. Consider a center BS with nine RNs and one tier of six BSs each with nine RNs, then there are 62 interfering RNs besides one serving RN and 2^{63} channel states for a UT served by RN. In principle, the analytic method presented here is applicable to scenarios with any number of RNs per cell, but requires excessive computation cost owing to a large number of possible interferers and their combinatorial complexity. Thus, rigorous simplification of interference modeling is needed for a UT served by

RN. Radio propagation conditions between RN and UT are assumed to be NLoS for those interfering RNs, which are quite far away from the UT, namely those for which LoS probability is below a threshold of 5%. This assumption reasonably reduces the combinatorial complexity of the interference modeling, so that the analytic method is able to evaluate performance of systems with three RNs per sector cell.

6.2 Uplink

Transmit power control is standardized for LTE uplink [3GP10e] and the power control equation for PUSCH is specified as Eq. (6.10). $\alpha \cdot PL$ is the open-loop path loss compensation component, where α and PL denote the fractional compensation factor and the downlink path loss estimate, respectively. P_0 represents the semi-static base level of transmit power. Then, $P_0 + \alpha \cdot PL$ constitutes the basic open-loop operating point for transmit power per RB. Δ_{TF} denotes the MCS dependent component, which allows transmit power to be adapted according to information data rate. $f(\Delta_{TPC})$ represents the component depending on user specific transmit power control commands. Then, $\Delta_{TF} + f(\Delta_{TPC})$ constitutes the dynamic offset of transmit power per RB. $10\log_{10}M$ is the bandwidth factor, where M denotes the number of RBs actually allocated to UE in a subframe. The total transmit power of UE in the subframe $P_0 + \alpha \cdot PL + \Delta_{TF} + f(\Delta_{TPC}) + 10\log_{10}M$ must be limited by the maximum transmit power of UE P_{max} .

$$P_{tx} = \min \{ P_{max}, P_0 + \alpha \cdot PL + \Delta_{TF} + f(\Delta_{TPC}) + 10\log_{10}M \} \quad (6.10)$$

Since SINR is independent on the number of allocated RBs, the bandwidth factor is eliminated by taking one RB into consideration. Further, the dynamic offset updated from subframe to subframe is neglected, while the basic open-loop operating point derived from static or semi-static parameters signalled by BS is taken into account. In consequence, the power con-

trol equation is simplified to Eq. (6.11) [BRRH11], which is applied to the following SINR calculation. Since radio propagation condition can be either LoS or NLoS, the path loss between a UT and its serving BS is calculated according to Eq. (3.5) and Eq. (3.6) for LoS and NLoS cases, respectively, and the transmit power $P_{tx,LoS}$ and $P_{tx,NLoS}$ are determined according to Eq. (6.11) by $PL_{LoS}(d_s)$ and $PL_{NLoS}(d_s)$, respectively.

$$P_{tx,(N)LoS} = \min \{P_{max}, P_0 + \alpha \cdot PL_{(N)LoS}(d_s)\} \quad (6.11)$$

Considering various radio propagation conditions, receive signal power is calculated by Eq. (6.12) for LoS and NLoS conditions between a UT and its serving BS, respectively. The receive signal power under LoS condition $P_{rx,LoS}$ is obtained by the transmit power under LoS condition $P_{tx,LoS}$, plus both, the antenna gain at transmitter G_{tx} and the antenna gain at receiver G_{rx} , respectively, minus the path loss under LoS condition $PL_{LoS}(d_s)$. Eq. (3.11) calculates the antenna gain for both, transmitter and receiver. The receive signal power under NLoS condition $P_{rx,NLoS}$ is obtained in the same way.

$$P_{rx,(N)LoS} = P_{tx,(N)LoS} + G_{tx} + G_{rx} - PL_{(N)LoS}(d_s) \quad (6.12)$$

Taking shadow fading into account, Eq. (6.13) expresses Probability Density Function (PDF) of receive signal power. Since path loss is distributed log-normally under both LoS and NLoS radio propagation conditions as Eq. (3.7) and Eq. (3.8), respectively, receive power has a log-normal distribution in $[mW]$ domain for each case correspondingly. More precisely, the receive signal power P_{rx} in $[dBm]$ domain is distributed normally with mean $P_{rx,LoS}$ and variance σ_{LoS}^2 under LoS condition, and mean $P_{rx,NLoS}$ and variance σ_{NLoS}^2 under NLoS condition. The probabilities for LoS and NLoS conditions between a UT and its serving BS $p_{LoS}(d_s)$ and $p_{NLoS}(d_s)$ are obtainable from Eq. (3.1) and Eq. (3.2), respectively. Since radio wave propagates randomly under LoS and NLoS conditions, PDF of the receive signal power is the sum of these two

normal distributions weighted by their respective probabilities.

$$\begin{aligned}
 PDF[P_{rx,S}](x) = & \\
 & p_{LoS}(d_s) \cdot \frac{1}{\sqrt{2\sigma_{LoS}^2\pi}} e^{-\frac{(x - P_{rx,LoS})^2}{2\sigma_{LoS}^2}} + \\
 & p_{NLoS}(d_s) \cdot \frac{1}{\sqrt{2\sigma_{NLoS}^2\pi}} e^{-\frac{(x - P_{rx,NLoS})^2}{2\sigma_{NLoS}^2}}
 \end{aligned} \tag{6.13}$$

Considering various radio propagation conditions, receive interference power is calculated by Eq. (6.14), which is similar to but more complex than calculation of receive signal power. Accordingly, radio propagation condition from a UT to the BS serving the UT can be either LoS or NLoS, where $P_{tx,LoS}$ and $P_{tx,NLoS}$ denote respective transmit power. Radio wave can propagate from the UT to the reference BS interfered by the UT under either LoS or NLoS condition, where $PL_{LoS}(d_i)$ and $PL_{NLoS}(d_i)$ denote respective path loss. The BS of a sector cell, which performance is evaluated, is called here the reference BS. Either LoS or NLoS from the UT to the serving BS can be arbitrarily combined with either LoS or NLoS from the UT to the reference BS, where $P_{rx,LoS,LoS}$ denotes receive interference power for LoS to both the BSs, $P_{rx,NLoS,LoS}$ for NLoS to the serving BS but LoS to the reference BS, $P_{rx,LoS,NLoS}$ for LoS to the serving BS but NLoS to the reference BS, and $P_{rx,NLoS,NLoS}$ for NLoS to both the BSs.

$$P_{rx,(N)LoS,(N)LoS} = P_{tx,(N)LoS} + G_{tx} + G_{rx} - PL_{(N)LoS}(d_i) \tag{6.14}$$

Taking shadow fading into account, Eq. (6.15) expresses PDF of receive interference power. Four normal distributions are summed by their individual weight, which correspond to those four combinations specified above, respectively. For each combination, mean is calculated by Eq. (6.14), variance is dependent on the radio propagation condition between the UT and the

reference BS interfered by the UT, and weight is probability for the specific condition between the UT and the serving BS times probability for the specific condition between the UT and the reference BS.

$$\begin{aligned}
 PDF[P_{rx,I}](x) = & \\
 & p_{LoS}(d_s) \cdot p_{LoS}(d_i) \cdot \frac{1}{\sqrt{2\sigma_{LoS}^2\pi}} e^{-\frac{(x - P_{rx,LoS,LoS})^2}{2\sigma_{LoS}^2}} + \\
 & p_{NLoS}(d_s) \cdot p_{LoS}(d_i) \cdot \frac{1}{\sqrt{2\sigma_{LoS}^2\pi}} e^{-\frac{(x - P_{rx,NLoS,LoS})^2}{2\sigma_{LoS}^2}} + \\
 & p_{LoS}(d_s) \cdot p_{NLoS}(d_i) \cdot \frac{1}{\sqrt{2\sigma_{NLoS}^2\pi}} e^{-\frac{(x - P_{rx,LoS,NLoS})^2}{2\sigma_{NLoS}^2}} + \\
 & p_{NLoS}(d_s) \cdot p_{NLoS}(d_i) \cdot \frac{1}{\sqrt{2\sigma_{NLoS}^2\pi}} e^{-\frac{(x - P_{rx,NLoS,NLoS})^2}{2\sigma_{NLoS}^2}}
 \end{aligned} \tag{6.15}$$

Given a cochannel UT is located in a specific cell area, PDF of interference power received by the reference BS from the cochannel UT $PDF[I_{area}]$, is obtained by PDF of interference power received from the cochannel UT at some location $PDF[I_{(x,y)}]$ integrated over the specific area and then normalized by the area size, Eq. (6.16). $PDF[I_{(x,y)}]$ is expressed by Eq. (6.15).

$$PDF[I_{area}] = \iint_{(x,y) \in area} \frac{PDF[I_{(x,y)}]}{A_{area}} \tag{6.16}$$

The specific cell area, where a cochannel UT is located, varies dependent on reuse partitioning techniques applied. E.g., by applying hard frequency reuse, the cochannel UT may be located anywhere in a neighboring cell. By applying reuse partitioning, however, the cochannel UT is restricted to a certain

part of a neighboring cell. Reuse partitioning is presented in detail in Chapter 11.

Taking all interferences simultaneously received by the reference BS from multiple neighboring cells into consideration, Eq. (6.21) calculates PDF of total interference. $PDF[I_i]$, denoting PDF of interference from the i^{th} neighboring cell, is calculated by Eq. (6.16). In logarithmic $[dBm]$ domain total interference is the power sum of all interferences, and PDF of total interference is derived from PDFs of individual interference by logarithmic convolution⁴, equivalent to a sum of all interferences and a convolution of their PDFs in linear $[mW]$ domain. As individual interference is calculated in $[dBm]$ domain in previous steps, PDF of total interference is derived by recursive application of logarithmic convolutions to PDFs of individual interference from each neighboring cell.

$$PDF[I_{\Sigma}] = PDF[I_1] *_{log} PDF[I_2] *_{log} \dots *_{log} PDF[I_{\#cell-1}] \quad (6.21)$$

⁴Let X and Y be two independent random variables in logarithmic $[dB]$ domain, $g_X(x)$ and $g_Y(y)$ be PDFs for X and Y , respectively. Then, a power sum R of X and Y is defined as

$$R = 10 \log_{10} \left(10^{\frac{X}{10}} + 10^{\frac{Y}{10}} \right). \quad (6.17)$$

PDF for R , $g_R(r)$, is derived by logarithmic convolution of $g_X(x)$ and $g_Y(y)$, namely

$$g_R(r) = g_X(x) *_{log} g_Y(y). \quad (6.18)$$

Logarithmic convolution is calculated as Eqs. (6.19)-(6.20), which is analytically derived in [PS96].

$$g_R(r) = \int_{-\infty}^r g_X(z) g_Y(D(r, z)) dz + \int_{-\infty}^r g_X(D(r, z)) g_Y(z) dz \quad (6.19)$$

$$D(r, z) = 10 \log_{10} \left(10^{\frac{r}{10}} - 10^{\frac{z}{10}} \right) \quad (6.20)$$

Taking thermal noise besides cochannel interferences into consideration, Eqs. (6.22) and (6.23) calculate PDF of interference plus noise, which mathematical derivation is given in [MW11]. $PDF[I_{\Sigma}]$ denotes PDF of total interference and is calculated by Eq. (6.21). Noise power N in logarithmic [dBm] domain is calculated by Eq. (6.24), corresponding to its calculation in linear [mW] domain Eq. (6.6).

$$PDF[I_{\Sigma} \& N](x) = PDF[I_{\Sigma}](x) \cdot \frac{10 \overline{10}^{\frac{z}{N}}}{10 \overline{10} - 10 \overline{10}^{\frac{z}{N}}} \quad (6.22)$$

$$z = 10 \log_{10}(10 \overline{10}^{\frac{x}{N}} + 10 \overline{10}^{\frac{N}{N}}) \quad (6.23)$$

$$N = 10 \log_{10}(10^{\frac{-174 + n_f}{10}} \cdot \#sch \cdot 180 \cdot 10^3) \quad (6.24)$$

Eq. (6.25) calculates PDF of SINR received at a BS for a UT location served by the BS. In linear domain SINR is the quotient of signal power from a UT at the location, and total cochannel interference power from UTs in neighboring cells plus thermal noise power. Then, in logarithmic domain SINR is the sum of signal power and negative interference plus noise power. I.e., PDF of SINR $PDF[SINR]$ is convolution of PDF of signal power $PDF[P_{rx,S}]$ and PDF of negative interference plus noise power $PDF[I_{\Sigma} \& N](-x)$, which is the reflection of PDF of positive interference plus noise power $PDF[I_{\Sigma} \& N](x)$ in the y-axis. $PDF[P_{rx,S}]$ and $PDF[I_{\Sigma} \& N](x)$ are calculated by Eq. (6.13) and Eq. (6.22), respectively.

$$PDF[SINR](x) = PDF[P_{rx,S}](x) * PDF[I_{\Sigma} \& N](-x) \quad (6.25)$$

To get probabilities from PDF of SINR, an integral of a probability density over a certain interval is needed to find a probability mass. The probability that the (continuous) random variable falls in an interval is the area under the PDF curve

sandwiched by the interval. If the interval is infinitesimally small, this approximation is good enough for the probability that the (discrete) random variable equals the median of the interval. Accordingly, PDF of SINR is sequentially divided into 0.1 *dB* intervals. For each of these intervals, the probability is the probability of a channel state and the median is the SINR in the channel state.

6.3 Maximum Ratio Combining

In HARQ with soft combining, incorrectly received TBs are stored at the receiver rather than discarded, and when a retransmitted TB is received, all the received TBs are combined. Chase Combining (CC) and IR are two main soft combining methods in HARQ. In CC, every retransmission contains same data and parity bits, and the receiver uses Maximum Ratio Combining (MRC) to combine the received bits with the same bits from previous transmissions.

In MRC, received signals from all diversity branches are combined to maximize the SINR at combiner output. The output SINR of MRC γ_{MRC} is given by Eq. (6.26) [WW99], where γ_i denotes the instantaneous SINR of the i^{th} diversity branch. After the N^{th} transmission, signal powers of an initial transmission and all subsequent $N - 1$ retransmissions are summed up to calculate the SINR resulting from MRC.

$$\gamma_{MRC} = \sum_{i=1}^N \gamma_i \quad (6.26)$$

In our model the estimated SINR of the first transmission of a TB is assumed to be the same as retransmissions following, namely γ_i is identical with γ_1 for all $i = 2, 3, \dots, N$. Then, the output SINR of MRC after the N^{th} transmission is N times the SINR of the first transmission in linear domain. E.g., energy addition after the second transmission gives a 3 *dB* diversity gain in logarithmic domain compared to the first transmission.

Signal Flow Graph Models

Content

7.1	Mathematic Fundamentals	77
7.2	SFG Models for LTE Performance Evaluation	82
7.3	SFG Model for AMC Scheme of PHY Layer	83
7.3.1	Block Error Rate	87
7.3.2	Number of Physical Resource Block Pairs	88
7.4	SFG Model for HARQ Protocol of MAC Layer	90
7.5	SFG Model for ARQ Protocol of RLC Layer	100

7.1 Mathematic Fundamentals

In this chapter behavior of communication protocols and performance of mobile radio networks are statistically analyzed by means of SFG, where both data transmission errors and signaling failures are taken into account.

Thinking of the SFG as a signal transmission system: Each branch of the graph may be associated with a unilateral amplifier, so that the signal traversing some branch is multiplied by the gain of that branch; Each node acts as an adder and ideal repeater, which receives and algebraically sums the signals from every incoming branch and then transmits the resulting signal along each outgoing branch.

Various graph topologies and some reduction rules of SFGs are discussed in details in [Mas53] and [Mas56]. Three basic topologies, namely cascade, parallel and self-loop, and their equivalence rules are most often applied in [Geh07] to analyze communication protocols.

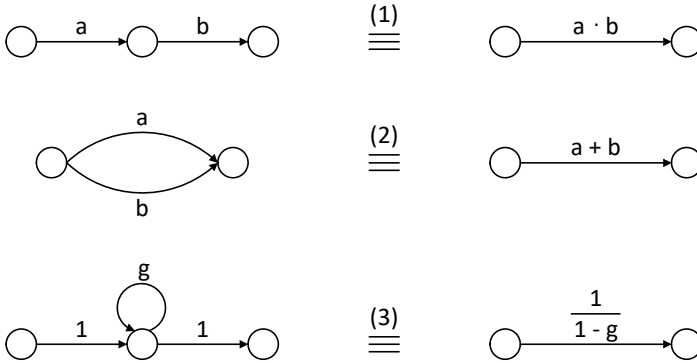


Figure 7.1: Basic equivalences of SFGs

Fig. 7.1 illustrates three basic equivalences: The cascade equivalence (1) eliminates the intermediate node by multiplying both branch gains; The parallel equivalence (2) merges two branches by summing their gains; The self-loop equivalence (3) replaces the loop and its node by a single branch, whose gain is the reciprocal of the loop difference $(1 - g)$, where g is the loop gain.

Generally, these basic equivalences permit successive reductions to an SFG, until the only branch appears in the residual graph. In this context, original branch gains are associated algebraically, i.e. with addition, multiplication and division, to form the gain of the residual branch.

Originally, SFGs are introduced by [Mas53] in order to analyze electronic circuits. In [LC89] and [LC93] SFGs are used to find MGFs of the transmission time in order to analyze the mean throughput and delay of ARQ protocols. This model has been extended by [AN07] to matrix signal flow graphs to enable the analysis of ARQ protocols with a hidden Markov model for the forward and reverse channel.

In this thesis SFGs are applied to analyze LTE communic-

ation functions and protocols, namely AMC scheme of PHY Layer, HARQ protocol of MAC Layer and SR-ARQ protocol of RLC Layer, identify MGFs of resource consumption from their graphical description SFGs, and evaluate LTE system performance in terms of user throughput and cell capacity based on the stochastic specification MGFs. An SFG serves to graphically represent an MGF of resource consumption comprising a set of equations, that are required to calculate user throughput of an LTE protocol stack.

Suppose that K is a discrete random variable and its possible values are non-negative integers $k \in N_0$. Then a Probability Mass Function (PMF) $P_K(k)$ states the probability of the random variable K taking a certain value k . The total probability for all hypothetical outcomes of the random phenomenon is one.

$$\sum_{k=0}^{\infty} P_K(k) = 1 \quad (7.1)$$

In stochastic theory, a MGF of a discrete random variable is an alternative specification of its PMF. Thus, it provides the basis of an alternative route to derive analytical results instead of calculating directly with PMF. For a non-negative discrete random variable K a PMF can be transformed to a MGF as follows.

$$G_K(z) = \sum_{k=0}^{\infty} P_K(k) \cdot z^{-k} \quad (7.2)$$

The completeness condition must hold for MGF, just the same as for PMF.

$$G_K(z = 1) = 1 \quad (7.3)$$

Besides, mean and variance of a discrete random variable can be deduced straightforwardly from the first order and the second order derivative of its MGF, respectively.

$$\bar{K} = \frac{\partial}{\partial z} G_K(z)|_{z=1} \quad (7.4)$$

$$\sigma^2(K) = \frac{\partial^2}{\partial z^2} G_K(z)|_{z=1} \quad (7.5)$$

A given MGF can be retransformed to its corresponding PMF by k times derivative of $G_K(z)$ with respect to z as follows.

$$P_K(k) = \frac{1}{k!} \cdot \left(\frac{\partial^k}{\partial z^k} G_K(z) \right) |_{z=0} \quad (7.6)$$

Alternatively, $G_K(z)$ can be derived by the Z-transform from $P_K(k)$, while $P_K(k)$ is the inverse Z-transform from $G_K(z)$.

$$P_K(k) \circ \bullet G_K(z) \quad (7.7)$$

As an example, the discrete unit impulse function $\delta(k)$ is a simplest PMF, which is defied as follows. $\delta(k - k_0)$ denotes the PMF taking a time delay into account.

$$\delta(k) = \begin{cases} 1 & \text{for } k = 0 \\ 0 & \text{for } k \neq 0 \end{cases} \quad (7.8)$$

MGFs corresponding to $\delta(k)$ and $\delta(k - k_0)$ are given in the following common Z-transform pairs, respectively.

$$\delta(k) \circ \bullet 1 \quad (7.9)$$

$$\delta(k - k_0) \circ \bullet z^{-k_0} \quad (7.10)$$

Three basic properties of Z-transform are most interesting for our application here, namely linearity, convolution and deconvolution in co-domain correspond to linearity, multiplication and division in Z-domain, respectively.

$$a_1 f_1(k) + a_2 f_2(k) \circ \bullet a_1 F_1(z) + a_2 F_2(z) \quad (7.11)$$

$$f_1(k) * f_2(k) \circ \bullet F_1(z) \cdot F_2(z) \quad (7.12)$$

$$f_1(k) *^{-1} f_2(k) \circ \bullet \frac{F_1(z)}{F_2(z)} \quad (7.13)$$

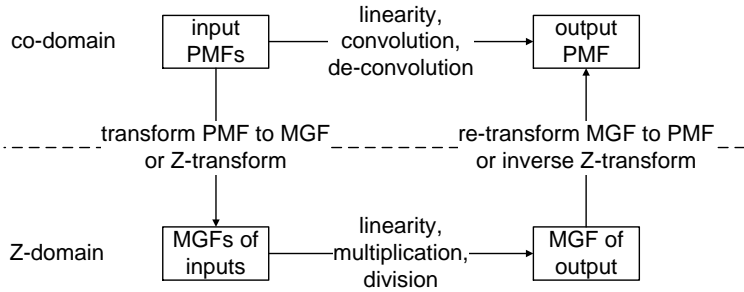


Figure 7.2: Calculation with PMFs in co-domain and with MGFs in Z-domain

It is worth mentioning that $f_1(k)$ and $f_2(k)$ are two co-domain functions, and $F_1(z)$ and $F_2(z)$ are their Z-transform functions; they can be PMFs and their corresponding MGFs, but they do not have to be.

As summarized in Fig. 7.2, there are two possible ways to derive a PMF resulting from given PMFs in our mathematical analysis, namely either mediately in Z-domain or directly in co-domain.

One option is firstly to transform the given PMFs to their corresponding MGFs, by Eq. (7.2) or Z-transform. And then algebraic calculations, namely linearity, multiplication and division, are applied to these MGFs to derive the MGF corresponding to the result PMF. Finally the result is retransformed from Z-domain to co-domain, by k times derivative as Eq. (7.6) or inverse Z-transform.

The other option is to derive the resulting PMF directly from the given PMFs, so that neither transform nor retransform between co-domain and Z-domain, nor algebraic calculation in Z-domain are necessary. Thereby, linearity, convolution and deconvolution are applied in co-domain, which correspond to linearity, multiplication and division in Z-domain, respectively.

A CDF $C_K(k)$ expresses the probability that a discrete random variable K has a value lower than or equal to k . Thus, $C_K(k)$ is a non-decreasing and right-continuous step function with the limits $\lim_{k \rightarrow 0} C_K(k) = 0$ and $\lim_{k \rightarrow +\infty} C_K(k) = 1$. The CDF can be derived by consecutively summing up the corresponding PMF.

$$C_K(k) = \sum_{i=0}^k P_K(i) \quad (7.14)$$

If a discrete random variable K attains values $k_1, k_2, \dots, k_i \dots$ with non-zero probabilities $P_K(k_1), P_K(k_2), \dots, P_K(k_i) \dots$, then the CDF of K is discontinuous and jumps at these points $k_1, k_2, \dots, k_i \dots$ and constant in between. The discontinuity of CDF is owing to the pulse form of PMF of the discrete random variable.

Referring to Eq. (7.2) a general expression of MGFs is a weighted sum of powers of the variable with non-positive integer exponents. For the sake of simplicity, a slightly amended form of MGFs is introduced into this work, where the integer exponents are non-negative instead of non-positive. And then, the amended MGFs are generally expressed as a weighted sum of powers of the variable with non-negative integer exponents. Thus, the following relationship holds for MGFs between their original form $G_K(z)$ and their amended form $G'_K(z)$.

$$G_K(z) = G'_K(z^{-1}) \quad (7.15)$$

In the following, unless otherwise stated, MGFs refer to the amended form and $G_K(z)$ denotes the amended form of MGFs.

7.2 SFG Models for LTE Performance Evaluation

The MGF of resource consumption for a lower protocol layer is an input to the SFG model of a next higher protocol layer to calculate the MGF of resource consumption for the higher

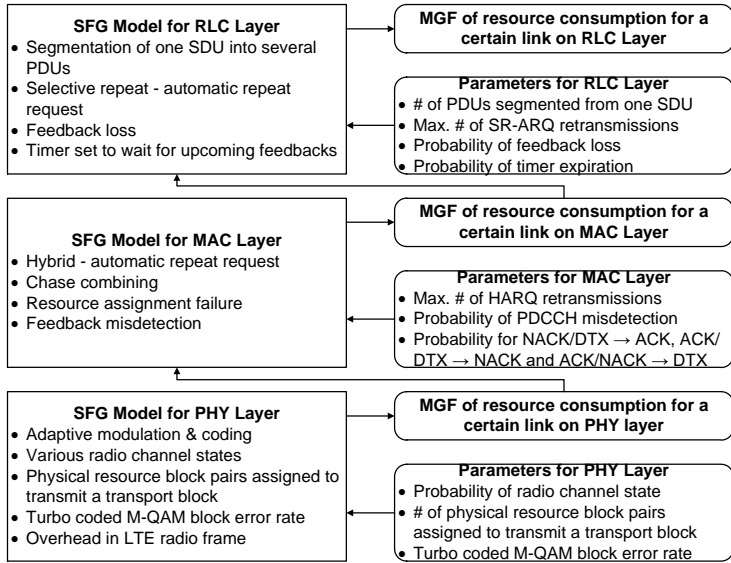


Figure 7.3: Signal flow graph models for LTE analysis

layer, see Fig. 7.3. Thereby, various aspects of the LTE system protocol layers are modeled and analyzed. On PHY layer, AMC scheme, various radio channel states, PRBPs assigned to transmit a TB, turbo coded M-QAM BLER and overhead in LTE radio frame are taken into account. On MAC layer, HARQ protocol, CC, resource assignment failure and feedback misdetection are accounted for. On RLC layer, segmentation of one RLC SDU into several RLC PDUs, SR-ARQ protocol, feedback loss and timer set to wait for upcoming feedbacks are considered.

7.3 SFG Model for AMC Scheme of PHY Layer

Following the AMC scheme [3GP10e] the SFG for PHY layer is shown in Fig. 7.4. $G_{K_{PHY}}(z)$ represents the MGF of the number of PRBPs consumed to transmit a TB on PHY layer.

The transmission on PHY layer is differentiated into N cases

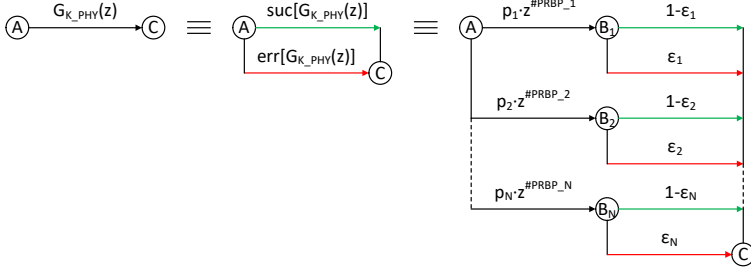


Figure 7.4: SFG for PHY layer

with respect to probability p_i of radio channel state and its related MCS. The i^{th} radio channel state consumes a number $\#PRBP_i$ of PRBPs to transmit a TB with a given size according to the MCS chosen for the i^{th} channel state. Each case $i = 1, 2, \dots, N$ is split into two branches with respect to the BLER ϵ_i resulting from the MCS and the channel state. The upper and lower branches represent transmission with success and failure, respectively. All the green paths in the figure represent correct transmission of TB on PHY layer and therefore belong to the group of successful transmission. All the red paths represent transmission in error and belong to the group of unsuccessful transmission. How to calculate $\#PRBP_i$ and ϵ_i in a channel state, is introduced in following subsections.

The SFG for PHY layer visualizes how the MGF of resource consumption for PHY layer $G_{K_{PHY}}(z)$ is composed of individual monomials $z^{\#PRBP_i}$ weighted by probability of channel state p_i . It also visualizes how the sequence of branches (green) corresponding to the successful group $suc[G_{K_{PHY}}(z)]$ and the other sequence (red) for the unsuccessful group $err[G_{K_{PHY}}(z)]$ are composed of individual monomials, respectively. It is worth mentioning owing to the amended form of MGFs introduced in Eq. (7.15) that all the powers of variable z have a positive exponent here; otherwise it should have a negative

exponent as specified in Eq. (7.10).

By applying basic equivalences of SFGs in Fig. 7.1 to the SFG for PHY layer in Fig. 7.4, the MGF for PHY layer, its success part and its failure part are deduced, respectively, as Eqs. (7.16), (7.17) and (7.18).

$$G_{K_{PHY}}(z) = suc[G_{K_{PHY}}(z)] + err[G_{K_{PHY}}(z)] \quad (7.16)$$

$$suc[G_{K_{PHY}}(z)] = \sum_{i=1}^N (p_i \cdot (1 - \epsilon_i) \cdot z^{\#PRBP_i}) \quad (7.17)$$

$$err[G_{K_{PHY}}(z)] = \sum_{i=1}^N (p_i \cdot \epsilon_i \cdot z^{\#PRBP_i}) \quad (7.18)$$

The total probability for all radio channel states is one.

$$\sum_{i=1}^N p_i = 1 \quad (7.19)$$

In order to show that the function $G_{K_{PHY}}(z)$ resulting from SFG model for PHY layer is a valid MGF, we prove that the completeness condition Eq. (7.3) is fulfilled for $G_{K_{PHY}}(z)$.

Proof:

Substituting Eqs. (7.18) and (7.17) into Eq. (7.16), we can get the following formulation for $G_{K_{PHY}}(z)$.

$$G_{K_{PHY}}(z) = \sum_{i=1}^N p_i \cdot z^{\#PRBP_i} \quad (7.20)$$

Let z be 1, then:

$$G_{K_{PHY}}(z = 1) = \sum_{i=1}^N p_i = 1 \quad (7.21)$$

because of Eq. (7.19).

I.e., the completeness condition is fulfilled for the function $G_{K_{PHY}}(z)$. Q.E.D.

By applying inverse Z-transform, more precisely, the common Z-transform pair Eq. (7.10) and the basic Z-transform property Eq. (7.11), Eqs. (7.16)-(7.18) in Z-domain are transformed to Eqs. (7.22)-(7.24) in co-domain, correspondingly. Please recall that both mathematic formulas, MGF in Z-domain and PMF in co-domain, can be adopted for our mathematic analysis.

$$P_{K_{PHY}}(k) = suc[P_{K_{PHY}}(k)] + err[P_{K_{PHY}}(k)] \quad (7.22)$$

$$suc[P_{K_{PHY}}(k)] = \sum_{i=1}^N p_i \cdot (1 - \varepsilon_i) \cdot \delta(k - \#PRBP_i) \quad (7.23)$$

$$err[P_{K_{PHY}}(k)] = \sum_{i=1}^N p_i \cdot \varepsilon_i \cdot \delta(k - \#PRBP_i) \quad (7.24)$$

Obviously, both the success part of the PMF for PHY layer $suc[P_{K_{PHY}}(k)]$ and the failure part $err[P_{K_{PHY}}(k)]$ are composed of individual impulse functions $\delta(k - \#PRBP_i)$. Consequently, the PMF for PHY layer $P_{K_{PHY}}(k)$, the sum of $suc[P_{K_{PHY}}(k)]$ and $err[P_{K_{PHY}}(k)]$, is also composed of these individual impulse functions.

The following Z-transform pairs hold between the PMF and the MGF for PHY layer. Readers are reminded here, owing to the amended form of MGFs introduced in Eq. (7.15), the MGF here is the Z-transform of the PMF, once its variable z is replaced with z^{-1} .

$$P_{K_{PHY}}(k) \circ \bullet G_{K_{PHY}}(z^{-1}) \quad (7.25)$$

$$err[P_{K_{PHY}}(k)] \circ \bullet err[G_{K_{PHY}}(z^{-1})] \quad (7.26)$$

$$suc[P_{K_{PHY}}(k)] \circ \bullet suc[G_{K_{PHY}}(z^{-1})] \quad (7.27)$$

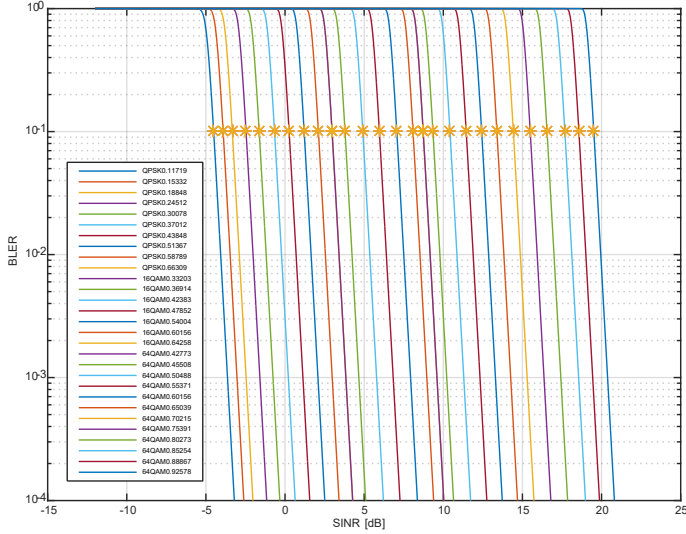


Figure 7.5: BLER versus SINR for MCSs of PDSCH

7.3.1 Block Error Rate

According to the turbo coded M-QAM BLER model [YRT09], BLER is a function of both, reference efficiency of MCS r and SINR γ .

$$BLER = P(r, \gamma) = 1 - \left(\frac{1}{1 + e^{-k_1\gamma + k_2 + k_3r + k_4r^2 + k_5r^3}} \right)^{k_6r} \quad (7.28)$$

with coefficients $k_1 = 5.3432$, $k_2 = -3.7311 \times 10^1$, $k_3 = 4.4981 \times 10^1$, $k_4 = -7.2544$, $k_5 = 6.3766 \times 10^{(-1)}$ and $k_6 = 9.7172$.

BLER versus SINR is shown with LTE MCSs as a parameter in Fig. 7.5 and Fig. 7.6 for PDSCH and PUSCH¹, respectively. They are calculated with Eq. (7.28) based on reference efficiency of MCSs in Table 2.4 and Table 2.5 for PDSCH and

¹Please remember that we only focus on user data channels on down- and uplink for calculating the throughput capacity of LTE systems.

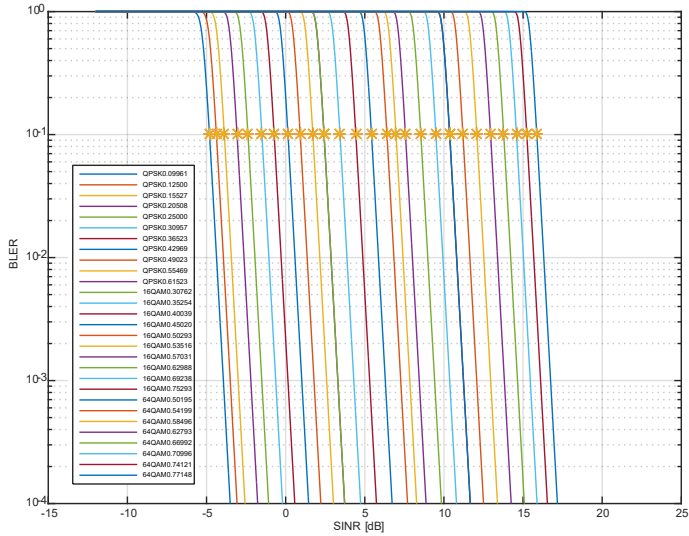


Figure 7.6: BLER versus SINR for MCSs of PUSCH

PUSCH, respectively. Curves from left to right in the figures correspond to MCSs from top to bottom in the tables.

AMC scheme of LTE systems chooses an appropriate MCS based on a BLER threshold of 10% [CNST09], namely for a given SINR of radio channel state the MCS providing a highest possible reference efficiency and ensuring BLER not exceeding the threshold is adopted. For each MCS, the asterisk on curve marks the SINR just achieving the BLER threshold and represents the switching point from a previous lower order MCS to this MCS.

7.3.2 Number of Physical Resource Block Pairs

A certain amount of radio resources are consumed to transmit a TB with a given size dependent on the MCS chosen for a specific radio channel state. The number of bits transmitted

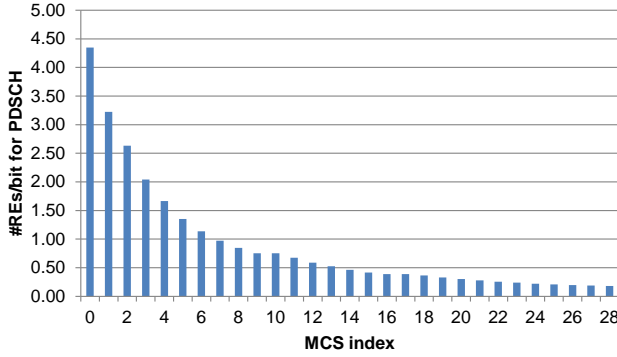


Figure 7.7: Number of REs per bit for MCSs of PDSCH

per PRBP is reference efficiency (the number of bits transmitted per RE) for the MCS $efficiency_{MCS}$ multiplied by 168 REs per PRBP excluding a percentage of overhead $ratio_{overhead}$ occupied for control signaling in a radio frame. Then, the number of PRBPs $\#PRBPs$ ² required to transmit the TB is equal to quotient of the number of bits in PHY PDU (TB plus CRC) $\#bits_{TB+CRC}$ and the number of bits transmitted per PRBP $efficiency_{MCS} \cdot 168 \cdot (1 - ratio_{overhead})$.

$$\#PRBPs = \frac{\#bits_{TB+CRC}}{efficiency_{MCS} \cdot 168 \cdot (1 - ratio_{overhead})} \quad (7.30)$$

The reciprocal term $\frac{1}{efficiency_{MCS}}$ in Eq. (7.30) merely depends on the MCS chosen. Since reference efficiency is the number of bits transmitted per RE for a MCS, the reciprocal of reference efficiency is interpreted as the number of REs consumed per bit for the respective MCS. Fig. 7.7 and Fig. 7.8

²Alternatively, calculation of resource consumption can be based on the number of REs $\#REs$. Then, the variable $\#PRBPs$ in all the equations involved is correspondingly replaced with the variable $\#REs$.

$$\#REs = \frac{\#bits_{TB+CRC}}{efficiency_{MCS} \cdot (1 - ratio_{overhead})} \quad (7.29)$$

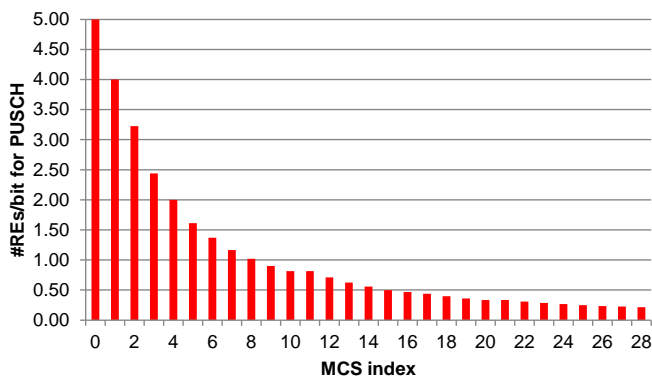


Figure 7.8: Number of REs per bit for MCSs of PUSCH

show the number of REs required per bit for different LTE MCSs of PDSCH and PUSCH, respectively, which correspond to reference efficiency in Table 2.4 and Table 2.5, respectively.

It is worth mentioning that in real systems a certain amount of PRBPs are scheduled to a user for transmission, and the size of TB to be mapped to these PRBPs is determined by the number of PRBPs available and the MCS chosen according to Table 7.1.7.2.1-1 in 3GPP spec [3GP10e]. In our model a TB is assumed to have an arbitrary but fixed length, and the number of PRBPs consumed to transmit the TB is calculated with the TB size assumed and the MCS chosen. Our model corresponds to real systems in this manner.

7.4 SFG Model for HARQ Protocol of MAC Layer

Referring to the HARQ protocol [3GP10h], the SFG for MAC layer is shown in Fig. 7.9. The SFG, which specifies the transmission of a MAC PDU with at most j times transmission of a TB on PHY layer, is recursively defined by the SFG, which describes the MAC transmission with at most $(j - 1)$ times PHY retransmission.

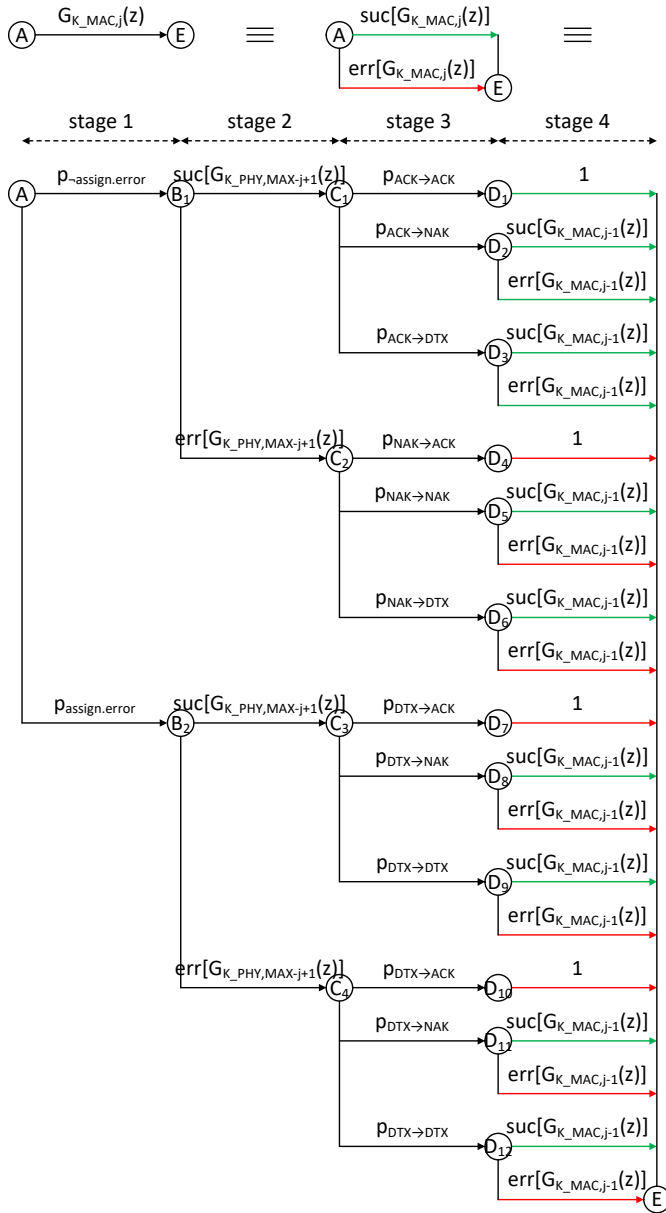


Figure 7.9: SFG for MAC layer: recursion

$G_{K_{MAC},j}(z)$ represents the MGF of the number of PRBPs required to transmit a MAC PDU conditioned on j transmissions of a TB on PHY layer. $G_{K_{PHY},MAX-j+1}(z)$ represents the MGF of resource consumption for the $(MAX - j + 1)^{th}$ transmission of the TB, where MAX transmissions of the TB are permitted by HARQ protocol at maximum. $G_{K_{PHY},1}(z)$, $G_{K_{PHY},2}(z)$, ..., $G_{K_{PHY},MAX}(z)$ are derived with the SFG model for AMC scheme of PHY layer based on the output SINR of MRC (cf. Chapter 6) after the 1^{st} , 2^{nd} , ..., MAX^{th} (final) transmission, respectively.

The SFG for MAC layer consists of four stages, see Fig. 7.9. In stage 1, the transmission on MAC layer distinguishes between successful and unsuccessful resource assignment, where $p_{assign.error}$ stands for the probability of control signaling resource assignment failure. Both stage 1 subgraphs branch into two stage 2 subgraphs, which represent correct and erroneous user data transmission on PHY layer, respectively. All the four stage 2 subgraphs branch into three stage 3 subgraphs. ACK represents the feedback for correct transmission, NAK for erroneous transmission and DTX for resource assignment failure. $p_{A \rightarrow B}$ stands for the probability that A is detected as B , since any feedback ACK, NAK and DTX can be detected or misdetected as ACK, NAK and DTX. In stage 4, no retransmission is caused for the detected ACK, but retransmission is triggered by detecting either NAK or DTX, which initiates a recursion.

According to Table 2.6, all the green paths representing a correct transmission of MAC PDU are collected into the successful group and all the red paths for an erroneous transmission are collected into the unsuccessful group.

The exit condition for the recursion is shown in Fig. 7.10. The SFG specifies the transmission of MAC PDU with a final transmission on PHY layer.

The recursively calculated MGF of resource consumption for MAC layer is visualized by the respective SFG straightfor-

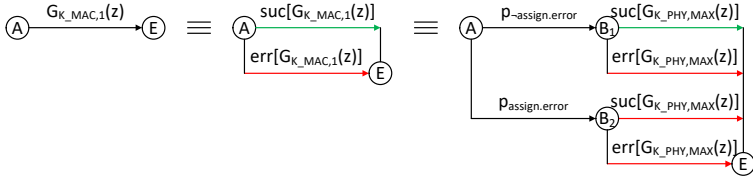


Figure 7.10: SFG for MAC layer: exit condition

wardly. The MGF of MAC layer for at most j times transmission of a TB on PHY layer $G_{K_{MAC},j}(z)$, is recursively defined by the MGF of MAC layer for at most $(j - 1)$ times transmission $G_{K_{MAC},j-1}(z)$. On the other hand, $G_{K_{MAC},j}(z)$ is elementarily composed of the MGF of PHY layer for the $(MAX - j + 1)^{th}$ transmission $G_{K_{PHY},MAX-j+1}(z)$. Moreover, it also visualizes how the MGF parts corresponding to error-free transmission $suc[G_{K_{MAC},j}(z)]$ and erroneous one $err[G_{K_{MAC},j}(z)]$ are made up of the MGF parts for success $suc[G_{K_{MAC},j-1}(z)]$ and $suc[G_{K_{PHY},MAX-j+1}(z)]$, and the MGF parts for failure $err[G_{K_{MAC},j-1}(z)]$ and $err[G_{K_{PHY},MAX-j+1}(z)]$.

Applying basic equivalences in Fig. 7.1 to the SFG for the recursion of MAC layer, the respective MGF is deduced and can be stated as follows.

$$G_{K_{MAC},j}(z) = suc [G_{K_{MAC},j}(z)] + err [G_{K_{MAC},j}(z)] \quad (7.31)$$

$$\begin{aligned} & suc [G_{K_{MAC},j}(z)] = \\ & p\text{-assign.error} \cdot p_{ACK \rightarrow ACK} \cdot suc [G_{K_{PHY},MAX-j+1}(z)] + \\ & [p\text{-assign.error} \cdot (p_{ACK \rightarrow NAK} + p_{ACK \rightarrow DTX}) + \\ & p_{assign.error} \cdot (p_{DTX \rightarrow NAK} + p_{DTX \rightarrow DTX})] \cdot \\ & suc [G_{K_{PHY},MAX-j+1}(z)] \cdot suc [G_{K_{MAC},j-1}(z)] + \\ & p\text{-assign.error} \cdot (p_{ACK \rightarrow NAK} + p_{ACK \rightarrow DTX}) \cdot \\ & suc [G_{K_{PHY},MAX-j+1}(z)] \cdot err [G_{K_{MAC},j-1}(z)] + \end{aligned}$$

$$\begin{aligned}
 & [p_{\text{assign.error}} \cdot (p_{NAK \rightarrow NAK} + p_{NAK \rightarrow DTX}) + \\
 & p_{\text{assign.error}} \cdot (p_{DTX \rightarrow NAK} + p_{DTX \rightarrow DTX})] \cdot \\
 & err [G_{K_{PHY,MAX-j+1}}(z)] \cdot suc [G_{K_{MAC,j-1}}(z)] \quad (7.32)
 \end{aligned}$$

$$\begin{aligned}
 & err [G_{K_{MAC,j}}(z)] = \\
 & p_{\text{assign.error}} \cdot p_{DTX \rightarrow ACK} \cdot suc [G_{K_{PHY,MAX-j+1}}(z)] + \\
 & (p_{\text{assign.error}} \cdot p_{NAK \rightarrow ACK} + p_{DTX} \cdot p_{DTX \rightarrow ACK}) \cdot \\
 & err [G_{K_{PHY,MAX-j+1}}(z)] + \\
 & p_{\text{assign.error}} \cdot (p_{DTX \rightarrow NAK} + p_{DTX \rightarrow DTX}) \cdot \\
 & suc [G_{K_{PHY,MAX-j+1}}(z)] \cdot err [G_{K_{MAC,j-1}}(z)] + \\
 & [p_{\text{assign.error}} \cdot (p_{NAK \rightarrow NAK} + p_{NAK \rightarrow DTX}) + \\
 & p_{\text{assign.error}} \cdot (p_{DTX \rightarrow NAK} + p_{DTX \rightarrow DTX})] \cdot \\
 & err [G_{K_{PHY,MAX-j+1}}(z)] \cdot err [G_{K_{MAC,j-1}}(z)] \quad (7.33)
 \end{aligned}$$

Both Eqs. (7.32) and (7.33) are a sum of four terms. Interpreting from the equations, transmission within at most j attempts is successful or not, basically dependent on whether the transmission succeeds in the $(MAX - j + 1)^{th}$ (this) attempt and upcoming $(j - 1)$ attempts or not. Consider this transmission attempt succeeds and no retransmission follows, if the resource assignment of this attempt is correctly detected, the MAC PDU is successfully transmitted, see Eq. (7.32) 1st term; Otherwise unsuccessful, Eq. (7.33) 1st term. This attempt fails, however, no retransmission follows, which obviously results in an unsuccessful transmission of the MAC PDU, Eq. (7.33) 2nd term. Both in case this attempt succeeds and upcoming retransmissions also succeed, and in case this attempt fails but upcoming retransmissions succeed, transmission of the MAC PDU is successful, see Eq. (7.32) 2nd and 4th terms. This attempt succeeds but upcoming retransmissions fail, which result also depends on the resource assignment of this attempt, Eq. (7.32) 3rd term and Eq. (7.33) 3rd term. This attempt fails and upcoming retransmissions also fail, which clearly leads to an unsuccessful transmission of the MAC PDU, Eq. (7.33) 4th term.

The SFG for the exit condition visualizes how the respective MGF of resource consumption for MAC layer with a final transmission $G_{K_{MAC,1}}(z)$ is composed of the MGF of PHY layer for the MAX^{th} transmission $G_{K_{PHY,MAX}}(z)$. Further, it also visualizes how the MGF parts corresponding to error-free and erroneous transmission of a MAC PDU, $suc[G_{K_{MAC,1}}(z)]$ and $err[G_{K_{MAC,1}}(z)]$, are composed of the MGF parts for successful and unsuccessful transmission of a PHY TB, $suc[G_{K_{PHY,MAX}}(z)]$ and $err[G_{K_{PHY,MAX}}(z)]$, as follows.

$$G_{K_{MAC,1}}(z) = suc [G_{K_{MAC,1}}(z)] + err [G_{K_{MAC,1}}(z)] \quad (7.34)$$

$$suc [G_{K_{MAC,1}}(z)] = p_{-assign.error} \cdot suc [G_{K_{PHY,MAX}}(z)] \quad (7.35)$$

$$\begin{aligned} err [G_{K_{MAC,1}}(z)] = \\ p_{assign.error} \cdot suc [G_{K_{PHY,MAX}}(z)] + err [G_{K_{PHY,MAX}}(z)] \end{aligned} \quad (7.36)$$

Both resource assignment and feedback signaling can be detected either correctly or incorrectly. Obviously, the sum of probabilities for a detection and a misdetection is always one.

$$p_{-assign.error} + p_{assign.error} = 1 \quad (7.37)$$

$$p_{ACK \rightarrow ACK} + p_{ACK \rightarrow NAK} + p_{ACK \rightarrow DTX} = 1 \quad (7.38)$$

$$p_{NAK \rightarrow NAK} + p_{NAK \rightarrow ACK} + p_{NAK \rightarrow DTX} = 1 \quad (7.39)$$

$$p_{DTX \rightarrow DTX} + p_{DTX \rightarrow ACK} + p_{DTX \rightarrow NAK} = 1 \quad (7.40)$$

In order to verify that the SFG model for MAC layer illustrated by Fig. 7.9 and Fig. 7.10 results in a valid MGF, it is checked in the following that the completeness condition Eq. (7.3) holds for the respective MGF for MAC layer formulated by Eqs. (7.31)-(7.33) and Eqs. (7.34)-(7.36).

Proof by mathematical induction:

Base case: Show that the statement holds for 1, i.e. $G_{K_{MAC},1}(z = 1) = 1$.

Substitute Eqs. (7.35) and (7.36) into Eq. (7.34), then:

$$\begin{aligned} G_{K_{MAC},1}(z) = & \\ & p_{\neg assign.error} \cdot suc [G_{K_{PHY},MAX}(z)] + \\ & p_{assign.error} \cdot suc [G_{K_{PHY},MAX}(z)] + err [G_{K_{PHY},MAX}(z)] \end{aligned} \quad (7.41)$$

Because of Eq. (7.37), then:

$$G_{K_{MAC},1}(z) = G_{K_{PHY},MAX}(z) \quad (7.42)$$

Let z be 1, then:

$$G_{K_{MAC},1}(z = 1) = 1 \quad (7.43)$$

because the MGF for PHY layer is proved to be valid in general i.e. $G_{K_{PHY},MAX}(z = 1) = 1$.

Inductive step: Assume that the statement holds for $k - 1$, i.e. $G_{K_{MAC},k-1}(z = 1) = 1$, show that the statement also holds for k , i.e. $G_{K_{MAC},k}(z = 1) = 1$.

Substitute Eqs. (7.32) and (7.33) into Eq. (7.31) and let j be k , then:

$$\begin{aligned} G_{K_{MAC},k}(z) = & suc [G_{K_{MAC},k}(z)] + err [G_{K_{MAC},k}(z)] = \\ & (p_{\neg assign.error} \cdot p_{ACK \rightarrow ACK} + p_{assign.error} \cdot p_{DTX \rightarrow ACK}) \cdot \\ & suc [G_{K_{PHY},MAX-k+1}(z)] + \\ & (p_{\neg assign.error} \cdot p_{NAK \rightarrow ACK} + p_{assign.error} \cdot p_{DTX \rightarrow ACK}) \cdot \\ & err [G_{K_{PHY},MAX-k+1}(z)] + \\ & \{ [p_{\neg assign.error} \cdot (p_{ACK \rightarrow NAK} + p_{ACK \rightarrow DTX}) + \\ & p_{assign.error} \cdot (p_{DTX \rightarrow NAK} + p_{DTX \rightarrow DTX})] \cdot suc [G_{K_{PHY},MAX-k+1}(z)] + \\ & [p_{\neg assign.error} \cdot (p_{NAK \rightarrow NAK} + p_{NAK \rightarrow DTX}) + \\ & p_{assign.error} \cdot (p_{DTX \rightarrow NAK} + p_{DTX \rightarrow DTX})] \cdot err [G_{K_{PHY},MAX-k+1}(z)] \} \cdot \end{aligned}$$

$$G_{K_{MAC},k-1}(z) \quad (7.44)$$

Let z be 1 and apply the assumption $G_{K_{MAC},k-1}(z = 1) = 1$, then:

$$\begin{aligned} G_{K_{MAC},k}(z = 1) = & [p_{\text{assign.error}} \cdot (p_{ACK \rightarrow ACK} + p_{ACK \rightarrow NAK} + p_{ACK \rightarrow DTX}) + \\ & p_{\text{assign.error}} \cdot (p_{DTX \rightarrow ACK} + p_{DTX \rightarrow NAK} + p_{DTX \rightarrow DTX})] \cdot \\ & suc [G_{K_{PHY},MAX-k+1}(z = 1)] + \\ & [p_{\text{assign.error}} \cdot (p_{NAK \rightarrow ACK} + p_{NAK \rightarrow NAK} + p_{NAK \rightarrow DTX}) + \\ & p_{\text{assign.error}} \cdot (p_{DTX \rightarrow ACK} + p_{DTX \rightarrow NAK} + p_{DTX \rightarrow DTX})] \cdot \\ & err [G_{K_{PHY},MAX-k+1}(z = 1)] \end{aligned} \quad (7.45)$$

Substitute Eqs. (7.37)-(7.40) into the equation above, then:

$$G_{K_{MAC},k}(z = 1) = G_{K_{PHY},MAX-k+1}(z = 1) \quad (7.46)$$

Since the MGF for PHY layer is proved to be valid in general i.e. $G_{K_{PHY},MAX-k+1}(z = 1) = 1$, then $G_{K_{MAC},k}(z = 1) = 1$.

Since both, base case and inductive step have been performed by mathematical induction, the completeness condition holds for the MGF for MAC layer. Q.E.D.

Applying inverse Z-transform, namely the basic Z-transform property Eqs. (7.11) and (7.12), MGFs Eqs. (7.31)-(7.33) and Eqs. (7.34)-(7.36) are transformed into PMFs Eqs. (7.47)-(7.49) and Eqs. (7.50)-(7.52), respectively. Please recall that PMFs provide another way in co-domain for our mathematic analysis as an alternative to MGFs in Z-domain.

$$P_{K_{MAC},j}(k) = suc [P_{K_{MAC},j}(k)] + err [P_{K_{MAC},j}(k)] \quad (7.47)$$

$$suc [P_{K_{MAC},j}(k)] =$$

$$\begin{aligned}
 & p_{\text{assign.error}} \cdot p_{ACK \rightarrow ACK} \cdot \text{suc} [P_{K_{PHY,MAX-j+1}}(k)] + \\
 & [p_{\text{assign.error}} \cdot (p_{ACK \rightarrow NAK} + p_{ACK \rightarrow DTX}) + \\
 & p_{\text{assign.error}} \cdot (p_{DTX \rightarrow NAK} + p_{DTX \rightarrow DTX})] \cdot \\
 & \text{suc} [P_{K_{PHY,MAX-j+1}}(k)] * \text{suc} [P_{K_{MAC,j-1}}(k)] + \\
 & p_{\text{assign.error}} \cdot (p_{ACK \rightarrow NAK} + p_{ACK \rightarrow DTX}) \cdot \\
 & \text{suc} [P_{K_{PHY,MAX-j+1}}(k)] * \text{err} [P_{K_{MAC,j-1}}(k)] + \\
 & [p_{\text{assign.error}} \cdot (p_{NAK \rightarrow NAK} + p_{NAK \rightarrow DTX}) + \\
 & p_{\text{assign.error}} \cdot (p_{DTX \rightarrow NAK} + p_{DTX \rightarrow DTX})] \cdot \\
 & \text{err} [P_{K_{PHY,MAX-j+1}}(k)] * \text{suc} [P_{K_{MAC,j-1}}(k)] \quad (7.48)
 \end{aligned}$$

$$\begin{aligned}
 & \text{err} [P_{K_{MAC,j}}(k)] = \\
 & p_{\text{assign.error}} \cdot p_{DTX \rightarrow ACK} \cdot \text{suc} [P_{K_{PHY,MAX-j+1}}(k)] + \\
 & (p_{\text{assign.error}} \cdot p_{NAK \rightarrow ACK} + p_{\text{assign.error}} \cdot p_{DTX \rightarrow ACK}) \cdot \\
 & \text{err} [P_{K_{PHY,MAX-j+1}}(k)] + \\
 & p_{\text{assign.error}} \cdot (p_{DTX \rightarrow NAK} + p_{DTX \rightarrow DTX}) \cdot \\
 & \text{suc} [P_{K_{PHY,MAX-j+1}}(k)] * \text{err} [P_{K_{MAC,j-1}}(k)] + \\
 & [p_{\text{assign.error}} \cdot (p_{NAK \rightarrow NAK} + p_{NAK \rightarrow DTX}) + \\
 & p_{\text{assign.error}} \cdot (p_{DTX \rightarrow NAK} + p_{DTX \rightarrow DTX})] \cdot \\
 & \text{err} [P_{K_{PHY,MAX-j+1}}(k)] * \text{err} [P_{K_{MAC,j-1}}(k)] \quad (7.49)
 \end{aligned}$$

$$P_{K_{MAC,1}}(k) = \text{suc} [P_{K_{MAC,1}}(k)] + \text{err} [P_{K_{MAC,1}}(k)] \quad (7.50)$$

$$\text{suc} [P_{K_{MAC,1}}(k)] = p_{\text{assign.error}} \cdot \text{suc} [P_{K_{PHY,MAX}}(k)] \quad (7.51)$$

$$\begin{aligned}
 & \text{err} [P_{K_{MAC,1}}(k)] = \\
 & p_{\text{assign.error}} \cdot \text{suc} [P_{K_{PHY,MAX}}(k)] + \text{err} [P_{K_{PHY,MAX}}(k)] \quad (7.52)
 \end{aligned}$$

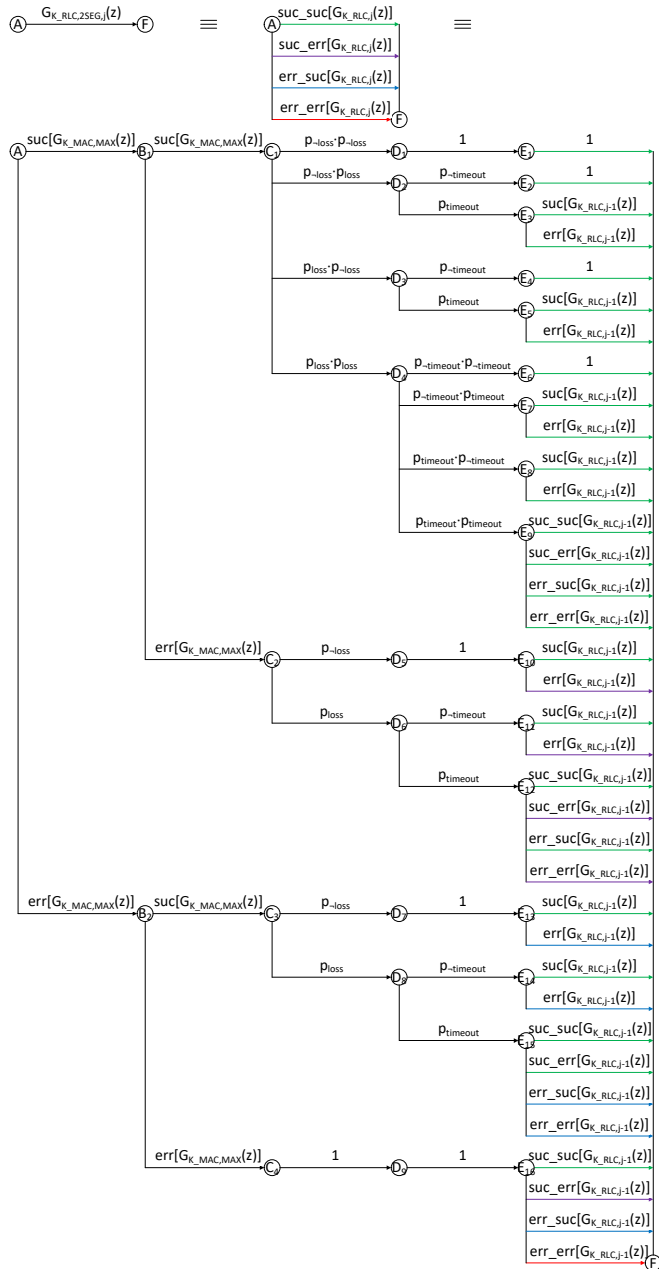


Figure 7.11: SFG for RLC layer: recursion for 2 segments

7.5 SFG Model for ARQ Protocol of RLC Layer

According to the ARQ protocol [3GP10i], an example SFG for RLC layer is shown in Fig. 7.11. Without loss of generality, it is assumed that 1 RLC SDU is segmented into 2 RLC PDUs. The model is generally applicable to any number of segments. Similar to the SFG for MAC layer, the SFG for the transmission of RLC SDU is specified as a recursion.

Firstly, the 1st segment is either transmitted successfully or unsuccessfully on MAC layer, where MAX stands for the maximum of transmissions permitted by HARQ protocol. Secondly, the transmission of the 2nd segment either succeeds or fails. Thirdly, the ACK feedback for the correctly transmitted segment is received or lost, where p_{loss} stands for the probability of ACK loss. Fourthly, the timer supervising upcoming feedbacks in case of ACK loss is either run out or not, where $p_{timeout}$ stands for the probability of timer expiration. Finally, retransmission is carried out for erroneously transmitted segments and for the segments, which are correctly transmitted but experience ACK loss and timer expiration. There is no retransmission performed for all the other cases.

According to Table 2.7, the transmission of a certain segment succeeds, if the corresponding MAC SDU is correctly transmitted on MAC layer, or the transmission on MAC layer is unsuccessful but one of the next retransmissions is successful. The transmission of the segment fails for all the other cases. Similar to the SFG for MAC layer, a path is classified to the green group, if both segments are successfully transmitted, or to the purple group, if the 1st segment is transmitted correctly but the 2nd one is in error, or to the blue group, if transmission of the 1st segment is erroneous but the 2nd one is correct, or to the red group, if both transmissions are unsuccessful. Merely the green group represents a successful transmission of RLC SDU, while all the other groups represent an erroneous transmission.

There is the case in retransmissions, that only one of the both segments is transmitted. The SFG for the transmission of 1 seg-

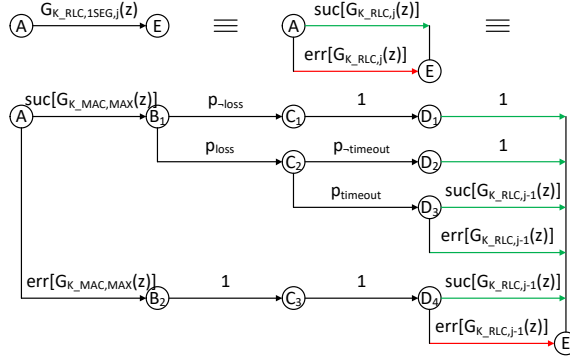


Figure 7.12: SFG for RLC layer: recursion for 1 segment

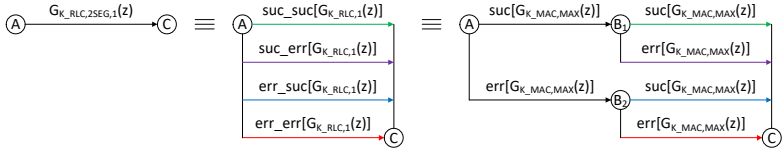


Figure 7.13: SFG for RLC layer: exit condition for 2 segments

ment is shown in Fig. 7.12.

As exit conditions for the recursions, the SFGs for the transmission of 2 segments and 1 segment within a final transmission on MAC layer are shown in Fig. 7.13 and Fig. 7.14, respectively.

The MGF of resource consumption for the exit condition is visualized by the respective SFG. The parts corresponding to green, purple, blue and red groups are given as follows, respectively.

$$G_{K_{RLC},2SEG,1}(z) = suc_suc[G_{K_{RLC},1}(z)] + suc_err[G_{K_{RLC},1}(z)] + err_suc[G_{K_{RLC},1}(z)] + err_err[G_{K_{RLC},1}(z)] \quad (7.53)$$

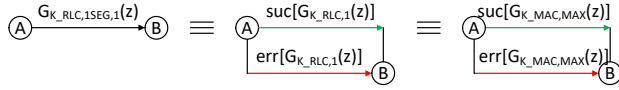


Figure 7.14: SFG for RLC layer: exit condition for 1 segment

$$suc_suc[G_{K_{RLC,1}}(z)] = suc[G_{K_{MAC,MAX}}(z)] \cdot suc[G_{K_{MAC,MAX}}(z)] \quad (7.54)$$

$$suc_err[G_{K_{RLC,1}}(z)] = suc[G_{K_{MAC,MAX}}(z)] \cdot err[G_{K_{MAC,MAX}}(z)] \quad (7.55)$$

$$err_suc[G_{K_{RLC,1}}(z)] = err[G_{K_{MAC,MAX}}(z)] \cdot suc[G_{K_{MAC,MAX}}(z)] \quad (7.56)$$

$$err_err[G_{K_{RLC,1}}(z)] = err[G_{K_{MAC,MAX}}(z)] \cdot err[G_{K_{MAC,MAX}}(z)] \quad (7.57)$$

The MGFs of resource consumption for the recursions are also visualized by the respective SFGs straightforwardly and their mathematical formulas are omitted here.

Throughput Capacity Calculation

Content

8.1 Resource, Error and Efficiency	103
8.2 User Throughput	104
8.3 Cell Capacity	105
8.3.1 Relay Enhanced Cell	106
8.4 Cell Spectral Efficiency	107

8.1 Resource, Error and Efficiency

Without loss of generality, assume that Eq. (8.1) is the MGF of resource consumption for a certain protocol layer. p_i represents the probability that an SDU with a given size is transmitted on this protocol layer under the i^{th} case. $\#PRBP_i$ represents the number of PRBPs consumed for such a transmission. As Eq. (8.2), $G_{K_{Layer}}(z)$ can be rewritten to consist of two parts, namely a success part $suc[G_{K_{Layer}}(z)]$ and a failure part $err[G_{K_{Layer}}(z)]$. e_i in Eq. (8.3) is the probability that the transmission is performed but fails and $(p_i - e_i)$ in Eq. (8.4) is the probability that the transmission is carried out and succeeds. The conditional probability $\frac{e_i}{p_i}$ is the error rate of such a transmission, while $\frac{p_i - e_i}{p_i}$ is the success rate.

$$G_{K_{Layer}}(z) = \sum_{i=1}^N (p_i \cdot z^{\#PRBP_i}) \quad (8.1)$$

$$G_{K_{Layer}}(z) = suc[G_{K_{Layer}}(z)] + err[G_{K_{Layer}}(z)] \quad (8.2)$$

$$err[G_{K_{Layer}}(z)] = \sum_{i=1}^N (e_i \cdot z^{\#PRBP_i}) \quad (8.3)$$

$$suc[G_{K_{Layer}}(z)] = \sum_{i=1}^N ((p_i - e_i) \cdot z^{\#PRBP_i}) \quad (8.4)$$

Consequently, p_i is the probability for consumption of resource $\#PRBP_i$, Eq. (8.5). p_i is the probability for error ratio equal to $\frac{e_i}{p_i}$, Eq. (8.6).

$$Prob[Resource = \#PRBP_i] = p_i, i = 1, 2, \dots, N \quad (8.5)$$

$$Prob[Error = \frac{e_i}{p_i}] = p_i, i = 1, 2, \dots, N \quad (8.6)$$

Spectral efficiency measured in $[bit/s/Hz]$ is the number of correctly received user data bits normalized by the consumed resource in time duration and in frequency bandwidth [CW13]. *Payload* represents the number of transmitted bits and, therefore, $Payload \cdot (\frac{p_i - e_i}{p_i})$ is the number of correctly received bits. $\#PRBP_i$ represents the number of consumed PRBPs, each of which occupies 1 *ms* in time domain and 180 *kHz* in frequency domain. Hence, $\#PRBP_i \cdot (10^{-3} \cdot 180 \cdot 10^3)$ is the consumed resource in $[s \cdot Hz]$. Consequently, p_i is the probability for spectral efficiency equal to $\frac{payload \cdot \frac{(p_i - e_i)}{p_i}}{\#PRBP_i \cdot (10^{-3} \cdot 180 \cdot 10^3)}$, Eq. (8.7).

$$Prob[Efficiency[\frac{bit}{s \cdot Hz}]] = \frac{payload \cdot \frac{p_i - e_i}{p_i}}{\#PRBP_i \cdot (10^{-3} \cdot 180 \cdot 10^3)} = p_i, \quad i = 1, 2, \dots, N \quad (8.7)$$

8.2 User Throughput

User throughput measured in $[bit/s]$ is the number of data bits correctly transmitted by consuming the radio resources assigned to the user within one second. *resource* represents the

number of PRBPs assigned to the user per second and, therefore, $\frac{resource}{\#PRBP_i}$ is the number of data packets, that can be transmitted for the user within one second. Obviously, $\frac{resource}{\#PRBP_i} \cdot \frac{p_i - e_i}{p_i}$ is the number of data packets correctly transmitted within one second. *payload* represents the number of data bits in a data packet and, hence, $payload \cdot \frac{resource}{\#PRBP_i} \cdot \frac{p_i - e_i}{p_i}$ is the number of data bits correctly transmitted per second. Consequently, p_i is the probability for user throughput equal to $payload \cdot \frac{resource}{\#PRBP_i} \cdot \frac{p_i - e_i}{p_i}$, Eq. (8.8).

$$Prob[throughput[\frac{bit}{s}]] = payload \cdot \frac{resource}{\#PRBP_i} \cdot \frac{p_i - e_i}{p_i} = p_i, \\ i = 1, 2, \dots, N(8.8)$$

This equation is generally applied to calculate both, throughput of direct/access link for UEs located in a donor/relay subcell and throughput of backhaul link for RNs, which is regarded as a user from its DeNB's perspective.

By implementing resource fair scheduling (cf. Chapter 4), *resource* assigned to a user in a certain subcell is then the number of PRBPs available to the subcell divided by the number of users located in the subcell. By configuring resource partitioning (cf. Chapter 10) among donor subcell, relay subcells and backhaul links in a relay enhanced cell, the number of PRBPs allocated to a certain subcell is just the number of PRBPs available to a sector cell multiplied by the resource percentage configured for this subcell.

8.3 Cell Capacity

Assume that $P_1, P_2, \dots, P_{\#point}$ are all grid elements in a cell/subcell and $f_{P_1}(r), f_{P_2}(r), \dots, f_{P_{\#point}}(r)$ represent PMFs of user throughput at the respective grid elements. $f_{P_{avg}}(r)$, which represents PMF of throughput for a user located somewhere in the cell/subcell, is then the average of $f_{P_1}(r), f_{P_2}(r), \dots, f_{P_{\#point}}(r)$, since the user has an equal chance to be located

at any grid element in the cell/subcell, Eq. (8.9).

$$f_{P_{avg}}(r) = \frac{f_{P_1}(r) + f_{P_2}(r) + \dots + f_{P_{\#point}}(r)}{\#point} \quad (8.9)$$

Assume that users $U_1, U_2, \dots, U_{\#user}$ are served by a same cell/subcell and $f_{U_i}(r)$ represents PMF of throughput for each of these user U_i . Since capacity of a cell/subcell is the sum of all user throughput achieved in the cell/subcell, $f_{U_{sum}}(r)$ representing PMF of cell/subcell capacity is the convolution of $f_{U_1}(r), f_{U_2}(r), \dots, f_{U_{\#user}}(r)$, Eq. (8.10).

$$f_{U_{sum}}(r) = f_{U_1}(r) * f_{U_2}(r) * \dots * f_{U_{\#user}}(r) \quad (8.10)$$

8.3.1 Relay Enhanced Cell

For a relay subcell, backhaul link and access links usually achieve different throughput and capacity, respectively. Capacity of two-hop links is the lower one of throughput on backhaul link and capacity on access links, since either backhaul link or access links may be the bottleneck limiting the performance of two-hop links.

If probability for backhaul link to have a throughput of $r_{backhaul}$ equals to $p_{backhaul}$, Eq. (8.11), and probability for access links to have a capacity of r_{access} equals to p_{access} , Eq. (8.12), then probability for two-hop links to have a capacity of $\min(r_{backhaul}, r_{access})$ equals to $p_{backhaul} \cdot p_{access}$, Eq. (8.13), assuming independence of backhaul link and access links. I.e., if PMF of throughput on backhaul link and PMF of capacity on access links are available, then PMF of capacity on two-hop links is derived straightforwardly.

$$Prob[throughput_{backhaul}[\frac{bit}{s}] = r_{backhaul}] = p_{backhaul} \quad (8.11)$$

$$Prob[capacity_{access}[\frac{bit}{s}] = r_{access}] = p_{access} \quad (8.12)$$

$$Prob[capacity_{2hop}[\frac{bit}{s}] = min(r_{backhaul}, r_{access})] = p_{backhaul} \cdot p_{access} \quad (8.13)$$

Assume that a relay enhanced cell consists of several subcells $C_1, C_2, \dots, C_{\#subcell}$, namely one donor subcell and $\#subcell - 1$ relay subcells. $f_{C_i}(r)$ represents PMF of capacity for the i^{th} subcell. As capacity of a relay enhanced cell is the sum of capacity achieved in each of its subcells, $f_{C_{\Sigma}}(r)$ representing PMF of cell capacity is the convolution of $f_{C_1}(r), f_{C_2}(r), \dots, f_{C_{\#subcell}}(r)$, Eq. (8.14).

$$f_{C_{\Sigma}}(r) = f_{C_1}(r) * f_{C_2}(r) * \dots * f_{C_{\#subcell}}(r) \quad (8.14)$$

8.4 Cell Spectral Efficiency

CSE is one of the performance measures for IMT-A systems as addressed in ITU-R performance requirements [IR08a]: "CSE [$bit/s/Hz/cell$] is defined as the aggregate throughput of all users divided by the channel bandwidth divided by the number of cells." Obviously, the CSE value is exactly the throughput capacity [bit/s] of a whole sector cell normalized by the total system bandwidth [Hz], which is available to each cell [$cell$].

Results for Downlink

Content

9.1	Scenario and System Parameters	109
9.1.1	UMa Scenario Parameters	110
9.1.2	Relay Deployment Parameters	113
9.1.3	LTE System Parameters	121
9.2	Resource, Error and Efficiency	122
9.2.1	Protocol Layers	124
9.2.2	Maximum of Retransmissions	126
9.3	Throughput and Capacity	127
9.3.1	Map of User Throughput	128
9.3.2	CDF of Aggregate Throughput	132
9.3.3	Mean of Aggregate Throughput	134
9.4	Validation	136
9.4.1	Impact of Scheduling on Capacity	137

9.1 Scenario and System Parameters

The analytical model comprises various scenario and system parameters without focusing concrete parameter values, cf. Chapters 6, 7 and 8. Concrete parameter values are for the first time introduced now, prior to discussing performance evaluation results.

From implementation point of view, the analytical model is implemented as a program. Parameters are defined as program variables and their values are read in during program runtime. Thereby, the program variables can be bound to any specific values and the analytical model can be applied flexibly to any

scenario assumptions and system configurations under consideration.

To be able to validate the analytical model, parameter values are selected to align this work with Sambale's work [Sam13], so that our analytical results can be compared to Sambale's system level simulation results in [Sam13].

Furthermore, a variety of resource partitioning configurations, which parameter values are other than Sambale's configuration, are examined to investigate their effect on the performance of relay enhanced systems.

9.1.1 UMa Scenario Parameters

Sambale states in [Sam13] Chapter 3 page 44, that the base coverage urban test environment is investigated in his work. Referring to [Sam13] Table 3.1 page 46, this test environment corresponds to the deployment scenario UMa. In compliance with Sambale's work, we evaluate the LTE system in the UMa scenario, cf. Chapter 3. Table 9.1 summarizes UMa scenario parameters and their values as studied in this work taken from IMT-A evaluation guidelines [IR08b] as follows.

- The number of BS antenna elements is allowed up to 8 for reception and up to 8 for transmission, and the number of UT antenna elements is allowed up to 2 for reception and up to 2 for transmission, according to [IR08b] Table 8-2 page 13. In [Sam13] Chapter 4 page 63, in order to validate results of the capacity model against simulation results, MIMO transmission is not considered and SINR is mapped to data rate according to MCS. In other words, in Sambale's simulation results the throughput capacity is evaluated based on Single Input Single Output (SISO) transmission and reception. In this work, one antenna element is employed for transmission and another one for reception at both BS and UT, since we aim to validate our

Table 9.1: Parameters of UMa scenario

BS antenna height	25 m, above rooftop
number of BS antenna elements	1 tx, 1 rx
total BS transmit power	46 dBm for 10 MHz
BS antenna down tilt angle	12°
UT antenna height	1.5 m
number of UT antenna elements	1 tx, 1 rx
maximal UT transmit power	24 dBm
minimum distance between UT and BS	≥ 25 m
carrier frequency	2 GHz
layout	hexagonal grid
inter-site distance	500 m
channel model	UMa model
user distribution	randomly and uniformly distributed over area
BS antenna gain	17 dBi (boresight)
UT antenna gain	0 dBi (omni)
BS noise figure	5 dB
UT noise figure	7 dB
thermal noise level	-174 dBm/Hz
traffic source	full buffer
bandwidth	10 + 10 MHz (FDD)
number of users per cell	200
scheduling	resource fair

results against other work related to SISO systems¹.

¹To be able to evaluate a system employing multiple antenna elements and supporting MIMO transmission and reception, our analytical model would just need to take the array gain on each parallel stream of a MIMO link into account in the SINR calculation introduced in Chapter 6. The MIMO gain is mathematically derived in [GJP02]. Our analysis method would then be well suited for MIMO based LTE-A and 5G systems, too, without introducing much computational complexity.

- "BS down tilt angle should be provided by proponents per deployment scenario", as specified in [IR08b] Section 8 page 17. It is proposed in [Sam13] Chapter 5 page 126, that optimal BS antenna down tilt is about 12° in BS only scenarios. Further, it appears reasonable to keep 12° down tilt unchanged when RNs are deployed, since different down tilt angles do not change cell capacity much. Following this, a BS antenna down tilt angle of 12° is assumed throughout this work.
- Number of users per cell is 10 in [IR08b] Table 8-5 page 15. In [Sam13] Chapter 5 page 100, 200 UTs are placed per cell instead of 10 UTs to reduce the coefficient of variation in system level simulation resulting from too small number of UTs per cell. We parameterize our scenario accordingly.
- "Packets are scheduled with an appropriate packet scheduler(s) proposed by the proponents for full buffer and VoIP traffic models separately", as specified in [IR08b] Section 7 page 6. In [Sam13] Chapter 1 page 2, rate fair scheduling is applied to achieve a same user experience ubiquitously independent of user locations within the cell. However, it is introduced in Minelli's paper [MMCG15] that PF and RR (resource fair) are two most commonly used schedulers. Thus, we do not take rate fair scheduling into consideration. Further, it is found in [MMCG15] that RR scheduling is a better choice than PF scheduling to achieve maximum cell capacity for relay enhanced LTE-A systems with more than 3 RNs per sector cell, cf. Chapter 4. Therefore, resource fair scheduling is our favorite for this work ².

²To be able to evaluate a system with PF scheduling, our analytical model should just take the scheduling gain into account in Eq. (8.8). The scheduling gain is mathematically derived in [CEA11] as the ratio between the throughput obtained with a PF scheduler and the throughput with an RR scheduler.

- BS antenna height, total BS transmit power, maximal UT transmit power, minimum distance between UT and BS and carrier frequency are given in [IR08b] Table 8-2 page 13.
- UT antenna height is given in [IR08b] Table A1-2 page 30.
- Layout, ISD, channel model, user distribution, BS antenna gain, UT antenna gain, BS noise figure, UT noise figure and thermal noise level are given in [IR08b] Table 8-4 page 14.
- Traffic source and bandwidth are given in [IR08b] Table 8-5 page 15.

Fig. 9.1 illustrates the UMa scenario. Six BSs are placed around one central BS, each establishing a site. Three sectorized antennas with a down tilt of 12° are employed by the BS and mounted above rooftop in height of 25 m at 30° , 150° and 270° , respectively, each establishing a cell. The performance of the central site is evaluated; the other sites serve to contribute interference to the central site.

9.1.2 Relay Deployment Parameters

Besides parameters for a basic scenario, additional parameters are required to represent relay deployment. Table 9.2 summarizes supplementary parameters for a relay enhanced UMa scenario, which can be categorized into three groups: infrastructure optimization related, resource configuration related, and channel model assumption related parameters.

For parameters of relay infrastructure, following values are found as optimum in Sambale's work [Sam13].

- The number of RNs per cell is set to 3 as a best solution to optimize system capacity, see [Sam13] Chapter 5 page 108. Three relays per cell appear to be the best

Table 9.2: Parameters supplemented for relay enhanced UMa scenario

number of RNs per cell	3
locations of RNs	$(0.95 \times (2/3 \times 500) \text{ m}, 0^\circ)$ $(0.7 \times (2/3 \times 500) \text{ m}, 18^\circ)$ $(0.7 \times (2/3 \times 500) \text{ m}, -18^\circ)$
RN antenna height	6.5 m, below rooftop
number of RN antenna elements	1 tx, 1 rx
total RN transmit power	20 dBm for 10 MHz
association SINR offset	0 dB
resource allocation between BS and RNs	orthogonal
resource allocation among RNs of a cell	reused
resource percentage for direct links (BS \leftrightarrow UT)	46 %
resource percentage for backhaul links (BS \leftrightarrow RN)	41 %
resource percentage for access links (RN \leftrightarrow UT)	13 %
RN antenna gain	0 dBi (omni)
RN noise figure	7 dB
path loss between RN and UT	UMa model
path loss between BS and RN	UMa model
path loss between BS and UT	UMa model
LoS probability between RN and UT	UMi model
LoS probability between serving BS and RN	1
LoS probability between interfering BS and RN	0
LoS probability between BS and UT	UMa model

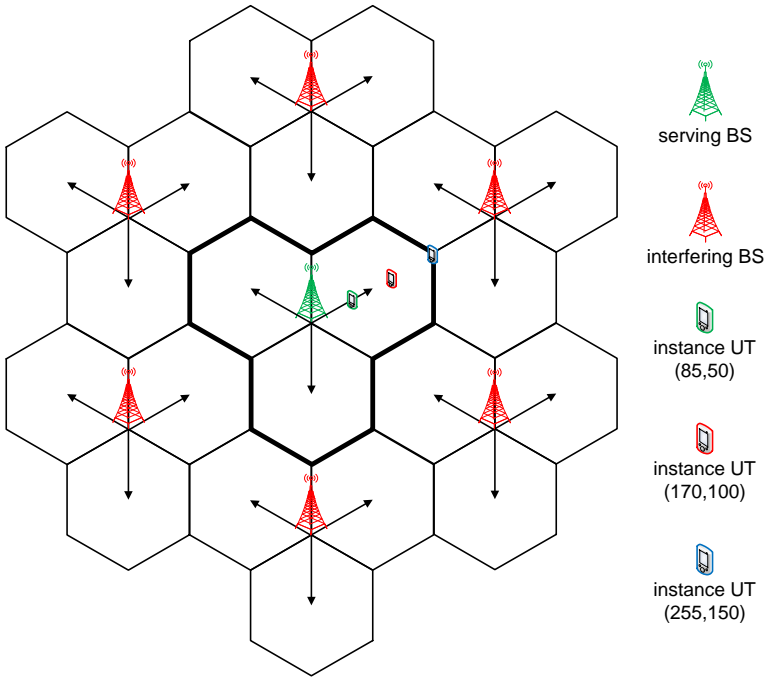


Figure 9.1: UMa scenario

compromise between performance gain and infrastructure cost, since the highest cell capacity increase per additional relay is achieved for up to three relays. Four or more relays per cell are not worth considering owing to limited possible cell capacity increase. Table 4.1 confirms that deploying about 3 RNs per cell is a good choice, since nine out of twelve different research teams participating in 3GPP self-evaluation have also evaluated scenarios with 3 to 4 RNs per cell.

- Locations of RNs are given in [Sam13] Chapter 5 page 104: For three RNs per cell, one RN is placed in BS antenna boresight direction at a distance of 0.95 times cell

diameter, where one cell diameter equals two thirds of ISD. The other two RNs are placed symmetrically 18° apart from BS antenna boresight at a distance of 0.7 times cell diameter. Placing three RNs properly at cell edge almost completely achieves maximal possible cell capacity increase.

- RN antenna height of 6.5 *m* is optimal for 3 RNs per cell, as shown in [Sam13] Figure 5.19 page 115.
- Association SINR offset of 0 *dB* appears to provide a close to optimal capacity for 3 RNs per cell in [Sam13] Chapter 5 page 116, where a UT is either associated to a BS or an RN dependent on best received mean SINR.
- RN transmit power of 20 *dBm* is found suitable for a cost efficient and capacity close to optimal operation of 3 RNs per cell, see [Sam13] Chapter 5 page 124.
- In Sambale's simulation results, MIMO transmission is not considered, see [Sam13] Chapter 4 page 63. In this work, RNs employ one antenna element for transmission and another one for reception, the same number of antennas as BSs and UTs.

Besides these parameter values, diverse relaying deployment scenarios can be studied with our model, i.e. any number of RNs per cell, any locations of RNs, any RN antenna height, any RN transmit power and any association SINR offset.

3GPP technical report [3GP10b] Annex A Table A.2.1.1.4-3 page 72 also specifies reference parameter values for deployment of RNs in Case 1 scenario (cf. Chapter 3): Maximal RN transmit power is set to 30 *dBm* for 10 *MHz* bandwidth; RN antenna is mounted at a height of 5 *m*; RN employs 2/4 transmit and 2/4 receive antenna ports; The number of RNs per cell and locations of RNs are not specified. Sambale's study optimizes the number of RNs per cell and RNs' locations in a cell, and

then finds out a complete set of optimum values for the other parameters based on the optimal relay placement, cf. Chapter 4. Hence, Sambale's optimum values are regarded as default in our study, instead of 3GPP's reference values, especially for the purpose of validating our results.

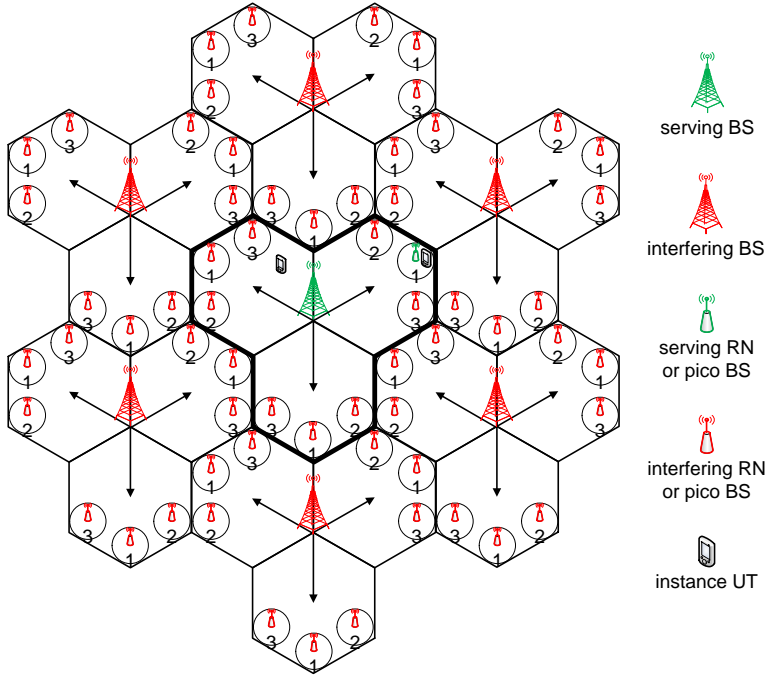


Figure 9.2: Relay enhanced UMa scenario

Fig. 9.2 illustrates the relay enhanced UMa scenario, which is developed based on the basic UMa scenario illustrated in Fig. 9.1. Three RNs per cell are placed 0.95, 0.7 and 0.7 cell diameter away from the center BS in antenna boresight direction, counter clockwise 18° and clockwise 18° rotated from the boresight direction, respectively. One omnidirectional antenna is employed by the RN and mounted below rooftop in height of 6.5 m. One

tier of six BSs each with nine RNs is taken into account for interference consideration in the analytical evaluation.

Parameters with respect to radio resource are configured in [Sam13] as follows.

- Resource allocation is illustrated in [Sam13] Figure 5.12(b) page 108: In the first partition of a radio frame a BS serves its UTs. In the second partition the BS transmits to its RNs sequentially. In the third partition all RNs serve their UTs simultaneously, while the BS is not transmitting. In other words, a BS and its RNs operate on orthogonal radio resources, while resources allocated to RNs of a cell are reused among them. Besides, resources for backhaul links are exclusively reserved and not available to direct links and access links.

Further, Sambale addresses in another paper [SW12], that a simultaneous transmission from BS and RNs to UTs in same subframes, works only for one RN per BS. Otherwise, BS would interfere other RNs within the same cell. In other word, BS and RNs shall use orthogonal radio resources in time or frequency domain, since otherwise mutual interference would be too high to get any capacity gain from deployment of relays.

- Resource partitioning is specified in [Sam13] Chapter 5 page 107: About 85% of frame resources are occupied by BS, roughly 50% for serving UTs via direct links and 35% to feed RNs via backhaul links. About 15% of frame resources are used by RNs to serve UTs via access links. Further, resource percentage can be measured more precisely from [Sam13] Figure 5.12(b) page 108: 46% for direct links, 41% for backhaul links, 13% for access links.

With these parameters, diverse resource allocation and resource partitioning can be studied, no matter whether resources are allocated between a BS and its RNs on an orthogonal or reused basis, and no matter how much percentage of

resources are partitioned for direct, backhaul and access links, respectively.

During 3GPP self-evaluation process several companies have studied whether same radio resources shall be reused by eNB and RNs to serve UEs, cf. Chapter 4. Following studies show that in interference limited environment just like 3GPP Case 1 or ITU-R UMa scenario (cf. Chapter 3), allocation of orthogonal instead of reused radio resources to eNB and RNs to serve its macro UEs and their relay UEs, respectively, is a good choice.

1. ZTE's study [ZTE09] assumes frequency reuse across eNB and RNs. It turns out that deployment of relays in this way does not bring any gain but a loss of 2% compared to deployment without relays. Results reveal that strong interference from eNB to UEs served by RNs significantly limits data rate on access links, since eNB and RNs are geographically crowded with aggressive frequency reuse.
2. Qualcomm's study [Qua10] proposes a cooperative silencing scheme, where macro cells do not transmit and remain silent for a number of subframes during each radio frame, and these subframes are used exclusively by relays to serve relay UEs, so that relay UEs do not see interference from macro cells. As a result, dominant interference from macro cells to UEs served by relays is effectively mitigated. It turns out that the cooperative silencing scheme contributes an additional gain of 21%.
3. LG Electronics' study [LG 10] observes that macro UEs naturally enjoy a cooperative silencing effect of relays during backhaul subframes, namely all the relays simultaneously turn off their transmission to receive backhaul signal from the macro cell. The study proposes that transmission to macro UEs experiencing severe interference in access subframes is multiplexed with transmission to

RNs in backhaul subframes. As a consequence, interference from relays to a considerable number of UEs served by macro cells is mitigated. It turns out that the cooperative silencing effect contributes an additional gain of 6%.

Parameters of channel model are taken from [Sam13] as follows.

- Path loss, both between RN and UT and between BS and RN, follows the UMa model in [Sam13] Chapter 3 page 49, since path loss model for the UMa scenario is also valid for typical relay antenna heights expected to be down to 5 m. This is exactly what IMT-A evaluation guidelines specify in [IR08b] Annex 1 page 28: "The link from a relay to a mobile station can be modeled with the same models as the conventional link from a base station to a mobile station. The links from base stations to relay stations can be modeled with conventional links."
- LoS probability between RN and UT follows the Urban Micro-cell (UMi) model ³ in [Sam13] Chapter 3 page 49, because the optimized RN antenna height is expected to be in the range of 5-10 m, which is much closer to the BS antenna height in the UMi scenario. According to IMT-A evaluation guidelines [IR08b] Table A1-3 page 31 and Table 8-2 page 13, LoS probability has individual functions for UMa and UMi scenario, where BS antenna is mounted in height of 25 m and 10 m, respectively.
- RN backhaul condition is assumed optimal in [Sam13] Chapter 5 page 117. RNs are carefully placed below rooftop so that the radio link to their serving BS is LoS

³In UMi channel model [IR08b], LoS Probability p_{LoS} is defined as a function of distance d in m as follows.

$$p_{LoS}(d) = \min(18/d, 1) \cdot (1 - \exp(-d/36)) + \exp(-d/36) \quad (9.1)$$

and the radio link to each of their interfering BSs is NLoS, which leads to a highest possible SINR on backhaul link. In other words, LoS probability is set to 1 between serving BS and RN and 0 between interfering BSs and RN.

- Both Path loss and LoS probability between BS and UT in the relay enhanced UMa scenario comply with the UMa model, which is nothing other than in the basic UMa scenario.
- RN antenna pattern is assumed omnidirectional in [Sam13] Table 5.1 page 97. Consequently, RN antenna gain is set to 0 *dBi*.
- RN noise figure is assumed 7 *dB* in [Sam13] Table 3.6 page 57.

It is stated in 3GPP technical report [3GP10b] Annex A page 70: "For 3GPP Case 1 relay scenario, the placement of relay could be taken by two major steps. 1) Virtual relay placement: A virtual relay is placed trying to enhance the cell edge throughput or overall cell throughput. 2) Relay site planning: Finding an optimal place among N candidate relay sites around the virtual relay which offers optimization of LoS probability and etc. The site planning procedure provides benefit on backhaul SINR." Obviously, the optimization of RN locations achieves step 1, while the assumption of RN backhaul condition reflects step 2.

9.1.3 LTE System Parameters

LTE system parameters relevant to this work and their standard values from experience are summarized in Table 9.3. These parameter values have been used earlier for system performance evaluation by Ericsson Eurolab [Hoy13]. Ericsson researchers say that some target values of LTE system parameters appeared in early versions of 3GPP specs, but are no longer contained in the current version.

Table 9.3: LTE system parameters

max. number of HARQ retransmissions	4-8
max. number of SR-ARQ retransmissions	1-3
probability of scheduling misdetection	1%
probability of ACK/NAK/DTX misdetection	0.1%
probability of ACK/NAK loss on RLC	0.1%
probability of ACK/NAK timeout on RLC	0.1%

- Maximal number of transmission repetitions is proposed 4-8 for HARQ protocol on MAC layer and 1-3 for SR-ARQ protocol on RLC layer, respectively.
- Probability of PDCCH misdetection on PHY layer is set to 1%, which is used for system evaluation by all 3GPP proponents;
- Probability of HARQ feedback misdetection on MAC layer is set to 0.1%, where a NAK or DTX is erroneously interpreted decoded as an ACK, ACK or DTX as NAK, and ACK or NAK as DTX;
- Probability of SR-ARQ feedback loss on RLC layer and probability of SR-ARQ feedback timeout on RLC layer are both assumed 0.1% in this work. In case of feedback loss, an ACK or NAK is lost. In case of feedback timeout, the timer waiting for an ACK or NAK is run out.

With these parameters, diverse HARQ and SR-ARQ processes can be studied, e.g. no retransmission, only one repeated transmission, and multiple repetitions, respectively.

9.2 Resource, Error and Efficiency

In this section, resource consumption, error rate and spectral efficiency, which are closely related to user throughput and

cell capacity, are analytically calculated with SFG models for user locations within the basic UMa scenario with predefined parameters, taking LTE protocol specific characteristics into account. For a user location, each performance measure is a random variable owing to randomness of radio channel conditions and control signaling errors.

Performance measures on MAC layer are presented as an example here, assuming that one retransmission is permitted for HARQ protocol at maximum. Results for RLC layer and based on the assumption that more retransmissions are allowed, do not differ much, which are shown in following subsections.

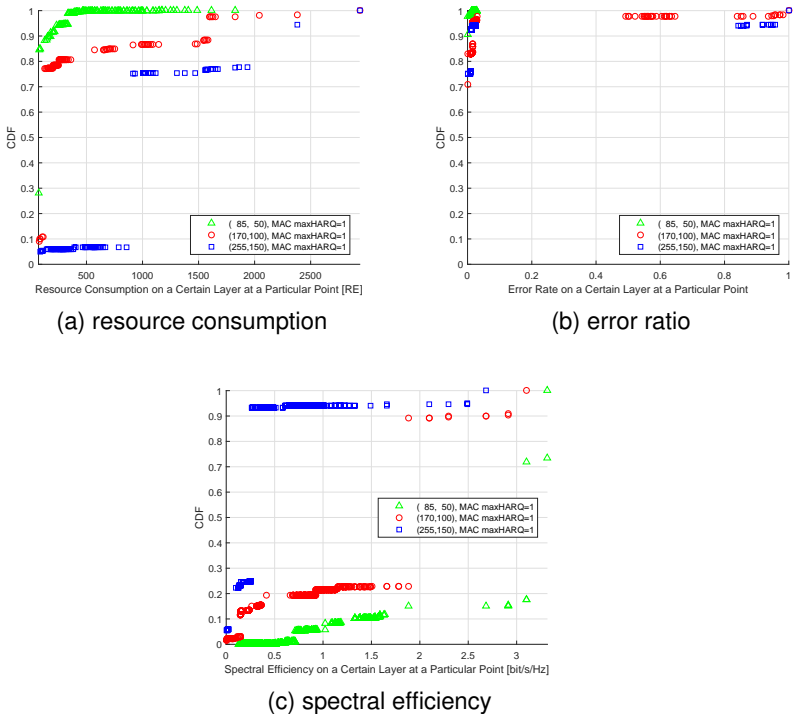


Figure 9.3: CDFs of performance criteria on MAC layer at three locations

CDFs of resource consumption, error ratio and spectral efficiency are shown for example locations in Fig. 9.3a, Fig. 9.3b and Fig. 9.3c, respectively. Three example locations are as specified in Fig. 9.1 in the north east cell of the central site in the basic UMa scenario, namely green, red and blue locations in antenna boresight direction and $1/3$, $2/3$ and 1 cell radius away from the center BS, respectively. One cell radius corresponds to $2/3$ ISD.

It is worth mentioning, that all the performance measures here are discrete random variables, which CDF is a step function with left closed and right open intervals, and takes a jump at values of probability masses. Besides, CDF is plotted here only for values, where its corresponding PMF has a non-null probability. This leads to both jumps and spaces of a CDF curve in diverse figures.

Owing to best radio channel conditions, a user at green location consumes fewest resources, experiences lowest error ratio and achieves highest spectral efficiency. Due to worst channel conditions, a user at blue location consumes most resources, experiences highest error ratio and achieves poorest spectral efficiency. Then, the three example locations (85, 50), (170, 100), and (255, 150) represent a best, medium and worst case, respectively.

9.2.1 Protocol Layers

CDFs of resource consumption, error ratio and spectral efficiency are plotted in Fig. 9.4a, Fig. 9.4b and Fig. 9.4c, respectively, for the worst example location (255, 150). Performance measures on PHY, MAC and RLC layers are calculated assuming that at maximum one retransmission is permitted by HARQ protocol on MAC layer and another one retransmission is allowed by SR-ARQ protocol on RLC layer to reduce residual errors.

Even at the worst example location, there is only a neglectable discrepancy in expected value of spectral efficiency

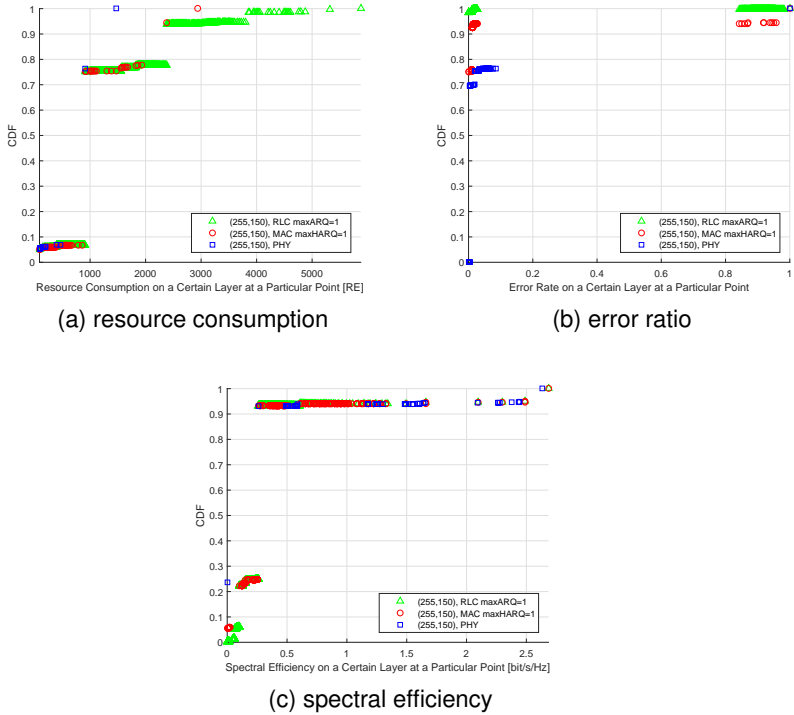


Figure 9.4: CDFs of performance criteria on three protocol layers

between MAC layer and RLC layer.

Compared to PHY layer, the spectral efficiency of MAC layer is improved; The error ratio is significantly reduced, since most of the residual errors from PHY layer are corrected by retransmission; Additional resources are consumed for retransmission by HARQ protocol. Compared to MAC layer, the spectral efficiency of RLC layer is further slightly improved; The extra resource consumption is caused by SR-ARQ retransmission; The error ratio is reduced further because of the correction of residual errors resulting from MAC layer by retransmission. Hence, error ratio is minimized not at a cost of spectral efficiency, but

resource consumption.

9.2.2 Maximum of Retransmissions

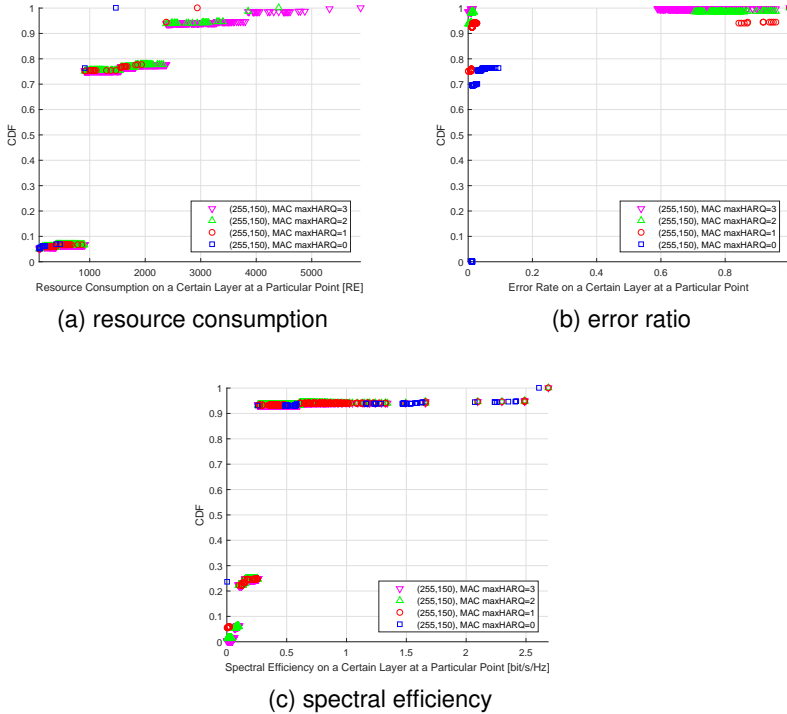


Figure 9.5: CDFs of performance criteria for increasing maximums of HARQ retransmissions

In the MAC layer model, the maximal number of retransmissions by the HARQ protocol is regarded as a most important parameter. Impact of the maximum of retransmissions on system performance is investigated for the worst example location (255, 150) in Figs. 9.5a-9.5c. No retransmission is performed in blue case, and maximal 1-3 retransmissions in red, green and pink cases, respectively.

CDFs of resource consumption in Fig. 9.5a increase with the number 0-3 of retransmissions, while CDFs of error ratio in Fig. 9.5b decrease and CDFs of spectral efficiency in 9.5c increase correspondingly. Clearly, retransmissions cause resource consumption but reduce error ratio and improve spectral efficiency.

Results of blue case are almost the same as results of PHY layer, except that PDCCH misdetection is not taken into account for error ratio calculation on PHY layer but for MAC layer, and MAC header is considered to be overhead for spectral efficiency calculation on MAC layer, but payload for PHY layer.

Even at the worst example location, the discrepancy in expected value of spectral efficiency is already at an acceptable level among different maximums of retransmissions, so long as more than one retransmission is performed by HARQ protocol in MAC layer model.

Increasing the maximum number of retransmissions, expected value of resource consumption is slightly increased and saturate, while error ratio is significantly reduced approaching zero. Of particular importance, expected value of spectral efficiency is raised converging to 0.3598 bit/s/Hz . It is found that by employing HARQ protocol on MAC layer in LTE systems, increasing the maximum number of retransmissions does not deteriorate expected value of spectral efficiency, but improves it a little bit. It is concluded that retransmissions of erroneously received data, although consuming extra resources, revise residual errors left over by previous transmissions not at a cost of spectral efficiency, but delay.

9.3 Throughput and Capacity

In this section results for both, user throughput and cell capacity are shown for downlink. Results are presented for three system types, namely macro cell only, macro cell enhanced

with three RNs connected by wireless backhaul, and macro cell enhanced with three pico BSs connected by wired backhaul.

In both systems RNs/pico BSs are equally placed according to relay deployment parameters in Table 9.2. Further, in both systems radio resources are identically partitioned following Table 9.2. In particular, radio resources allocated to backhaul links in the RN enhanced system are unused in the pico BS enhanced system.

9.3.1 Map of User Throughput

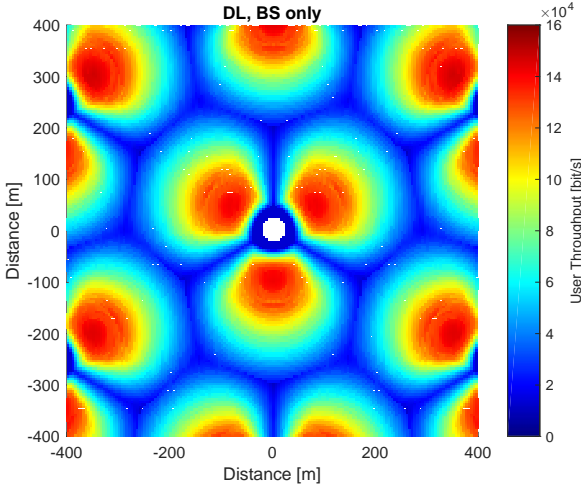


Figure 9.6: DL throughput map of BS only system

In the multi-cell scenario a $5\text{ m} \times 5\text{ m}$ grid is introduced over an $800\text{ m} \times 800\text{ m}$ service area of the scenario. A multi-cell scenario map of user throughput shows for each grid element in the service area the mean throughput of a single user located at the grid element.

Fig. 9.6, serving as baseline, shows the multi-cell scenario map of user throughput for a system with macro cells only.

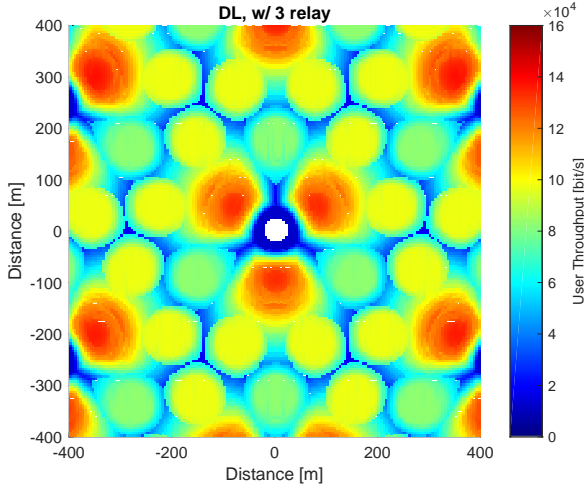


Figure 9.7: DL throughput map of RN enhanced system

User throughput map for a system enhanced by three RNs per cell is shown in Fig. 9.7⁴, while user throughput map for a system enhanced by three pico BSs per cell is shown in Fig. 9.8. If radio resources allocated to backhaul links were also utilized in the pico BS enhanced system, Fig. 9.8 would then be scaled up dramatically.

It is visible in Fig. 9.6 that cell areas in antenna boresight and nearby BSs achieve highest user throughput $\geq 12 \times 10^4 \text{ bit/s}$ thanks to good radio channel conditions. Site edges, borders between adjacent cells and circular areas close by BSs suffer from strong cochannel interference from either neighbor BSs or adjacent cells resulting in worst user throughput $\leq 4 \times 10^4 \text{ bit/s}$.

Donor cells and relay cells in Fig. 9.7 have exactly the same coverage as donor cells and pico cells in Fig. 9.8, respectively. Area sizes served by RNs/pico BSs 1, 2 and 3 (specified in Fig. 9.2) are 19%, 18% and 18% of a whole cell size, respectively.

⁴The computational cost for e.g. the result in Fig. 9.7 is about 10 days on a 64 computer cluster.

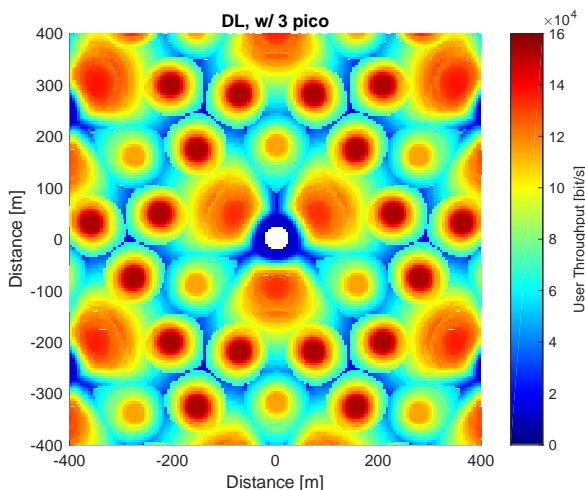


Figure 9.8: DL throughput map of pico BS enhanced system

Relay/pico cells (hereafter referred to as small cell in common) 2 and 3, which are placed axis-symmetrically to antenna boresight of a BS and partially lie in transition region between cell edge and cell center, have the same but less coverage than small cell 1 located in boresight of BS antenna at cell edge. A donor cell and all three small cells together cover 45% and 55% of a cell, respectively.

Comparing Fig. 9.7 with Fig. 9.8 to find their common trait, areas in antenna boresight of the macro BS and nearby, and center areas in small cells benefit from highest throughput, respectively, thanks to good radio channel condition. Edge areas of macro cells and edge areas of their small cells suffer from lowest throughput, respectively, owing to strong cochannel interference by adjacent macro cells and small cells, respectively.

Besides, small cells 2 and 3 have a same behavior in terms of throughput owing to symmetry. small cell 2 has slightly higher throughput than small cell 1, since radio resources assigned to access links per user in small cell 2 are a little bit more than

those in small cell 1, which results from the fact that the same amount of radio resources is reused between small cells 1 and 2, but there are less users due to less coverage in small cell 2 than in small cell 1.

Comparing Fig. 9.7 to Fig. 9.8 to discover their characteristic feature, users served by macro BSs see a same local throughput in both pico BS enhanced and RN enhanced systems, owing to use of a same macro BS antenna. Pico cell users are served with higher throughput than relay cell users, because pico cells have a wired backhaul not limiting any throughput on access links as is the case with wireless backhaul of relay cells. Throughput of the area served by relay cells is slightly lower than that of the area directly served by macro cell, while throughput of pico cells is a little bit higher than that of macro cell.

In addition, relay cell centers have lower throughput than pico cell centers, but relay cell edges and pico cell edges have comparable throughput. Access links of UTs located in center-/edge areas of a relay cell and access links of UTs in center-/edge areas of a pico cell apply comparably high/low valued MCSs. For UTs of pico cells throughput is just determined by their access links, while for UTs of relay cells throughput may be limited by their backhaul links besides their access links. A backhaul link of two-hop UTs, regardless whether located in center or at edge of a relay cell, apply same MCSs merely depending on radio channel conditions between donor BS and RN. For UTs in center of relay cells the MCSs applied on backhaul links are not high enough to satisfy the MCSs applied on access links and then backhaul links become a bottleneck reducing the throughput provided on access links⁵. In contrast, for UTs at edge of relay cells the MCSs applied on backhaul links are high enough to support the MCSs applied on access links and thus there exists such a bottleneck effect only marginally.

⁵During 3GPP self-evaluation process Intel (UK) [Int10] has observed the same behavior and proposed to apply MIMO transmission on backhaul to overcome the bottleneck, cf. Chapter 4.

Intuitively, in Fig. 9.7 RNs bring yellow, green and cyan colors to areas, that otherwise would appear in blue in Fig. 9.6. Pico BSs bring even red and orange in addition to these areas in Fig. 9.8. In summary, RNs contribute much and pico BSs contribute even more to improve user throughput. It is further visible, that UTs are served with a high location dependent variance of throughput in Fig. 9.6, while UTs are served much more fairly over the cell area in both Fig. 9.7 and Fig. 9.8. Summarizing, both RN enhanced and pico BS enhanced systems have better fairness in terms of location dependent user throughput compared to a system with macro BS only.

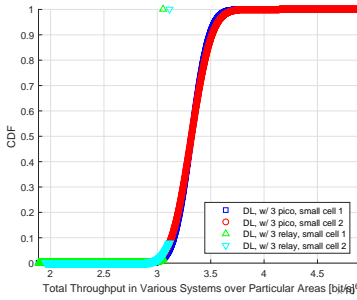
9.3.2 CDF of Aggregate Throughput

An aggregate throughput for a certain area is a total of user throughputs of all users located within the area considered. Since user locations, radio channel conditions and control signaling errors etc. are all random variables, the aggregate throughput is also a random variable which probability distribution can be presented by a CDF. Grid elements introduced in last section are considered as potential user locations in this section.

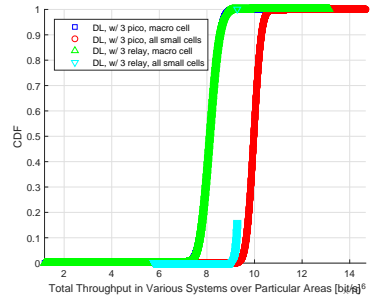
CDFs of aggregate throughput are shown in Fig. 9.9a for areas of small cell 1 and small cell 2, in Fig. 9.9b for areas of donor cell and all the three small cells together, and in Fig. 9.9c for area of a whole sector cell. Please note the abscissa scales of these three figures are different from each other; Order of magnitude is $\times 10^6$ in the former two figures and $\times 10^7$ in the latter one figure. Small cell 3 omitted here has a same aggregate throughput as small cell 2, because they are placed axis-symmetrically to antenna boresight of a macro BS.

CDFs are plotted only for throughput values, for which corresponding PMFs have non-null probability. E.g., the cyan CDF of Fig. 9.9a jumps sharply from a probability of 9% to 100% at the throughput of $3.1 \times 10^6 \text{ bit/s}$, because its corresponding PMF has a probability of 91% for this throughput value. Sim-

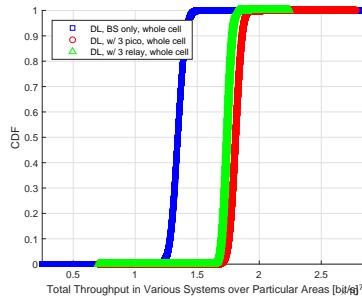
ilar jumps can be found in the green curve of Fig. 9.9a and the cyan curve of Fig. 9.9b.



(a) single small cells



(b) donor cell and all small cells together



(c) whole sector cell

Figure 9.9: CDFs of DL aggregate throughput for various cell areas

In Fig. 9.9a relay cell 2 has a slightly higher throughput than relay cell 1, since the wireless backhaul link from BS to RN 2 has better radio channel conditions than the backhaul from BS to RN 1. Pico cells 1 and 2 have a comparable throughput, because the wired backhaul from BS to pico BS 1 is not other than the wired backhaul from BS to pico BS 2. In Fig. 9.9b both RN enhanced system and pico BS enhanced system provide a rather higher throughput over their small cells than over their

donor cell, as desired.

In Fig. 9.9a pico cell 1 has a higher throughput than relay cell 1, as expected. CDF for pico cell 1 also reveals the throughput that can be provided by access links in relay cell 1. CDF for relay cell 1 first follows CDF for pico cell 1 during its flat phase, and then the relay CDF rockets when the pico CDF just begins to surge steeply at a threshold of $3.1 \times 10^6 \text{ bit/s}$. The threshold reflects the throughput that can be provided by the backhaul link for relay cell 1. It is worth mentioning that such a threshold shall be well selected as high as necessary and as low as possible. If the threshold was too low, then the throughput of access links could not be covered by the throughput of backhaul link; If the threshold was too high, then the throughput of backhaul link could not be exhausted by the throughput of access links. This observation is also valid for other small cells and, as a consequence, for the case of all small cells together in Fig. 9.9b. Besides, donor cell has a same throughput in both systems enhanced with small cells, no doubt.

In Fig. 9.9c, the RN enhanced system raises the throughput significantly compared to the BS only system, owing to good radio channel condition on access links associating two-hop UTs to RNs and radio resource reuse on access links among multiple relay cells. The pico BS enhanced system further boosts the throughput in comparison to the RN enhanced system, thanks to not only retaining both good channel condition and resource reuse on access links but also employing wired backhauls instead of wireless ones. If radio resources reserved for backhaul links were utilized by access and direct links in the pico BS enhanced system, CDFs for each individual pico cell, a donor cell, all pico cells together and a whole sector cell would be shifted to the right dramatically.

9.3.3 Mean of Aggregate Throughput

Referring to the green CDF in Fig. 9.9c as an example, there is a 99% probability that the random parameter of aggregate

throughput lies within an interval ⁶ of $(1.65, 1.85) \times 10^7 \text{ bit/s}$. Similarly, intervals can be identified for other CDFs in Figs. 9.9a-9.9c aiming at a certain probability.

A mean of aggregate throughput is given for each area in the form of both numbers in Table 9.4 and bar charts in Fig. 9.10. In particular, the mean aggregate throughput for a whole sector cell (cell capacity) is a most widely used performance measure in 3GPP related works, cf. Table 4.1.

Table 9.4: DL aggregate throughput over some area in some system $\times 10^7 \text{ [bit/s]}$

	BS only	3 RNs	3 pico BSs (59% resource)	3 pico BSs (100% resource)
donor cell	1.3441	0.8115	0.8115	1.3754
small cell 1	-	0.3053	0.3322	0.5631
small cell 2	-	0.3109	0.3321	0.5629
small cell 3	-	0.3109	0.3329	0.5642
all small cells	-	0.9272	0.9972	1.6902
whole cell	1.3441	1.7386	1.8086	3.0654

The pico BS enhanced system is listed for two cases: The first case, which utilizes the 59% radio resources only, allocates 46% to direct links and 13% to access links just the same as the RN enhanced system, cf. Table 9.2; The second case, which fully utilizes the 100% radio resources in full, allocates besides the 59% the other 41% radio resources reserved for backhaul links to direct links and access links according to their respective ratios. Based on the first case, the second case raises the mean of aggregate throughput for donor cell and pico cells, and consequently the cell capacity by $69\% = \frac{1}{1-41\%} - 1$.

Three LTE system types considered are compared against one another in terms of cell capacity. Compared to a system

⁶The probability and the interval here are something like but, in a strict sense, shall not be misinterpreted as a confidence level and a confidence interval, respectively.

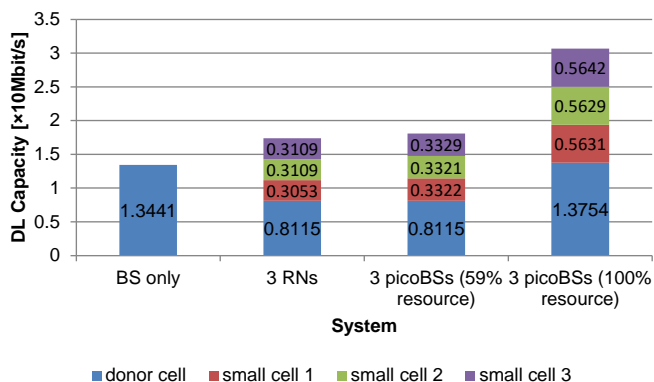


Figure 9.10: DL aggregate throughput over various areas in different systems [$\times 10^7 \text{ bit/s}$]

with BS only, a system enhanced with three RNs per cell improves cell capacity from $1.3441 \times 10^7 \text{ bit/s}$ by 29% to $1.7386 \times 10^7 \text{ bit/s}$. A system enhanced with three pico BSs per cell improves cell capacity by 35% and 128% to $1.8086 \times 10^7 \text{ bit/s}$ and $3.0654 \times 10^7 \text{ bit/s}$ in case of 59% and 100% resource usage, respectively. Hence, the pico BS enhanced system is the winner in terms of cell capacity.

9.4 Validation

Results based on system level simulation are used to validate results derived from our analytical model. Sambale's work [Sam13] is taken into account as the first reference. Saleh's work [SmBR⁺11] is considered as the second reference.

Figure 9.11 shows CSE bar charts for deployments with and without RNs from Sambale's, Saleh's and our works, respectively. Sambale's CSE results are measured from CSE bar charts for 0 and 3 RNs marked as simulation in [Sam13] Figure 5.5 page 100. Saleh's CSE results are derived from CDFs of UE throughput for eNB only and 4 RNs cases in [SmBR⁺11] Figure

4, which are also explicitly given in CSE bar charts for a cell with BS only and a cell with RNs marked as external results in [Sam13] Figure 5.8 page 103. In this work, CSE values are unambiguously derived from aggregate throughput of a whole sector cell in Table 9.4 for a cell with BS only and a cell with 3 RNs, respectively, normalized by the total downlink bandwidth in Table 9.1.

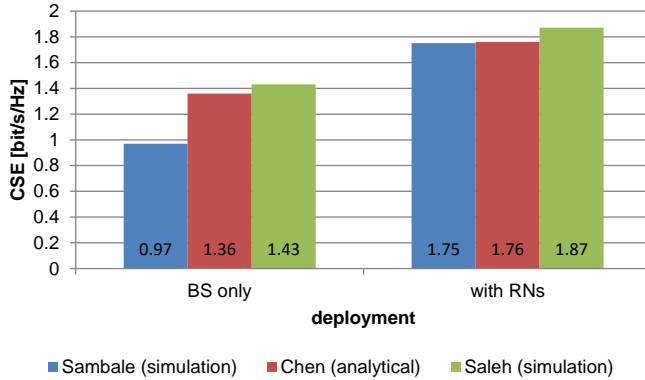


Figure 9.11: Validation of analytical results against system level simulation based references

Compared to Saleh’s results, our results deviate by only -5% for both, a cell with BS only and a cell with RNs. A comparison to Sambale’s results shows a neglectable discrepancy of 1% for a cell with RNs but a large discrepancy of 40% for a cell with BS only.

9.4.1 Impact of Scheduling on Capacity

It is impossible to find an external work based on exactly the same assumptions as made in this work. As described in detail at the beginning of this chapter, most of our assumptions align with Sambale’s, however, there is still one exception: Sambale assumes rate fair scheduling among users, while Saleh and we

assume resource fair scheduling.

Intuitively, a most possible reason for the discrepancy in CSE figures for BS only case is the difference between scheduling strategies applied. With resource fair scheduling, all users no matter at cell edges or in cell centers get a same amount of radio resources. In contrast, with rate fair scheduling, cell edge users applying lower order MCSs drain too much radio resource, whilst cell center users applying higher order MCSs obtain very limited radio resource. In consequence, applying rate fair instead of resource fair scheduling leads to a loss in CSE.

Taking deployment of relays into consideration, most macro cell edges of a basic scenario turn into relay subcell centers of a relay enhanced scenario. In other words, the amount of users located in edge/center areas of macro cells in a basic scenario are much more/less than the amount of users located in edge/-center areas of both donor and relay subcells in a relay enhanced scenario. Then, applying rate fair instead of resource fair scheduling in a basic scenario leads to a substantial resource exhaustion at cell edges and a serious resource shortage in cell centers, and consequently an obvious CSE loss compared to a relay enhanced scenario.

This explains why there is a large discrepancy for a cell with BS only but a neglectable discrepancy for a cell enhanced with RNs between Sambale's CSE results and both Saleh's and our CSE results in Fig. 9.11. Furthermore, the comparison reveals that non-relay systems are sensitive to scheduling strategies with respect to CSE, whilst relay enhanced systems are much more tolerant towards scheduling strategies.

Resource Partitioning in Relay Enhanced Cells

Content

10.1	Introduction	139
10.2	Results for Downlink of Relay Enhanced Systems .	140

10.1 Introduction

Resource partitioning shall be well configured for relay enhanced cells to gain a maximum of system performance. Radio resources available to a cell are divided into partitions and resource partitions are assigned to BS and RNs in an orthogonal or reused manner for transmission on direct links between BS and UTs, backhaul links between BS and RNs and access links between RN and UTs.

According to configuration parameters in Table 9.2 for a relay enhanced cell, all RNs reuse the same radio resources, while BS and RNs use orthogonal radio resources in time or frequency domain. Radio resources are partitioned 50% for direct links, 35% for backhaul links, and 15% for access links, respectively. Under this circumstance capacity maximum is achieved. However, throughput fairness so far is not taken into consideration for users located in different cell areas.

In this chapter optimum resource partitioning for relay enhanced cells is investigated to achieve not only maximum cell capacity but also fair user throughput. Our analytical framework is applied to calculate throughput of a user at various locations and capacity of all users in a cell under different resource

partitioning conditions. The percentage of radio resources assigned to donor subcell, backhaul links and relay subcells are studied to find out the optimum, as all the other configuration parameters in Table 9.2 are kept unchanged.

10.2 Results for Downlink of Relay Enhanced Systems

Radio resources (RRs) of a cell are partitioned into exclusive RRs to be (1) reused by RNs, (2) used as backhaul for RNs, and (3) used by the donor BS. In order to identify optimum resource partitioning aiming at highest cell capacity, we study various RR assignments to the three partitions mentioned.

For each way of partitioning of RRs represented by the % RRs assigned to relay subcells versus % RRs assigned to backhaul links we calculate cell capacity, Fig. 10.1; The remaining RRs are assigned to the donor subcell to directly serve its UTs. Visible from Fig. 10.1 is that there are ways of partitioning RRs (highlighted by hatched bars on the subdiagonal in Fig. 10.1) that approximately maximize capacity, namely combinations of % RRs assigned to relays/backhaul, respectively, as follows: 5%/10%, 10%/25%, 15%/35%, 20%/45%, 25%/60%. Other combinations of RR assignment to relays/backhaul result in lower capacity since bottlenecks appear in some partitions, then.

Cell capacity for the best combinations is shown in Fig. 10.2, where the red and green shares of a bar represent the capacity share contributed from donor subcell and relay subcells, respectively. Obviously, if RNs (plus backhaul) get more and BS gets less RRs, relay subcells increasingly contribute more to cell capacity while capacity contributed by the donor subcell decreases. Cell capacity for all combinations of RRs shown in Fig. 10.2 is more or less the same.

Fig. 10.3 for a multi-cell scenario shows the user throughput map of 3-RN-enhanced cells for a capacity optimal resource

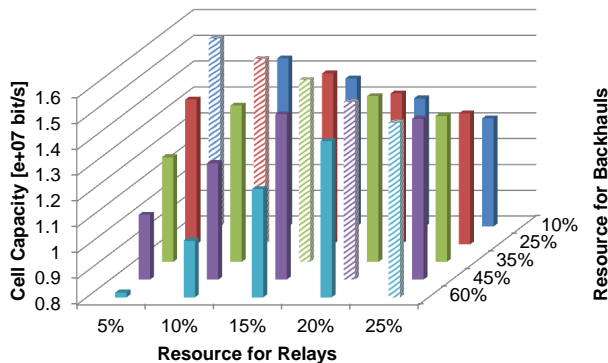


Figure 10.1: Cell capacity for various combinations of resource for relays and resource for backhauls

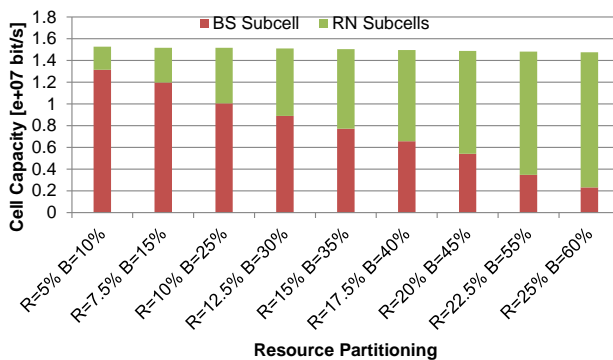


Figure 10.2: Cell capacity for capacity optimal resource partitioning

partitioning, where 15%, 35% and 50% of RRs are assigned to relay subcells, backhauls and donor subcell, respectively. Most part of the subcells served by BSs appears in red since well served. Areas served by RNs appear in green and are better served than by a BS without RNs. Clearly, users in subcells served by BSs and by RNs see quite different local through-

put and there is a high location dependent variance of user throughput throughout the cell. It would be preferable (under optimal choice of the respective MCSs) throughput to be independent of location in the cell since UTs then would be served more fairly. This also would reduce variance of packet delay, since a scheduler then needs not to wait for a UT roaming in a badly served cell area to occasionally have better channel condition to be served then.

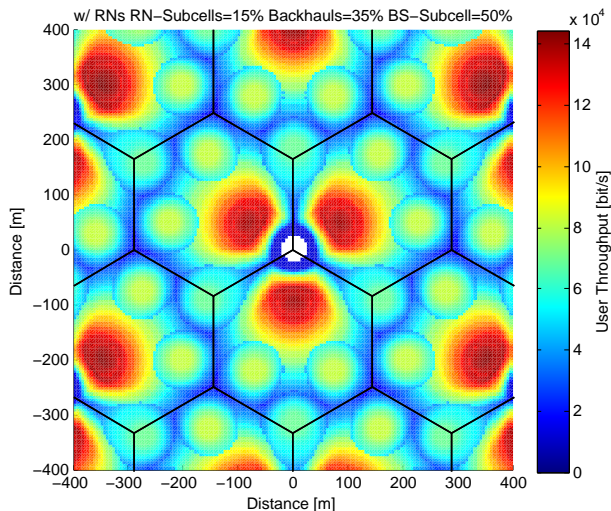


Figure 10.3: DL throughput map for relay=15% backhaul=35%

Bar charts of standard deviation of user throughput shown in Fig. 10.4 for capacity optimal partitioning combinations discussed in Fig. 10.2 reveal that resource partitioning can be optimized for better fairness. Red bars represent standard deviation of 3-RN-enhanced cells with different combinations of RR partitioning. The smallest standard deviation is achieved for partitioning RRs into 20% for relay subcells, 45% for backhaul and 35% for the donor subcell. At this point of operation of RRs according to Fig. 10.2 cell capacity is contributed in the amount of 64% by relay subcells and 36% by the donor subcell,

respectively.

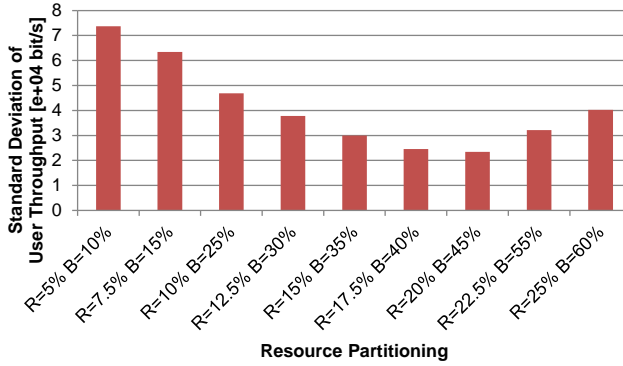


Figure 10.4: Standard deviation of user throughput for capacity optimal resource partitioning

If too many RRs are assigned to relay subcells and their related backhauls, and at the same time too few RRs to the donor subcell, subcells served by RNs would appear in a Fig. 10.3 like user throughput map in red and the subcell served by BS would be green. The opposite would happen if the BS gets too many RRs, see Fig. 10.3.

User throughput map under both, optimal cell capacity and minimum throughput standard deviation (maximum fairness) is shown in Fig. 10.5. From bird's view the service by relay cells appears to be small yellow cells of about equal size arranged regularly across the area similar to service by pico cells with omnidirectional antennas. There are still blue areas representing bad radio coverage owing to cochannel interference but the area shown in blue in Fig. 10.5 is smaller compared to Fig. 10.3 and there is less dark blue in Fig. 10.5.

Our model presumes that UTs are homogeneously distributed in cells and always have data to transmit. A real world system would need RRs assigned to RNs and to related backhaul, respectively, to be assigned dynamically dependent on

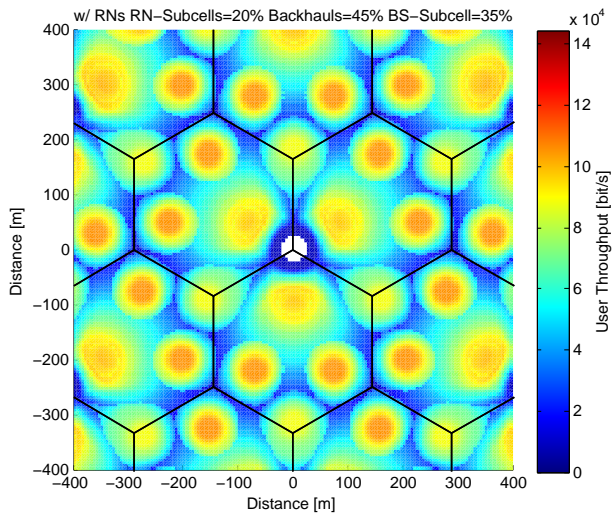


Figure 10.5: DL throughput map for relay=20% backhaul=45%

local load to be able to keep the capacity maximal that otherwise cannot be reached owing to wasted RRs.

Uplink under Reuse Partitioning

Content

11.1 Introduction	145
11.2 Reuse Partitioning	147
11.3 New Concept Reuse Partitioning	148
11.4 Results for Uplink under Reuse Partitioning	152
11.5 Results for Uplink of Relay Enhanced Systems	160

11.1 Introduction

In UMa scenario introduced in Chapter 3, a reference UT located in a certain cell, besides the signal from the BS antenna of this cell, simultaneously receives cochannel interferences from up to 20 neighbor BS antennas on downlink. On uplink the reference UT transmits the signal to the BS antenna of this cell, and up to 20 other UTs each located in one of 20 neighbor cells contribute cochannel interferences to this BS antenna. It is worth noting that downlink interferers are stationary BS antennas at fixed location, while uplink interferers are roaming UTs at random location in their respective cells.

Intuitively, both downlink and uplink cochannel interference can be mitigated with the Reuse Partitioning (RUP) concept. In this chapter we study uplink interference mitigation based on the following idea: Radio resources assigned to a reference UT located in a given cell, in cochannel cells are allocated at the same time to that UT, which among all UTs is the farthest away from the BS serving the reference UT. This maximizes distance and thereby path loss between interfering UTs and the serving

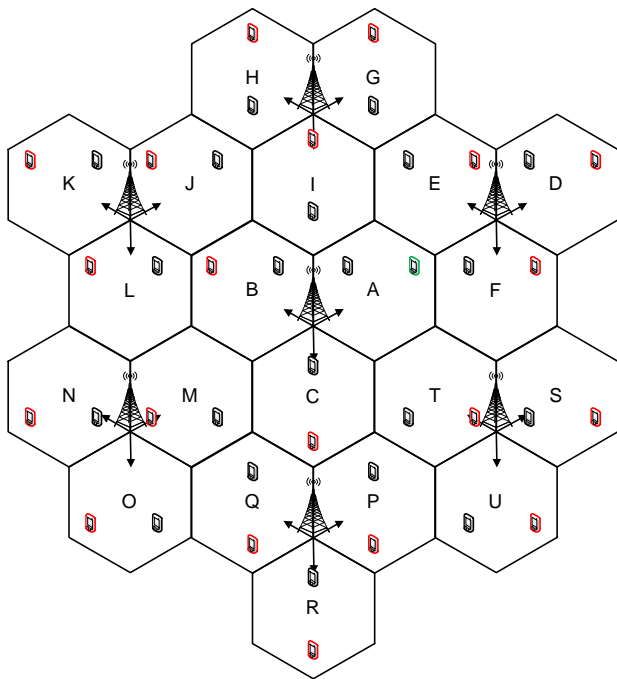


Figure 11.1: UMa scenario

BS. No matter, whether the reference UT is located in cell center or at cell edge, this idea should on average minimize cochannel interference on uplink. An example in Fig. 11.1 shows the reference UT in green in cell A, its serving BS in scenario center, and twenty cochannel UTs in red in cells B - U, respectively, where UTs are assumed randomly and uniformly distributed over cell area in UMa scenario.

In cellular networks UTs located nearby BSs according to better signal quality are better served, while UTs located far away have poor service. This leads to unfairness when comparing UTs in site center and UTs at site edge. This problem exists for both, downlink and uplink. We study possibilities to mitigate

interference on uplink by RUP with a special focus on site edge in this work.

11.2 Reuse Partitioning

Fractional Frequency Reuse (FFR) and Soft Frequency Reuse (SFR) follow the RUP concept to mitigate cochannel interference in cellular systems. In RUP, each cell is divided into two or more concentric subcells (zones), and the channel reuse distance, i.e. the distance between cells using the same channel, can be smaller for inner zones than for outer zones [KN96].

FFR described in [SOAS03] partitions the given bandwidth into an inner and an outer part. The inner part resources are completely reused by all cells with a Frequency Reuse Factor (FRF) of one while the outer part resources are further partitioned into three subsets and are reused among three adjacent cells with a FRF of three in a classical reuse three pattern.

SFR proposed in [Hua05a], [Hua05b] is characterized by FRF of one for the central region of a cell and FRF of three for outward cell regions. One third of the total bandwidth is allocated to the outer zone of a cell and thereby the outer zones of every three adjacent cells have orthogonal subcarriers. The inner zone of a cell may access the entire bandwidth. Maximum transmission power density allowed is higher on subcarriers allocated to both cell edge and cell center than on subcarriers for cell center only.

The concept proposed in this chapter applies RUP. In common with FFR and SFR, cells are divided into zones, radio resources are partitioned into subsets and resource subsets are allocated to zones. Both FFR and SFR apply FRF of one for cochannel inner zones and FRF of three for cochannel outer zones. Instead, our concept maximizes distance between cochannel zones of adjacent cells applying FRF one for both, inner and outer zones. To the best of our knowledge this is a new concept of RUP to mitigate cochannel interference in

cellular systems.

11.3 New Concept Reuse Partitioning

To mitigate uplink interference, a novel RUP concept is proposed. Each cell is divided into a certain number of partitions. The set of radio resources of a cell is divided into orthogonal subsets, one resource subset per cell partition. Radio resources of a certain resource subset are only granted to UTs located in the respective cell partition, but not to UTs in other partitions of the same cell. This concept results in orthogonal radio resources assigned to different cell partitions. The number of cell partitions must equal the number of resource subsets. Size of resource subsets may be proportional to area size of cell partitions.

The advantage of assigning resource subsets to cell partitions is that a UT located in a given cell partition, say x , is only interfered by UTs located in the same partitions x of neighbor cells, but not by UTs in other partitions. One drawback of forming resource subsets assigned to cell partitions is that trunking gain is reduced compared to a system without resource subsets dedicated to specific cell partitions. Trunking gain will be discussed later, when we study options with cells having different cell partition sizes.

RUP must be designed such that all sites throughout the cellular network achieve a comparable improvement in terms of uplink interference mitigation.

In our system design, the cellular network is made up from grey and white sites that appear as grey and white stripes, respectively, if an infinitely two dimensional network is considered. Fig. 11.2 and Fig. 11.3 show the UMa scenario for evaluation of a white site and a grey site, respectively, placed in the center of the scenario. Each white site has two white sites in stripe directions and four grey sites in other directions as its six neighboring sites. Similarly, each grey site has two grey

sites in stripe directions and four white sites in other directions as its neighborhoods. We limit our consideration to these sites inside the figure, since interference from UTs to the central site BS is not affected by those sites outside the figure. Cells are divided into six divisions of equal size as an example. Enumerating clockwise from BS position, each white cell is composed of divisions a, b, c, d, e, f in turn, whilst each grey cell has divisions d, e, f, a, b, c in turn. Please note, in this way the cellular network can be regularly expanded to any size, where all the sites apply either white or grey site patterns.

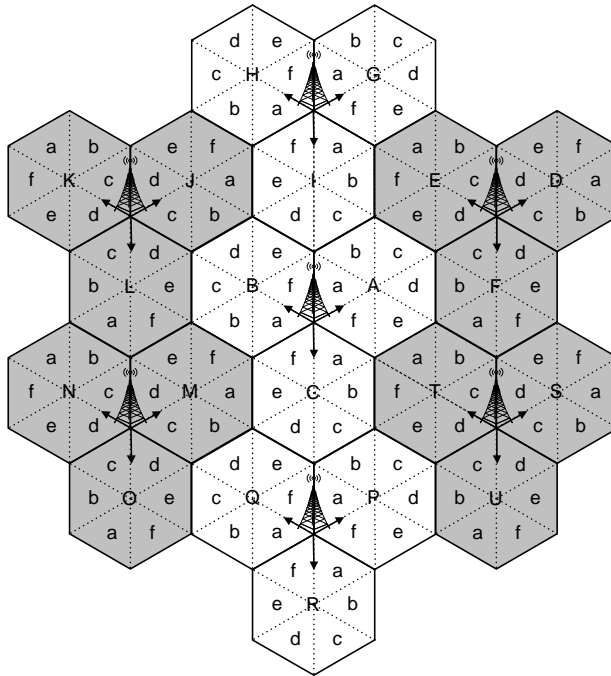


Figure 11.2: UMa scenario under cell partitioning with white site in center

Cell partitions can be designed arbitrarily according to the needs and are made up from cell divisions. One cell partition

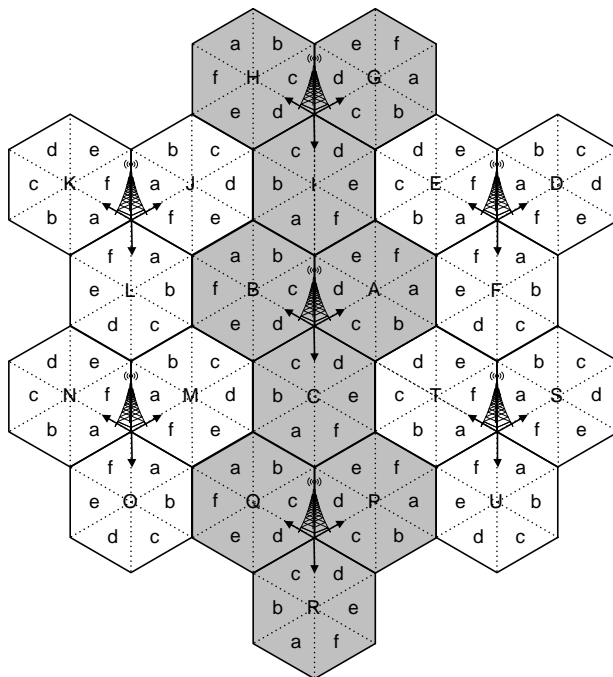


Figure 11.3: UMa scenario under cell partitioning with grey site in center

may comprise one or more divisions and another partition of the cell may comprise the same or a different number of other divisions of the cell.

Accordingly, the total radio resources are divided into six parts of equal size, namely resource parts *a - f* correspond to cell divisions *a - f*, respectively. Resource subsets are closely related to cell partitions: A resource subset assigned to a cell partition is made up from resource parts corresponding to cell divisions belonging to the cell partition. Thereby, the amount of radio resources assigned to a cell partition results from the ratio of the number of divisions that the partition is built from divided by the total number of divisions in a cell.

E.g., cell division a forms the first cell partition (a), divisions b, c the second partition (b, c), and divisions d, e, f the third partition (d, e, f). Hence, resource subset (a), subset (b, c), and subset (d, e, f) are allocated to the respective cell partitions, where the first, second and third partitions are assigned one sixth, one third, and one half of the radio resources available per cell, respectively. In the extreme, all six divisions of a cell constitute one cell partition only, which corresponds to a system without cell partitions and without RUP.

The notion Case is introduced to distinguish between different ways of cell and reuse partitioning. We study the following five Cases:

1. In Case (a, b, c, d, e, f) all six divisions of a cell form one partition only;
2. In Case $(a)(b)(c)(d)(e)(f)$ each division forms its own partition;
3. In Case $(a, f)(b, e)(c, d)$ divisions a, f form a first partition, divisions b, e a second, and divisions c, d a third;
4. In Case $(a, f)(b, c, d, e)$ divisions a, f form a first partition, and divisions b, c, d, e a second;
5. In Case $(a, b, e, f)(c, d)$ divisions a, b, e, f form a first partition, and divisions c, d a second.

Please note, white and grey sites in a given cellular network, although arranging cell divisions with different pattern, apply the same cell and reuse partitioning. There may be better arrangements of cell divisions and partitions, since we have not found an algorithm to mathematically optimize cell and reuse partitioning for interference minimization.

In order to evaluate the pros and cons of this novel way of RUP, the analytical model developed in this work is applied. It calculates per small grid element, e.g. $5 \text{ m} \times 5 \text{ m}$, uplink SINR

taking uplink power control into account and assuming the antenna pattern and the radio propagation model. From SINR of a grid element its uplink spectral efficiency (SE) is calculated accounting for LTE PHY layer characteristics like AMC, various radio channel states, PRBPs consumed to transmit a TB, turbo coded M-QAM BLER and overhead in LTE radio frame.

11.4 Results for Uplink under Reuse Partitioning

In the UMa scenario considered a $5\text{ m} \times 5\text{ m}$ grid is artificially overlaid to an $800\text{ m} \times 800\text{ m}$ center site of the scenario made up from three cells served by the central BS. Using the analytical model mentioned SE is calculated as PMF for each grid element. The mean of SE PMF for each grid element is shown as a colored map for the multi-cell scenario shown in Fig. 11.2. SE PMFs for a cell and its partitions are calculated by summarizing over SE PMFs of all grid elements contained in the respective partition and are normalized to the number of grid elements involved. Expected value and standard deviation of SE for the cell and the partitions are derived straightforwardly from the respective SE PMF. Our results serve to compare the contribution of various ways of cell and reuse partitioning to uplink interference mitigation.

In Case (a,b,c,d,e,f) there is one partition (a,b,c,d,e,f) per cell and all radio resources available to the cell are allocated to this partition. This case has the same SE map for both, white and grey sites and serves as a reference.

All SE maps shown in the following have the same scale from 0 to 1.4 bit/s/Hz . Fig. 11.4 shows the SE map of the center site for reference Case (a,b,c,d,e,f) . Trivially, site center divisions of a cell, e.g. divisions a, f in white sites, achieve highest SE, while site edge divisions, e.g. divisions c, d in white sites, experience lowest SE, because SINR at the BS antenna is much higher for UTs located in site center divisions than for UTs located in site edge divisions.

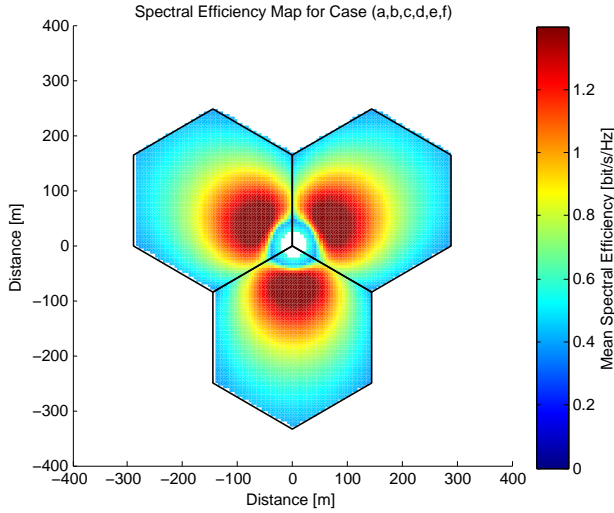


Figure 11.4: UL spectral efficiency map for Case (a,b,c,d,e,f)

In Case (a)(b)(c)(d)(e)(f) we study, whether the proposed uplink interference mitigation method has the potential for improving SE. There are six partitions per cell and each partition is made up from one division. One sixth of a cell's radio resources are allocated to each partition. In this Case both white and grey sites have the same SE map.

The resulting SE map for the center site is shown in Fig. 11.5¹. Divisions *a* and *f* show red, yellow and green instead of dark red and red in Fig. 11.4. Divisions *c* and *d* show red, yellow and green instead of green and blue in Fig. 11.4. Divisions *b* and *e* show red, yellow and green similar to Fig. 11.4. Furthermore, in Fig. 11.4 one half of the cell area is covered by red, yellow

¹Figs. 11.5-11.8 do not show SE on downlink but on uplink. Jumps in SE values (color jumps) when passing borders between adjacent partitions do not happen on downlink but on uplink under our new concept RUP. Such jumps simply reflect that a grid element at the boarder of a partition may contribute a quite different SINR than an adjacent grid element at the boarder of a neighboring partition.

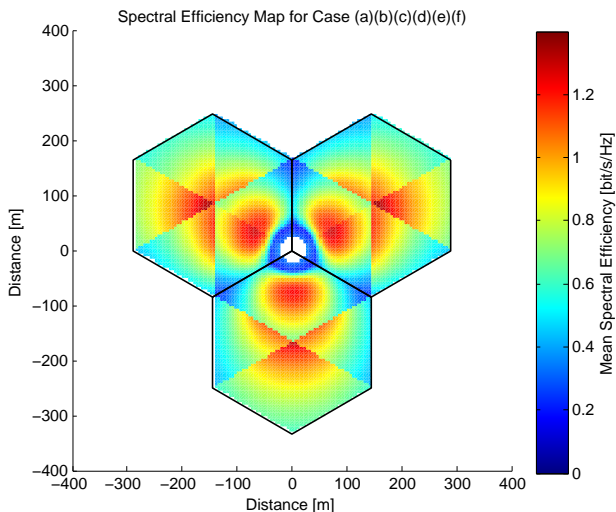


Figure 11.5: UL spectral efficiency map for Case (a)(b)(c)(d)(e)(f)

and green and the other half is covered by dark red and blue, respectively, while in Fig. 11.5 red, yellow and green appear for most of the cell area, but dark red and blue almost disappear.

It is obvious that Case (a)(b)(c)(d)(e)(f) compared to Case (a,b,c,d,e,f) significantly improves SE of UTs located at site edge at the cost of a degradation of SE of UTs located in site center. Clearly, introducing six partitions instead of one substantially reduces uplink cochannel interference for UTs located in site edge divisions, but increases interference for UTs located in site center divisions. Low SE at site edge as visible in Fig. 11.4 is a big problem for cellular networks, since it consumes much radio resources to serve UTs fair, whilst higher SE at site edge as visible from Fig. 11.5 is desired for real world systems, since more fairness of UTs located there is possible. Moreover, large SE difference across a cell resulting from large SINR difference between site center and site edge as visible in Fig. 11.4 is also problematic, since channel estimation is more difficult owing to high variance of SINR, whilst a more homogeneous SE distri-

bution resulting from a more homogeneous SINR distribution over the whole cell as visible from Fig. 11.5 is desirable.

In the following three ways of partitioning, namely Case $(a,f)(b,e)(c,d)$ with three partitions, Case $(a,f)(b,c,d,e)$ with two partitions, and Case $(a,b,e,f)(c,d)$ with two partitions, are studied to explore, whether the new method can keep SE gain and SE homogeneity achieved in Case $(a)(b)(c)(d)(e)(f)$ with less than six partitions.

In Case $(a,f)(b,e)(c,d)$ we combine divisions a and f into a first partition (a,f) , divisions b and e into a second partition (b,e) , and divisions c and d into a third partition (c,d) , and allocate one third of radio resources to each partition. In this Case white sites have the same SE map as grey sites.

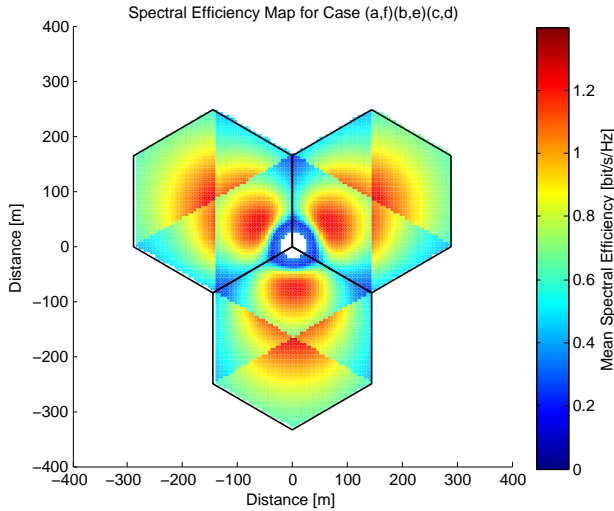


Figure 11.6: UL spectral efficiency map for Case $(a,f)(b,e)(c,d)$

From the SE map in Fig. 11.6 calculated for the center site, it is visible that SE of cell partition (a,f) is somewhat lower than in Fig. 11.4 but still acceptable. Cell partition (c,d) has much higher SE than in Fig. 11.4. SE in cell partition (b,e) is comparably high as in Fig. 11.4.

Case $(a,f)(b,c,d,e)$ combines two divisions a and f , namely site center divisions of white sites, which are site edge divisions of grey sites, into one partition (a,f) and combines the other four divisions b, c, d, e into the other partition (b,c,d,e) . One third of radio resources is assigned to partition (a,f) and two thirds of resources to partition (b,c,d,e) .

Case $(a,b,e,f)(c,d)$ combines two divisions c and d , namely site edge divisions of white sites, which are site center divisions of grey sites, into the first partition and combines the other four divisions a, b, e, f into the second partition. One third of radio resources is assigned to partition (c,d) and two thirds of resources to (a,b,e,f) .

Please note, in both Case $(a,f)(b,c,d,e)$ and Case $(a,b,e,f)(c,d)$ white sites and grey sites have different SE maps. However, in both Cases, all white sites and all grey sites, respectively, have the same SE map in common. Moreover, white sites in one of these two Cases have the same SE map as grey sites in the other Case of them. Hence, it is sufficient to display SE maps of a white site for Case $(a,f)(b,c,d,e)$ and Case $(a,b,e,f)(c,d)$ to also represent SE maps of a grey site for Case $(a,b,e,f)(c,d)$ and Case $(a,f)(b,c,d,e)$, respectively.

Fig. 11.7 shows SE map of the center site for Case $(a,f)(b,c,d,e)$. When comparing to the reference Case (a,b,c,d,e,f) SE appears to be substantially improved in four divisions b, c, d and e covering site edge. However, SE is somewhat reduced in site center divisions a and f still keeping an acceptable level.

Fig. 11.8 shows SE map of the center site for Case $(a,b,e,f)(c,d)$. When Comparing to reference Case (a,b,c,d,e,f) SE appears to be significantly higher in site edge divisions c and d but a little lower in four divisions a, b, e and f covering site center.

It is clear that Case $(a,f)(b,e)(c,d)$, Case $(a,f)(b,c,d,e)$ and Case $(a,b,e,f)(c,d)$ not only improve SE at site edge and provide more homogeneous SE throughout cells compared to Case (a,b,c,d,e,f) , but also come with a reduced number of three and two partitions, respectively, compared to six partitions in Case $(a)(b)(c)(d)(e)(f)$. Few instead of many partitions are desirable

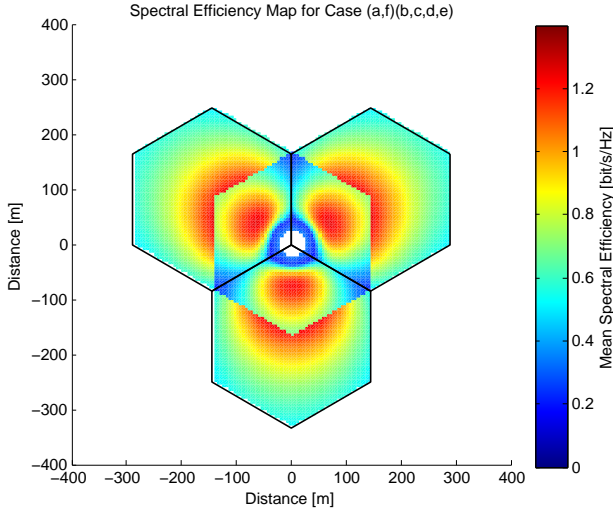


Figure 11.7: UL spectral efficiency map for Case (a,f)(b,c,d,e)

for real world systems, since the loss in trunking gain of radio resources assigned to specific partitions increases with the number of partitions per cell applied. Seen from this perspective Case (a,f)(b,e)(c,d) (Fig. 11.6) is less attractive than both, Case (a,f)(b,c,d,e) (Fig. 11.7) and Case (a,b,e,f)(c,d) (Fig. 11.8). Please remember, that for white and grey sites Case (a,f)(b,e)(c,d) has the same SE map, whilst Case (a,f)(b,c,d,e) and Case (a,b,e,f)(c,d) have individual SE maps that are different. From this perspective Case (a,f)(b,e)(c,d) has reference value for building a network with all sites having the same performance, but this is not a necessary goal of network planning.

Figs. 11.9, 11.10 and 11.11 show for various cell and reuse partitioning Cases bar charts of expected value, standard deviation of SE for cell A and expected value of SE for divisions a , b , c of cell A identified in Fig. 11.2, respectively. Compared to the reference Case (a,b,c,d,e,f), all RUP Cases increase expected value of SE for cell by up to 1%. Much more important is that all the partitioning Cases reduce standard deviation of SE up to

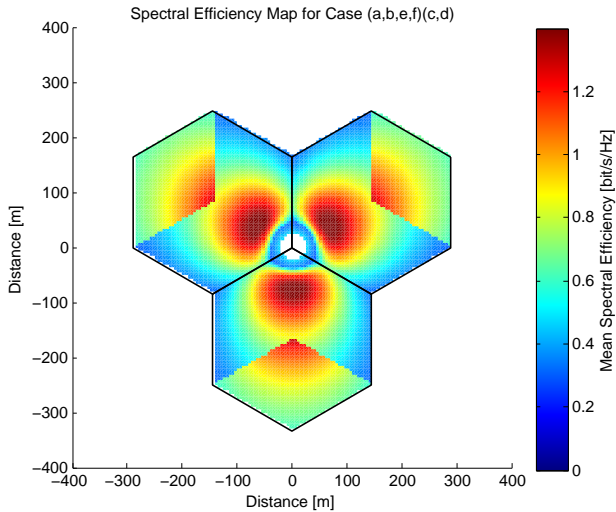


Figure 11.8: UL spectral efficiency map for Case (a,b,e,f)(c,d)

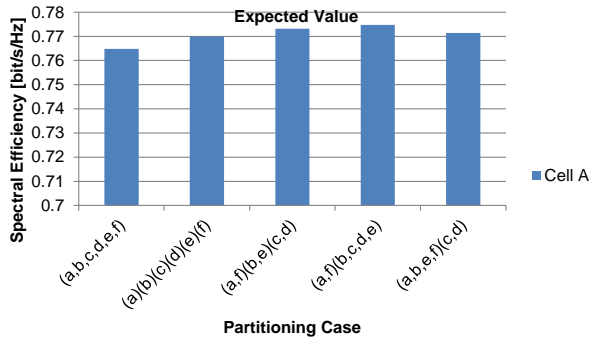


Figure 11.9: Expected value of spectral efficiency for cell A

30% underlining their potential to much more homogeneously serve UTs throughout the cell area. Most important is that all the partitioning Cases significantly boost expected value of SE in site edge divisions up to 44% showing their potential to reduce cochannel interference for UTs at site edge. Moreover, in

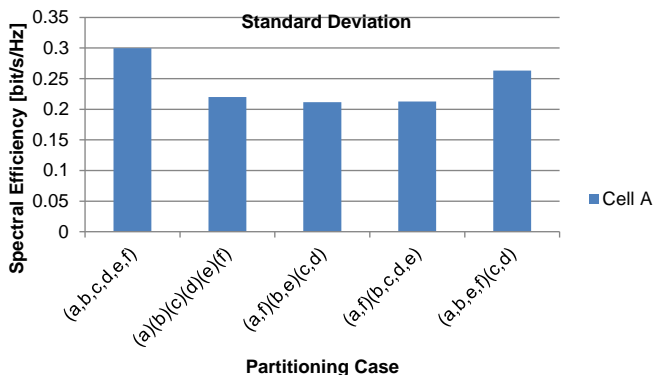


Figure 11.10: Standard deviation of spectral efficiency for cell A

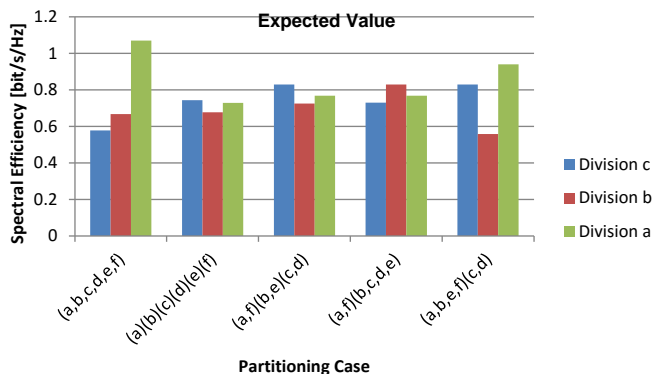


Figure 11.11: Expected value of spectral efficiency for divisions a, b and c

all the partitioning Cases expected value of SE for site center division is comparable to that for site edge division with a discrepancy ranging from -7% to 13% .

RUP on uplink presented here is a comparable technique to relay enhanced cells. This is because under RUP resource subsets are assigned to cell partitions, each partition with its ex-

clusive resources. In a relay enhanced cell orthogonal resources are allocated to direct, backhaul and access links, respectively. We expect that among all the RUP Cases, Case $(a,f)(b,c,d,e)$ (Fig. 11.7) is closest in terms of SE distribution to a cell enhanced with three relays, which uplink performance is evaluated in the following section.

11.5 Results for Uplink of Relay Enhanced Systems

Preliminary experiments are performed to evaluate throughput capacity for uplink of relay enhanced systems, where scenario and system parameters are configured with the same values as those for downlink according to Tables 9.1, 9.2 and 9.3.

Fig. 11.12 shows user throughput map for uplink of a relay enhanced system with 3 relays per cell. On uplink the relay enhanced system achieves a gain of 18% in throughput capacity compared to the non-relay system shown in Fig. 11.4. On downlink a performance gain of 29% is achieved, see Fig. 9.10. Preliminary results reveal that by deploying relays, the gain on uplink is about two thirds of that on downlink.

The parameter configuration optimized for downlink is not optimal for uplink, as e.g. seen from the contribution of the relay in antenna boresight of each sector cell in Fig. 11.12. The throughput capacity would be increased, if the parameters were properly configured. An optimization for uplink is not performed in this work, since there are no results suitable for validation in literature.

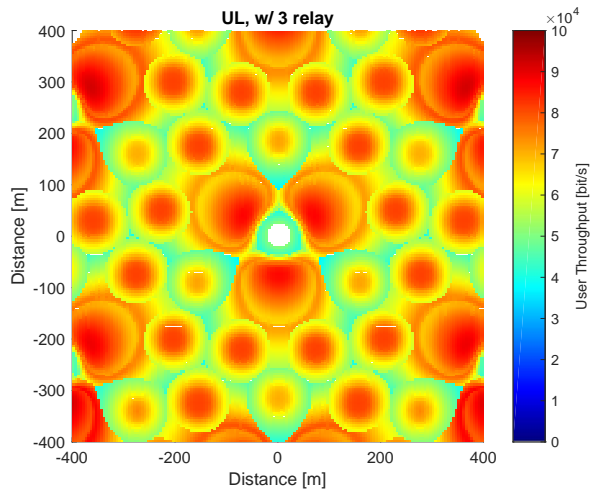


Figure 11.12: UL throughput map of RN enhanced system

Conclusions

Content

12.1 Conclusions	163
-----------------------------------	------------

12.1 Conclusions

A new analytical framework is presented to evaluate 3GPP LTE systems enhanced with multiple small cells per cell, namely either relay cells or pico cells. These systems are evaluated with respect to resource consumption, error ratio, spectral efficiency and user throughput for any small area element in a cell, as well as throughput capacity and CSE for a whole cell in a multi-cell scenario.

The most important protocol layer specific functions are modeled in very detail by using SFGs: On PHY layer, the SFG model of AMC scheme takes for various radio channel states the number of physical resource block pairs consumed to transmit a transport block and block error rate of turbo coded M-QAM into account; On MAC layer, the SFG model of HARQ protocol considers the number of retransmissions, resource assignment failure and feedback misdetection; On RLC layer, the SFG model of ARQ protocol includes the number of retransmissions, feedback loss and timer expiry for upcoming feedbacks.

This framework is used to evaluate the performance criteria resource consumption, error ratio and spectral efficiency at any user location of a cell. It is found that the HARQ protocol employed in MAC layer of LTE systems, although consuming resources for retransmission of erroneously received data, con-

tributes much not only to reduce error ratio but also to improve spectral efficiency, independent of the number of retransmissions permitted at maximum.

The framework is also used to evaluate the downlink performance with respect to local user throughput and throughput capacity of a whole cell. Two example LTE systems enhanced by small cells, one with three RNs and the other with three pico eNBs per cell positioned optimally (close to the cell edge), have a gain in cell capacity by 29% and 128%, respectively, compared to a system without small cells. Thus, it is concluded that cell capacity is raised substantially by pico cells compared to relay cells. The analytic results found in this work are validated by comparison to simulation results published by other researchers.

Further, resource partitioning of 3-relay-enhanced cells is optimized in terms of both cell capacity and user fairness across cell. Local user throughput and cell capacity on downlink of relay enhanced LTE systems are analytically evaluated for a variety of resource partitioning configurations. The optimal partitioning ratio is identified to maximize cell capacity and minimize standard deviation of local user throughput.

To optimize uplink spectral efficiency, we propose RUP in a new way to mitigate uplink cochannel interference in cellular networks. The uplink performance is analytically evaluated in terms of spectral efficiency per small area element and spectral efficiency per cell. It is shown possible to achieve a quite homogeneous spectral efficiency distribution across a cell with our new method compared to state-of-the-art resource allocation on uplink. It turns out that optimum RUP on uplink in cells without relays results in such a spectral efficiency distribution as can be expected from 3-relay enhanced cells.

List of Figures

2.1	LTE radio frame for downlink transmission . . .	7
2.2	LTE radio frame for uplink transmission	8
2.3	LTE user plane protocol stack (simplified) [ADF ⁺ 09]	11
2.4	Data flow through LTE protocol stack [LLM ⁺ 09]	20
2.5	Relay deployment example [HCM ⁺ 12]	21
2.6	One example of heterogeneous deployments [3GP10b]	23
2.7	Multiplexing between access and backhaul links [DPS11]	24
2.8	Relay DL backhaul design [HCM ⁺ 12]	26
2.9	LTE radio frame for downlink transmission in relay enhanced system	27
2.10	Uplink backhaul HARQ timing with 8 ms peri- odicity (FDD) [HLG ⁺ 11]	30
2.11	Illustration of 5G NR transmission structure and basic terminologies [LLB ⁺ 19]	32
3.1	Cellular coverage layout of UMa scenario [IR08b]	36
5.1	Capacity model	62
5.2	Capacity model extended for two-hop systems .	64
7.1	Basic equivalences of SFGs	78
7.2	Calculation with PMFs in co-domain and with MGFs in Z-domain	81
7.3	Signal flow graph models for LTE analysis . . .	83
7.4	SFG for PHY layer	84
7.5	BLER versus SINR for MCSs of PDSCH	87

List of Figures

7.6	BLER versus SINR for MCSs of PUSCH	88
7.7	Number of REs per bit for MCSs of PDSCH . . .	89
7.8	Number of REs per bit for MCSs of PUSCH . . .	90
7.9	SFG for MAC layer: recursion	91
7.10	SFG for MAC layer: exit condition	93
7.11	SFG for RLC layer: recursion for 2 segments . . .	99
7.12	SFG for RLC layer: recursion for 1 segment . . .	101
7.13	SFG for RLC layer: exit condition for 2 segments	101
7.14	SFG for RLC layer: exit condition for 1 segment .	102
9.1	UMa scenario	115
9.2	Relay enhanced UMa scenario	117
9.3	CDFs of performance criteria on MAC layer at three locations	123
9.4	CDFs of performance criteria on three protocol layers	125
9.5	CDFs of performance criteria for increasing max- imums of HARQ retransmissions	126
9.6	DL throughput map of BS only system	128
9.7	DL throughput map of RN enhanced system . .	129
9.8	DL throughput map of pico BS enhanced system	130
9.9	CDFs of DL aggregate throughput for various cell areas	133
9.10	DL aggregate throughput over various areas in different systems [$\times 10^7 bit/s$]	136
9.11	Validation of analytical results against system level simulation based references	137
10.1	Cell capacity for various combinations of re- source for relays and resource for backhauls . . .	141
10.2	Cell capacity for capacity optimal resource parti- tioning	141
10.3	DL throughput map for relay=15% backhaul=35%	142
10.4	Standard deviation of user throughput for capa- city optimal resource partitioning	143
10.5	DL throughput map for relay=20% backhaul=45%	144

11.1	UMa scenario	146
11.2	UMa scenario under cell partitioning with white site in center	149
11.3	UMa scenario under cell partitioning with grey site in center	150
11.4	UL spectral efficiency map for Case (a,b,c,d,e,f) .	153
11.5	UL spectral efficiency map for Case (a)(b)(c)(d)(e)(f)	154
11.6	UL spectral efficiency map for Case (a,f)(b,e)(c,d)	155
11.7	UL spectral efficiency map for Case (a,f)(b,c,d,e)	157
11.8	UL spectral efficiency map for Case (a,b,e,f)(c,d)	158
11.9	Expected value of spectral efficiency for cell A .	158
11.10	Standard deviation of spectral efficiency for cell A	159
11.11	Expected value of spectral efficiency for divi- sions a, b and c	159
11.12	UL throughput map of RN enhanced system . .	161

List of Tables

2.1	Typical numbers of PUCCH regions [LN09] . . .	9
2.2	Number of DM RS symbols per slot for different PUCCH formats [3GP10d]	10
2.3	Indices of DM RS symbols in a slot for different PUCCH formats [3GP10d]	10
2.4	LTE MCSs for PDSCH [Mot08]	14
2.5	LTE MCSs for PUSCH [EPM08]	14
2.6	HARQ protocol	16
2.7	Generalized SR-ARQ protocol	18
2.8	OFDM symbols usable for DeNB-to-RN transmission in the first slot [3GP10f]	26
2.9	OFDM symbols usable for DeNB-to-RN transmission in the second slot [3GP10f]	27
4.1	3GPP self-evaluation	46
9.1	Parameters of UMa scenario	111
9.2	Parameters supplemented for relay enhanced UMa scenario	114
9.3	LTE system parameters	122
9.4	DL aggregate throughput over some area in some system $\times 10^7$ [bit/s]	135

BIBLIOGRAPHY

- [3GP10a] 3GPP. TR 36.806 - Technical Specification Group Radio Access Network; Evolved Universal Terrestrial Radio Access (E-UTRA); Relay architectures for E-UTRA (LTE-Advanced) (Release 9). Technical report, 3rd Generation Partnership Project, 2010.
- [3GP10b] 3GPP. TR 36.814 - Technical Specification Group Radio Access Network; Evolved Universal Terrestrial Radio Access (E-UTRA); Further advancements for E-UTRA physical layer aspects (Release 9). Technical report, 3rd Generation Partnership Project, 2010.
- [3GP10c] 3GPP. TS 36.201 - Technical Specification Group Radio Access Network; Evolved Universal Terrestrial Radio Access (E-UTRA); LTE physical layer; General description (Release 10). Technical report, 3rd Generation Partnership Project, 2010.
- [3GP10d] 3GPP. TS 36.211 - Technical Specification Group Radio Access Network; Evolved Universal Terrestrial Radio Access (E-UTRA); Physical channels and modulation (Release 10). Technical report, 3rd Generation Partnership Project, 2010.
- [3GP10e] 3GPP. TS 36.213 - Technical Specification Group Radio Access Network; Evolved Universal Terrestrial Radio Access (E-UTRA); Physical layer procedures (Release 10). Technical report, 3rd Generation Partnership Project, 2010.

Bibliography

- [3GP10f] 3GPP. TS 36.216 - Technical Specification Group Radio Access Network; Evolved Universal Terrestrial Radio Access (E-UTRA); Physical layer for relaying operation (Release 10). Technical report, 3rd Generation Partnership Project, 2010.
- [3GP10g] 3GPP. TS 36.300 - Technical Specification Group Radio Access Network; Evolved Universal Terrestrial Radio Access (E-UTRA) and Evolved Universal Terrestrial Radio Access Network (E-UTRAN); Overall description; Stage 2 (Release 10). Technical report, 3rd Generation Partnership Project, 2010.
- [3GP10h] 3GPP. TS 36.321 - Technical Specification Group Radio Access Network; Evolved Universal Terrestrial Radio Access (E-UTRA); Medium Access Control (MAC) protocol specification (Release 10). Technical report, 3rd Generation Partnership Project, 2010.
- [3GP10i] 3GPP. TS 36.322 - Technical Specification Group Radio Access Network; Evolved Universal Terrestrial Radio Access (E-UTRA); Radio Link Control (RLC) protocol specification (Release 10). Technical report, 3rd Generation Partnership Project, 2010.
- [3GP15] 3GPP. TR 22.885 - Technical Specification Group Services and System Aspects; Study on LTE support for Vehicle to Everything (V2X) services (Release 14). Technical report, 3rd Generation Partnership Project, 2015.
- [3GP16] 3GPP. TR 22.886 - Technical Specification Group Services and System Aspects; Study on enhancement of 3GPP support for 5G V2X services (Re-

- lease 15). Technical report, 3rd Generation Partnership Project, 2016.
- [3GP19] 3GPP. TS 38.211 - Technical Specification Group Radio Access Network; NR; Physical channels and modulation (Release 15). Technical report, 3rd Generation Partnership Project, 2019.
- [AA09] Alcatel-Lucent Shanghai Bell and Alcatel-Lucent. R1-094632 - Downlink performance evaluation for relay-enhanced cellular systems with PF scheduler. Technical report, 3rd Generation Partnership Project, 2009. https://www.3gpp.org/ftp/tsg_ran/WG1_RL1/TSGR1_59/Docs/R1-094632.zip.
- [ADF⁺09] David Astély, Erik Dahlman, Anders Furuskär, Ylva Jading, Magnus Lindström, and Stefan Parkvall. LTE: The Evolution of Mobile Broadband. *IEEE Communications Magazine*, 2009.
- [AN07] Kamtorn Ausavapattanakun and Aria Nosratinia. Analysis of Selective-Repeat ARQ via Matrix Signal-Flow Graphs. *IEEE Transactions on Communications*, 2007.
- [BM11] Matthew Baker and Tim Moulsley. *LTE – The UMTS Long Term Evolution : From Theory to Practice : Second Edition*, chapter 9 Downlink Physical Data and Control Channels, pages 189–214. John Wiley & Sons, 2011.
- [BRRH11] Omer Bulakci, Simone Redana, Bernhard Raaf, and Jyri Hamalainen. Impact of power control optimization on the system performance of relay based lte-advanced heterogeneous networks. *Journal of Communications and Networks*, 2011.

- [CEA11] R. Combes, S. E. Elayoubi, and Z. Altman. Cross-Layer Analysis of Scheduling Gains: Application to LMMSE receivers in Frequency-Selective Rayleigh-Fading Channels. In *International Symposium of Modeling and Optimization of Mobile, Ad Hoc, and Wireless Networks*, 2011.
- [CMC09a] CMCC. R1-093726 - Text Proposal for Channel Model and Evaluation Methodology. Technical report, 3rd Generation Partnership Project, 2009.
- [CMC09b] CMCC. R1-094824 - Relay performance evaluation. Technical report, 3rd Generation Partnership Project, 2009. https://www.3gpp.org/ftp/tsg_ran/WG1_RL1/TSGR1_59/Docs/R1-094824.zip.
- [CNST09] Brian Classon, Ajit Nimbalkar, Stefania Sesia, and Issam Toufik. *LTE – The UMTS Long Term Evolution : From Theory to Practice*, chapter 10 Channel Coding and Link Adaptation, pages 207–242. John Wiley & Sons, 2009.
- [CW13] Yuan Chen and Bernhard Walke. Analysis of cell spectral efficiency in 3GPP LTE systems. In *IEEE 24th International Symposium on Personal, Indoor and Mobile Radio Communications*, 2013.
- [CW14] Yuan Chen and Bernhard Walke. Spectral Efficiency of LTE with Small Cells and Optimum Association Threshold. In *IEEE 25th International Symposium on Personal, Indoor and Mobile Radio Communications*, 2014.
- [DPS11] Erik Dahlman, Stefan Parkvall, and Johan Sköld, editors. *4G LTE / LTE-Advanced for Mobile Broadband*, chapter 16 Relaying, pages 331–345. Elsevier, 2011.

- [EPM08] Ericsson, Panasonic, and Motorola. R1-082091 - MCS and TBS Tables for PUSCH. Technical report, 3rd Generation Partnership Project, 2008.
- [EVW01] Norbert Esseling, Harbinder S. Vandra, and Bernhard Walke. A forwarding concept for hiperlan/2. *Computer Networks*, pages 25–32, 2001.
- [Geh07] Guido Gehlen. *Mobile Web Services - Concepts, Prototype, and Traffic Performance Analysis*. PhD thesis, RWTH Aachen University, 2007.
- [GJP02] D. Gore, R. W. Heath Jr., and A. Paulraj. On Performance of the Zero Forcing Receiver in Presence of Transmit Correlation. In *IEEE International Symposium on Information Theory*, 2002.
- [HCM⁺12] Christian Hoymann, Wanshi Chen, Juan Montojo, Alexander Golitschek, Chrysostomos Koutsimanis, and Xiaodong Shen. Relaying Operation in 3GPP LTE: Challenges and Solutions. *IEEE Communications Magazine*, 2012.
- [HLG⁺11] Eric Hardouin, J. Nicholas Laneman, Alexander Golitschek, Hidetoshi Suzuki, and Osvaldo Gonsa. *LTE – The UMTS Long Term Evolution : From Theory to Practice : Second Edition*, chapter 30 Relaying, pages 673–700. John Wiley & Sons, 2011.
- [Hoy13] Christian Hoymann. Rule of Thumb. Email, Ericsson Eurolab, 2013.
- [Hua05a] Huawei. R1-050507 - Soft Frequency Reuse Scheme for UTRAN LTE. Technical report, 3rd Generation Partnership Project, 2005.
- [Hua05b] Huawei. R1-050841 - Further Analysis of Soft Frequency Reuse Scheme. Technical report, 3rd Generation Partnership Project, 2005.

Bibliography

- [Hua09] Huawei. R1-094726 - Type 1 relay performance evaluation. Technical report, 3rd Generation Partnership Project, 2009.
https://www.3gpp.org/ftp/tsg_ran/WG1_RL1/TSGR1_59/Docs/R1-094726.zip.
- [Int10] Intel Corporation (UK) Ltd. R1-105427 - Downlink Relay System Performance Evaluation. Technical report, 3rd Generation Partnership Project, 2010.
https://www.3gpp.org/ftp/tsg_ran/WG1_RL1/TSGR1_62b/Docs/R1-105427.zip.
- [IR08a] ITU-R. M.2134 - Requirements related to technical performance for IMT-Advanced radio interface(s). Technical report, International Telecommunication Union Radiocommunication Sector, 2008.
- [IR08b] ITU-R. M.2135 - Guidelines for evaluation of radio interface technologies for IMT-Advanced. Technical report, International Telecommunication Union Radiocommunication Sector, 2008.
- [IR17a] ITU-R. M.2410 - Minimum requirements related to technical performance for IMT-2020 radio interface(s). Technical report, International Telecommunication Union Radiocommunication Sector, 2017.
- [IR17b] ITU-R. M.2412 - Guidelines for evaluation of radio interface technologies for IMT-2020. Technical report, International Telecommunication Union Radiocommunication Sector, 2017.
- [KN96] I. Katzela and M. Naghshineh. Channel assignment schemes for cellular mobile telecommunication systems: A comprehensive survey. *IEEE Personal Communications*, 1996.

- [LC89] Deng-Lin Lu and Jin-Fu Chang. Analysis of ARQ Protocols via Signal Flow Graphs. *IEEE Transactions on Communications*, 1989.
- [LC93] Deng-Lin Lu and Jin-Fu Chang. Performance of ARQ Protocols in Nonindependent Channel Errors. *IEEE Transactions on Communications*, 1993.
- [LG 10] LG Electronics. R1-102428 - Downlink Performance with Relay. Technical report, 3rd Generation Partnership Project, 2010. https://www.3gpp.org/ftp/tsg_ran/WG1_RL1/TSGR1_60b/Docs/R1-102428.zip.
- [LHX⁺10] Bin Lin, Pin-Han Ho, Liang-Liang Xie, Xuemin Shen, and Janos Tapolcai. Optimal relay station placement in broadband wireless access networks. *IEEE Transactions on Mobile Computing*, 2010.
- [LLB⁺19] Xingqin Lin, Jingya Li, Robert Baldemair, Jung-Fu (Thomas) Cheng, Stefan Parkvall, Daniel Chen Larsson, Havish Koorapaty, Mattias Frenne, Sorour Falahati, Asbjörn Grövlén, and Karl Werner. 5G New Radio: Unveiling the Essentials of the Next Generation Wireless Access Technology. *IEEE Communications Standards Magazine*, 2019.
- [LLM⁺09] Anna Larmo, Magnus Lindström, Michael Meyer, Ghyslain Pelletier, Johan Torsner, and Henning Wiemann. The LTE Link-Layer Design. *IEEE Communications Magazine*, 2009.
- [LN09] Robert Love and Vijay Nangia. *LTE – The UMTS Long Term Evolution : From Theory to Practice*, chapter 17 Uplink Physical Channel Structure, pages 377–404. John Wiley & Sons, 2009.
- [Mas53] Samuel J. Mason. Feedback Theory - Some Properties of Signal Flow Graphs. In *Proceedings of the*

Institute of Radio Engineers, Proceedings of the Institute of Radio Engineers, 1953.

- [Mas56] Samuel J. Mason. Feedback Theory - Further Properties of Signal Flow Graphs. In *Proceedings of the Institute of Radio Engineers*, 1956.
- [MMCG15] Mattia Minelli, Maode Ma, Marceau Coupechoux, and Philippe Godlewski. Scheduling Impact on the Performance of Relay-Enhanced LTE-A Networks. *IEEE Transactions on Vehicular Technology*, 2015.
- [Mot08] Motorola. R1-081638 - TBS and MCS Signaling and Tables. Technical report, 3rd Generation Partnership Project, 2008.
- [Mot09] Motorola. R1-094687 - Relay System Performance for Downlink with Latest Link Models. Technical report, 3rd Generation Partnership Project, 2009.
https://www.3gpp.org/ftp/tsg_ran/WG1_RL1/TSGR1_59/Docs/R1-094687.zip.
- [MW11] Maciej Mühleisen and Bernhard Walke. Analytical Evaluation of LTE Uplink Performance in the IMT-Advanced Indoor Hotspot Scenario. In *2011 IEEE 22nd International Symposium on Personal Indoor and Mobile Radio Communications*, 2011.
- [NEC10] NEC Group. R1-103835 - System Level Performance Evaluation for Relays. Technical report, 3rd Generation Partnership Project, 2010.
https://www.3gpp.org/ftp/tsg_ran/WG1_RL1/TSGR1_61b/Docs/R1-103835.zip.
- [NN10] Nokia Siemens Networks and Nokia. R1-106216 - Type-1 Relay Performance for Downlink. Technical report, 3rd Generation Partnership Project, 2010. https://www.3gpp.org/ftp/tsg_ran/WG1_RL1/TSGR1_61b/Docs/R1-106216.zip.

- [//www.3gpp.org/ftp/tsg_ran/WG1_RL1/TSGR1_63/Docs/R1-106216.zip](https://www.3gpp.org/ftp/tsg_ran/WG1_RL1/TSGR1_63/Docs/R1-106216.zip).
- [NTT11] NTT Docomo. R1-110244 - System Evaluation of Relay Performance. Technical report, 3rd Generation Partnership Project, 2011. https://www.3gpp.org/ftp/tsg_ran/WG1_RL1/TSGR1_63b/Docs/R1-110244.zip.
- [Pan10] Panasonic. R1-101273 - Downlink Relay Performance Evaluation. Technical report, 3rd Generation Partnership Project, 2010. https://www.3gpp.org/ftp/tsg_ran/WG1_RL1/TSGR1_60/Docs/R1-101273.zip.
- [PS96] Jan B. Punt and Dirk Sparreboom. Summing received signal powers with arbitrary probability density functions on a logarithmic scale. *Wireless Personal Communications*, 1996.
- [PWS⁺04] Ralf Pabst, Bernhard H. Walke, Daniel C. Schultz, Patrick Herhold, Halim Yanikomeroglu, Sayandev Mukherjee, Harish Viswanathan, Matthias Lott, Wolfgang Zirwas, Mischa Dohler, Hamid Aghvami, David D. Falconer, and Gerhard P. Fettweis. Relay-Based Deployment Concepts for Wireless and Mobile Broadband Radio. *IEEE Communications Magazine*, 2004.
- [Qua10] Qualcomm Incorporated. R1-103559 - Downlink performance for Type I relays with and without range expansion. Technical report, 3rd Generation Partnership Project, 2010. https://www.3gpp.org/ftp/tsg_ran/WG1_RL1/TSGR1_61b/Docs/R1-103559.zip.
- [Sam13] Klaus Sambale. *Cellular Radio Relay Placement for*

- Optimized Capacity*. PhD thesis, RWTH Aachen University, 2013.
- [SmBR⁺11] Abdallah Bou Saleh, Ömer Bulakci, Zhe Ren, Simone Redana, Bernhard Raaf, and Jyri Hämäläinen. Resource Sharing in Relay-enhanced 4G Networks - Downlink Performance Evaluation. In *European Wireless 2011*, 2011.
- [SOAS03] Mikael Sternad, Tony Ottosson, Anders Ahlen, and Arne Svensson. Attaining both Coverage and High Spectral Efficiency with Adaptive OFDM Downlinks. In *2003 IEEE 58th Vehicular Technology Conference*, 2003.
- [SW12] Klaus Sambale and Bernhard Walke. Cell Spectral Efficiency Optimization in Relay Enhanced Cells. In *IEEE 23rd International Symposium on Personal, Indoor and Mobile Radio Communications*, 2012.
- [TK09] Issam Toufik and Raymond Knopp. *LTE – The UMTS Long Term Evolution : From Theory to Practice*, chapter 12 Multi-User Scheduling and Interference Coordination, pages 285–300. John Wiley & Sons, 2009.
- [TLW09] Ylva Timner, Anna Larmo, and Henning Wiemann. Control Signaling Robustness in LTE. In *2009 IEEE 70th Vehicular Technology Conference Fall*, 2009.
- [WB85] Bernhard Walke and Roland Briechle. A local cellular radio network for digital voice & data transmission at 60 GHz. In *Cellular & Mobile Communications Intl: Online Publications*, 1985.
- [WPS03] B. Walke, R. Pabst, and D. Schultz. A mobile broadband system based on fixed wireless routers.

- In *International Conference on Communication Technology*, 2003.
- [WW99] Moe Z. Win and Jack H. Winters. Analysis of Hybrid Selection/Maximal-Ratio Combining in Rayleigh Fading. In *1999 IEEE International Conference on Communications*, 1999.
- [YRT09] Chia-Hao Yu, Kalle Ruttik, and Olav Tirkkonen. Approximate Rate Quantization of Adaptive Modulation and Coding with Near-Optimum Throughput. In *2009 IEEE 20th International Symposium on Personal, Indoor and Mobile Radio Communications*, 2009.
- [ZRM97] Michele Zorzi, Ramesh R. Rao, and Laurence B. Milstein. ARQ Error Control for Fading Mobile Radio Channels. *IEEE Transactions on Vehicular Technology*, 1997.
- [ZTE09] ZTE. R1-094748 - Preliminary Performance Study on Type 1 and Type 2 Relays. Technical report, 3rd Generation Partnership Project, 2009.
https://www.3gpp.org/ftp/tsg_ran/WG1_RL1/TSGR1_59/Docs/R1-094748.zip.

ACRONYMS

3GPP 3rd Generation Partnership Project

4G 4th Generation

5G 5th Generation

ACK Acknowledgement

AM Acknowledged Mode

AMC Adaptive Modulation and Coding

ARQ Automatic Repeat Request

BLER Block Error Rate

BS Base Station

CC Chase Combining

CDF Cumulative Distribution Function

CoMP Coordinated Multiple Point

CRC Cyclic Redundancy Check

CSE Cell Spectral Efficiency

CSI Channel State Information

DeNB Donor Enhanced Node-B

DFT Discrete Fourier Transform

DM RS Demodulation Reference Signal

DTX Discontinuous Transmission

Bibliography

- eNB** Enhanced Node-B
- FDD** Frequency Division Duplex
- FEC** Forward Error Correction
- FFR** Fractional Frequency Reuse
- FFT** Fast Fourier Transform
- FRF** Frequency Reuse Factor
- HARQ** Hybrid Automatic Repeat Request
- IEEE** Institute of Electrical and Electronics Engineers
- IMT-A** International Mobile Telecommunications-Advanced
- IMT-2020** International Mobile Telecommunications-2020
- IP** Internet Protocol
- IR** Incremental Redundancy
- ISD** Inter-site distance
- ITU-R** International Telecommunication Union Radiocommunication Sector
- LoS** Line-of-Sight
- LTE** Long Term Evolution
- LTE-A** Long Term Evolution-Advanced
- MAC** Medium Access Control
- MBSFN** Multicast Broadcast Single Frequency Network
- MCS** Modulation and Coding Scheme
- MGF** Moment Generating Function

MIMO Multiple Input Multiple Output

MRC Maximum Ratio Combining

MU-MIMO Multi-User Multiple Input Multiple Output

NAK Negative Acknowledgement

NLoS Non-Line-of-Sight

NR New Radio

OFDM Orthogonal Frequency Division Multiplexing

OFDMA Orthogonal Frequency Division Multiple Access

PBCH Physical Broadcast Channel

PCFICH Physical Control Format Indicator Channel

PDCCH Physical Downlink Control Channel

PDCP Packet Data Convergence Protocol

PDF Probability Density Function

PDSCH Physical Downlink Shared Channel

PDU Protocol Data Unit

PF Proportional Fair

PHICH Physical Hybrid-ARQ Indicator Channel

PHY Physical

PMF Probability Mass Function

PRBP Physical Resource Block Pair

PUCCH Physical Uplink Control Channel

PUSCH Physical Uplink Shared Channel

Bibliography

QAM Quadrature Amplitude Modulation

QPSK Quadrature Phase Shift Keying

RAP Radio Access Point

RB Resource Block

RE Resource Element

RLC Radio Link Control

RN Relay Node

RR Round Robin

RS Reference Signal

RTT Round Trip Time

RUP Reuse Partitioning

RV Redundancy Version

R-PDCCH Relay Physical Downlink Control Channel

SC-FDMA Single Channel Frequency Division Multiple Access

SDMA Spatial Division Multiple Access

SDU Service Data Unit

SFG Signal Flow Graph

SFR Soft Frequency Reuse

SINR Signal to Interference plus Noise Ratio

SISO Single Input Single Output

SRS Sounding Reference Signal

- SR-ARQ** Selective Repeat Automatic Repeat Request
- SU-MIMO** Single-User Multiple Input Multiple Output
- TB** Transport Block
- TCP** Transmission Control Protocol
- TDM** Time Division Multiplexing
- UE** User Equipment
- UMa** Urban Macro-cell
- UMi** Urban Micro-cell
- UMTS** Universal Mobile Telecommunications System
- UT** User Terminal
- V2X** Vehicle to Everything
- VoIP** Voice over IP
- WiMAX** Worldwide Interoperability for Microwave Access

CURRICULUM VITAE

Name: Yuan Chen
Date of Birth: August 31, 1980
Place of Birth: Shanghai, China
Nationality: German

09/1991 - 08/1998 Shixi High School, Shanghai, China

01/2000 - 06/2000 Preparatory Course for Foreign Students,
RWTH Aachen University

10/2000 - 03/2010 Studies in Computer Science,
RWTH Aachen University

03/2012 - 03/2017 Research Engineer,
Chair of Communication Networks,
RWTH Aachen University

since 06/2021 Engineer for Frequency Strategy,
Federal Agency for Public Safety Digital
Radio, Berlin, Germany

